Fisheries and Oceans Canada | Pêches et Océans Canada
Ecosystems and Oceans Science | Sciences des écosystèmes et des océans

Canadian Science Advisory Secretariat (CSAS)

Research Document 2021/060

Québec Region

Chemical and Biological Oceanographic Conditions in the Estuary and Gulf of St. Lawrence during 2020

M. Blais[1], P. S. Galbraith[1], S. Plourde[1], E. Devred[2], S. Clay[2], C. Lehoux[1] and L. Devine[1]

[1]Fisheries and Oceans Canada, Québec Region,
Maurice Lamontagne Institute,
P.O. Box 1000, Mont-Joli, Québec, G5H 3Z4

[2]Fisheries and Oceans Canada, Maritimes Region,
Bedford Institute of Oceanography,
P.O. Box 1006, Dartmouth, Nova Scotia, B2Y 4A2

October 2021

Canada

Foreword

This series documents the scientific basis for the evaluation of aquatic resources and ecosystems in Canada. As such, it addresses the issues of the day in the time frames required and the documents it contains are not intended as definitive statements on the subjects addressed but rather as progress reports on ongoing investigations.

Published by:

Fisheries and Oceans Canada
Canadian Science Advisory Secretariat
200 Kent Street
Ottawa ON K1A 0E6

http://www.dfo-mpo.gc.ca/csas-sccs/
csas-sccs@dfo-mpo.gc.ca

ISSN 1919-5044
ISBN 978-0-660-40307-6 Cat. No. Fs70-5/2021-060E-PDF

Correct citation for this publication:

Blais, M., Galbraith, P.S., Plourde, S., Devred, E., Clay, S., Lehoux, C. and Devine, L. 2021. Chemical and Biological Oceanographic Conditions in the Estuary and Gulf of St. Lawrence during 2020. DFO Can. Sci. Advis. Sec. Res. Doc. 2021/060. iv + 67 p.

Aussi disponible en français :

Blais, M., Galbraith, P.S., Plourde, S., Devred, E., Clay, S., Lehoux, C. et Devine, L. 2021. Les conditions océanographiques chimiques et biologiques dans l'estuaire et le golfe du Saint-Laurent en 2020. Secr. can. de consult. sci. du MPO, Doc. de rech. 2021/060. iv + 70 p.

TABLE OF CONTENTS

ABSTRACT

An overview of chemical and biological oceanographic conditions in the Gulf of St. Lawrence in 2020 is presented as part of the Atlantic Zone Monitoring Program (AZMP). AZMP data as well as data from regional monitoring programs are analyzed and presented in relation to long-term means in the context of a strong warming event that began in 2010. These long-term means are now calculated on data from 1999–2020 (1999–2015 in earlier reports). Oxygen levels at 300 m reached a record low concentration in the Estuary and at Rimouski station. Nitrate inventories in the surface layer (0–50 m) of the Gulf were either near or slightly above normal. Nitrate mid-layer inventories (50–150 m) were above normal in the northern and central Gulf, while they were close to normal in Magdalen Shallows and Cabot Strait. In the bottom layer (150 m–bottom), positive nitrate anomalies were found in all Gulf regions. Positive deep nitrate anomalies have been observed regularly since 2012 in Cabot Strait and the central Gulf in association with intrusions of warm and salty waters, but they have been rare in the Estuary over the last decade. The recent increase in the nitrate inventory of the bottom layer is mostly associated with negative anomalies of the N:P ratio and positive anomalies of the Si:N ratio. There were strong positive anomalies of vertically integrated chlorophyll *a* (chl *a*; 0–100 m) during late summer in the northeast Gulf, during fall in the Estuary, and, to a lesser extent, in the central Gulf during both seasons. Elsewhere, vertically integrated phytoplankton biomass was close to normal except in Cabot Strait, where it was below normal. Most regions have shown either near-normal or above-normal chl *a* inventories during fall since about 2014. In contrast, phytoplankton biomass derived from satellite data showed negative annual and fall anomalies in most of the ocean colour averaging areas over the last three years. Spring bloom metrics were mostly near normal, except for high bloom amplitudes and magnitudes in the Magdalen Shallows and Cabot Strait boxes. Zooplankton biomass was close to normal almost everywhere in the Gulf; it was only below normal in the central Gulf/Cabot Strait region. *Calanus finmarchicus*, *C. hyperboreus,* and large calanoid abundances were also generally close to normal, except that *C. hyperboreus* abundance was above normal in the northwest Gulf and below normal on the Magdalen Shallows. Small calanoid abundances were near normal everywhere despite record low abundance of *Pseudocalanus* spp. on the Magdalen Shallows and low abundances in the northwest Gulf and at Rimouski station. Abundances of warm-water-associated copepods were slightly above normal in most regions and at a record high on the Magdalen Shallows. The lack of sampling during spring precluded characterization of *Calanus finmarchicus* phenology at Rimouski station this year.

INTRODUCTION

The Atlantic Zone Monitoring Program (AZMP) was implemented in 1998 (Therriault et al. 1998) with the aim of (1) increasing Fisheries and Oceans Canada's (DFO) capacity to understand, describe, and forecast the state of the marine ecosystem and (2) quantifying the changes in the ocean's physical, chemical, and biological properties and the predator–prey relationships of marine resources. AZMP provides data to support the sound development of ocean activities. A critical element in the AZMP observational program is the annual assessment of the distribution and variability of nutrients and the plankton communities they support.

A description of the spatiotemporal distribution of dissolved oxygen, nutrients (nitrate, silicate, and phosphate), and chlorophyll a concentrations (chl a) provides important information on water-mass movements and on the location, timing, and magnitude of biological production cycles. A description of phytoplankton and zooplankton distributions provides important information on the organisms forming the base of the marine food web. Understanding plankton production cycles is essential for an ecosystem approach to fisheries management.

The AZMP derives its information on the state of the marine ecosystem from data collected at a network of sampling locations (high-frequency monitoring stations, cross-shelf sections) in each DFO region (Québec, Gulf, Maritimes, Newfoundland and Labrador; see Figure 1 for Québec region station locations) occupied at a frequency of weekly to once annually. The sampling design provides valuable information on the natural variability in physical, chemical, and biological properties of the Northwest Atlantic continental shelf: cross-shelf sections provide detailed geographic information but are limited in their seasonal coverage while strategically located high-frequency monitoring stations complement the sampling by providing more detailed information on seasonal-scale changes in ecosystem properties.

In this document, we review the chemical and biological oceanographic (lower trophic levels) conditions in the Gulf of St. Lawrence in 2020. Physical oceanographic conditions that prevailed in 2020 are described in Galbraith et al. (2021). The annual average freshwater discharge into the Estuary was above normal. The maximum volume of sea-ice was below normal, but the winter mixed layer volume was near normal. The May to November average sea-surface temperature was close to normal. The seasonally averaged minimum temperature of the cold intermediate layer (CIL) was near normal. Since 2009, deep-water temperatures (> 150 m) have been increasing overall in the Gulf, and new record highs were set at 200 m, 250 m, and 300 m in 2020. A strong mixing event occurred during September in the Estuary and northwestern Gulf. This report describes the 2020 production cycles and community composition of phytoplankton and zooplankton in the context of these physical conditions.

Due to the COVID-19 pandemic, there was no early summer oceanographic survey in the Gulf during 2020, and high-frequency monitoring stations were not sampled between early spring and July. Numerous changes were also incorporated into this year's report, including the extension of the climatology (now 1999–2020), the addition of late summer datasets collected during multidisciplinary surveys, and changes in the methods used to derive chl a estimates and spring bloom metrics from remote sensing.

METHODS

SAMPLE COLLECTION

All sample collection and processing steps meet the standards of the AZMP protocol (Mitchell et al. 2002). Field measurements included in this report were made along seven oceanographic

sections—along with stations located between these sections—during AZMP surveys carried out in winter, early summer, and fall (mainly in March, June, and November) of each year and at two high-frequency monitoring stations (Fig. 1). For the first time, field measurements made during multidisciplinary surveys (August and September; hereafter referred to as late summer surveys) and during the mackerel egg survey (June; zooplankton samples only) are included in our report for all years (2006–2020) for which these data are available. Sample collection during late summer surveys is a stratified random sampling strategy that is meant to cover all homogenous strata of the Gulf. During the mackerel egg survey, which mostly covers the Magdalen Shallows region, zooplankton samples are collected at 65 stations located on an equidistant grid. In this document, the seven sections as well as additional stations were grouped into four main regions for which biochemical indices will be presented (Fig. 2):

1. Estuary and northwestern Gulf: this region is generally deep (> 200 m) and cold in summer. It is strongly influenced by freshwater runoff from the St. Lawrence River and cold and dense waters from the Laurentian Channel;
2. Northeastern Gulf: this region, with deep channels and a relatively wide shelf (< 100 m), is characterized by high surface salinity and is influenced by the intrusion of water from the Labrador Shelf;
3. Central Gulf and Cabot Strait: this region is generally deep (> 200 m) and is directly influenced by a mixture of deep waters at the continental slope (warm North Atlantic Central Water that has a Gulf Stream signature and cold Labrador Current water) that enter the Gulf through Cabot Strait;
4. Magdalen Shallows: this region is shallow (< 100 m) and warm at the surface in summer. It is under the influence of the Gaspé Current.

These regions are slightly different than those used in previous reports and are meant to match the boxes used in the Gulf for the newly implemented DFO Ecosystem Approach to Fisheries Management. When sufficient data is available, biochemical indices are sometimes presented for region subdivisions (Fig. 1) to provide more details about spatial patterns. Since there are few biochemical data collected in Mecatina, Northumberland and Laurentien Hermitage (Fig. 1), indices will not be reported for these regions.

Table 1 provides details about the 2020 sampling surveys and Figures 2 and 3 summarize the sampling effort during the seasonal surveys and at the high-frequency monitoring stations, respectively. Rimouski station (depth 320 m) has been sampled since 1991—about weekly throughout the summer, once or twice a month in early spring and late fall, and rarely in winter (except during the winter survey) because of sea ice. It has been included in AZMP's annual review of environmental conditions since 2004 to represent conditions in the Estuary and northwestern Gulf. Since the beginning of AZMP, Shediac Valley station (depth 84 m) has represented conditions on the Magdalen Shallows and the Estuary outflow. However, sampling frequency at Shediac Valley station in good years is closer to monthly between May and November and decreases from January through April. Due to the COVID-19 pandemic, there was no early summer oceanographic campaign in the Gulf during 2020, and high-frequency monitoring stations were not sampled between mid-March and early July. Shediac Valley station was only visited on three occasions in 2020. Thus, while some results are presented for Shediac Valley, they are not discussed and annual anomalies were not calculated for Shediac Valley indices in 2020. In addition to the visits to high-frequency monitoring stations, Viking oceanographic buoys equipped with automatic temperature and salinity profilers carried out 212 full-depth casts at Shediac Valley station and 53 casts to 320 m at Rimouski station.

Sampling at oceanographic sections and high-frequency monitoring stations includes a CTD profile (temperature, salinity, fluorescence, dissolved oxygen) as well as water sampling using Niskin bottles (surface, 5 m, 15 m, 25 m, 50 m, 100 m, 200 m, 300 m, 400 m, bottom). Water from the Niskin bottles is collected for the analysis of dissolved oxygen (Winkler method), nutrients (Seal Analytical AutoAnalyzer 3 or Alpkem AutoAnalyzer), chl *a* (fluorometer), and phytoplankton enumeration (inverted microscopy) (Mitchell et al. 2002). Finally, mesozooplankton (< 1 cm) is sampled with bottom-to-surface vertical ring net tows (75 cm diameter, 200 µm mesh) for most of the surveys. During the mackerel egg survey, however, zooplankton sampling differs: the water column (surface to a maximum of 50 m) is sampled with 333 µm mesh bongo nets (61 cm diameter) using double oblique tows for a minimum of 10 min while cruising at ~2.5 kts (Ouellet 1987; Grégoire et al. 2014). A correction that accounts for the vertical distribution of mesozooplankton in the whole water column allows the estimation of their abundance in waters deeper than 50 m (Lehoux et al. 2020). Taxonomists are responsible for the identification, counts, and biomass measurements of zooplankton samples collected during regular AZMP surveys (early summer and fall surveys) whereas samples collected during the late summer multidisciplinary survey and during the mackerel egg survey are analyzed using a semi-automated procedure developed with the ZooImage 5.5.2 software package (Grosjean et al. 2018) following the methodology described in Plourde et al. (2019). Since methods are different and considering the larger size of net mesh used during the mackerel egg survey, large calanoid taxa indices developed with ZooImage analysis only include copepodite stages CIV – CVI and these data are not included in the annual anomaly estimates.

OXYGEN

Oxygen concentrations at 300 m are used as an indicator of hypoxic conditions in the Gulf. Oxygen concentration was measured using an oxygen probe (Sea-Bird SBE43) mounted on the CTD; the probe was calibrated against seawater samples collected and analyzed by Winkler titration on every cast (for the calibration procedure, see Sea-Bird application notes 61-1, -2, -3). Here, we present the mean annual distribution of deep oxygen in the Gulf derived from the CTD-mounted probe along with time series of annual concentrations of deep oxygen based on gridded (2 km x 2 km) inverse-distance-weighted interpolation.

NUTRIENTS AND PHYTOPLANKTON

Nutrient and chl *a* data collected along the AZMP sections and at the high-frequency monitoring stations were integrated over various depth intervals (i.e., 0–100 m for chl *a*; 0–50 m, 50–150 m, and 150 m–bottom for nutrients) using trapezoidal numerical integration. Chlorophyll *a* is used as a proxy for phytoplankton biomass. In 2016 and 2017, winter vertical profiles of nutrients were performed all over the Gulf and revealed that nitrate concentrations were relatively homogeneous in the upper 50 m of the water column during this season. Thus, for years when vertical nutrient profiles were not available, including 2020, integrated nitrate values for the winter survey were calculated using surface concentrations (2 m) × 50 m, assuming homogeneity of nitrate concentrations in the winter mixed layer.

In this document, detailed descriptions of the seasonal and interannual patterns are provided for different nutrient and phytoplankton indices. For the high-frequency monitoring stations, we present nitrate inventories in surface, mid, and deep water-column layers, chl *a* concentration, total phytoplankton abundance, and the relative abundance of its main taxa. Taxonomic identification of phytoplankton is performed for high-frequency monitoring stations only. The ratio between diatoms and flagellates or between diatoms and dinoflagellates can be used to provide information on the phytoplankton community size structure. In 2019 and 2020, samples from Shediac Valley were analyzed by a different taxonomist (same method), which led to a

large bias in flagellate counts. These counts were thus removed from anomaly calculations, although they may eventually be integrated into the time series once a reliable correction factor is found to relate the two taxonomists' counts. For the Gulf regions described above, time series of annual and/or seasonal inventories of nitrate, nutrient ratios (N:P and Si:N), and chl *a* integrated over different depth layers as well as their spatial distributions are presented. Spring nutrient drawdown was estimated using the difference between the March and June nitrate inventories (0–50 m) and is used as a proxy for phytoplankton spring production since sampling occurs after the spring bloom. Anomalies were computed for these indices (see Scorecards section below) for both high-frequency monitoring stations and Gulf regions.

SATELLITE REMOTE SENSING OF OCEAN COLOUR

Satellite ocean colour data provide large-scale images of surface phytoplankton biomass (chl *a*) over the Northwest Atlantic. We used daily satellite composite images for four ocean colour boxes (northwest Gulf, northeast Gulf, Magdalen Shallows, and Cabot Strait; see Fig. 4 for locations) to supplement our ship-based observations, especially regarding the spring bloom phenology, and to provide seasonal coverage and a large-scale context over which to interpret our survey data. However, since ocean colour imagery does not provide information on the dynamics that take place below the surface of the water column, it should be used as complementary information to the field data.

It should be noted that the ocean colour boxes have been revised in this report relative to previous ones to reduce the possible bias in chl *a* retrievals associated with coastal waters and freshwater input. All ocean colour boxes are located outside of the St. Lawrence River plume because satellite-based chl *a* estimates in this region are unreliable due to contamination by river inputs loaded with terrestrially derived coloured matter; boxes are not directly adjacent to the coast for the same reason. While knowledge on phytoplankton dynamics at the surface of the Estuary during spring is gathered using weekly sampling at Rimouski station, the temporal resolution is not always sufficient to allow calculations of the bloom metrics in the same statistical manner as the one discussed below. Thus, although spring bloom metrics are not presented for the Estuary, the seasonal and interannual variabilities of phytoplankton biomass are described.

Near-surface phytoplankton biomass has been estimated from ocean colour data collected by the Moderate Resolution Imaging Spectroradiometer (MODIS) "Aqua" sensor launched by NASA in July 2002 (4 km spatial resolution). In this report, MODIS data from 2003–2020 are used to construct a continuous time series of surface chl *a* in the four ocean colour boxes (Fig. 4). The continued calibration and data reprocessing done by NASA ensure data quality over the whole MODIS time series (Xiong et al. 2020). Previous reports used a combination of sensors (SeaWiFS, MODIS, VIIRS) to construct a time series starting in 1998. However, since the consistency between chl *a* estimates using these three sensors has not been compared in the waters of the Gulf, it was decided to use only one sensor to eliminate sensor bias over the time series.

Composite satellite images of remote sensing reflectance sourced from NASA's Goddard Space Flight Center were converted to chl *a* using an algorithm based on empirical orthogonal function (EOF) analysis (Laliberté et al. 2018). Daily chl *a* concentrations for pixel with minimal daily coverage of 20% were averaged over each ocean colour box and were extracted using the PhytoFit application v1.0.0 (Clay and Layton 2020). The timing (start and duration) of the spring phytoplankton bloom was defined using a symmetric shifted Gaussian function of time in days (Zhai et al. 2011) that was smoothed using a LOESS function (locally estimated scatterplot smoothing). While the start and duration of the spring bloom were derived from the smoothed Gaussian curve, the amplitude (maximum chl *a*) and magnitude (the integral of chl *a*

concentration under the Gaussian curve) of the spring bloom were calculated from the daily satellite-derived chl *a* within the spring bloom period rather than from the Gaussian curve. In addition, seasonal mean chl *a* biomass during spring (March to May), summer (June to August), and fall (September to November) as well as the annual average (March to November) were computed. For each of these metrics, we computed normalized annual anomalies (see Scorecards section below) to describe temporal trends for each ocean colour box. Note that January, February, and December were discarded due to lack of data (cloud, sea-ice cover, and low sun angles).

ZOOPLANKTON INDICES

We provide a detailed description of the seasonal patterns for different zooplankton indices, mostly at Rimouski (results for Shediac Valley in 2020 are presented but are not discussed nor were anomalies calculated) as well as for the Gulf regions described above. For the high-frequency monitoring stations, we present total mesozooplankton biomass (dry weight), total copepod abundance, and the relative abundances of the copepod species making up 95% of the total abundance. In addition, we include *Pseudocalanus* spp. (Rimouski station only) and *Calanus finmarchicus* abundances and stage composition. Because of its importance to the total zooplankton biomass in the Gulf, a detailed description of *Calanus hyperboreus* is provided for Rimouski and Shediac Valley stations. We also present the early summer and fall distribution and time series of total zooplankton biomass and total abundances of *C. finmarchicus*, *C. hyperboreus*, and *Pseudocalanus* spp. for the Gulf regions as well as similar indices (*C. finmarchicus*, *C. hyperboreus*, large calanoïds and small calanoïds) from the egg mackerel survey and the late summer survey (ZooImage). Since zooplankton samples are collected over the entire water column, zooplankton indices represent depth-integrated metrics.

We used the time series at Rimouski station to describe *C. finmarchicus* phenology and its changes through time because adequate sampling and stage identification started there more than 25 years ago (1994). However, sampling methodology has changed over time: from 1994 to 2004, prior to the use of AZMP standard nets (i.e., 75 cm diameter, 200 µm mesh bottom-to-surface ring net tows; Mitchell et al. 2002), *C. finmarchicus* copepodite stage abundance was determined using samples collected with 333 µm (CIV–CVI) and 73 µm (CI–III) mesh nets, towed from bottom to surface and from 50 m to surface, respectively. The 73 µm mesh nets were analyzed for only six years (1994, 1996–2000) of the time series (see Plourde et al. 2009 for details). In other years before 2004 for which 73 µm samples were not analyzed, the abundance of CI–III in the 333 µm samples was adjusted based on a comparison performed with a 158 µm mesh net (S. Plourde, DFO, Mont-Joli, QC; unpublished data). The phenology of *C. finmarchicus* was described using the following steps: (1) stage-relative abundances were normalized (proportion of a copepodite stage/maximum proportion for the stage) within each year for CI–III, CIV, CV, and CVI (male and female) and (2) stage proportions were smoothed using a LOESS function.

Finally, annual anomalies were computed for zooplankton biomass and for the abundance of several zooplankton indices that reflect either key copepod taxa, different functional groups, or groups of species indicative of cold- or warm-water intrusions and/or local temperature conditions specific to the Gulf (see Scorecards section below) for both high-frequency monitoring stations and Gulf regions. Only samples collected during regular AZMP surveys (early summer and fall) and analyzed by taxonomists were included in the calculation of regional zooplankton annual anomalies. A detailed list of species included in each large copepod index is presented in Appendix 1. Occasionally, taxonomists cannot distinguish *C. finmarchicus* from *C. glacialis* and record them in a common category. Since 2018, we use the results of a genetic study based on prosome length to distinguish these species (Parent et al. 2011).

SCORECARDS

Normalized anomalies for the chemical and biological indices presented in scorecards were computed for the high-frequency monitoring station and oceanographic regions. These anomalies are calculated as the difference between the variable's average for the season or for the complete year and the variable's average for the climatology (usually 1999–2020 unless otherwise noted); this number is then divided by the climatology's standard deviation. The 1999–2020 climatology represents a five-year extension to the climatology used in previous reports (1999–2015), which should increase stability over the time series and generally reduce the amplitude of the anomalies, painting a picture slightly different from those presented in previous reports.

Anomalies are presented as scorecards with positive anomalies depicted as shades of red, negatives as blues, and anomalies within ± 0.5 SD as white (considered as normal conditions, i.e., similar to the climatology). A standard set of indices representing anomalies of nitrate inventories, phytoplankton biomass and bloom dynamics, mesozooplankton biomass, and the abundance of dominant mesozooplankton species and groups (*C. finmarchicus, Pseudocalanus* spp., total copepods, and total non-copepods) are produced for each AZMP region. To visualize Northwest Atlantic shelf-scale patterns of environmental variation, a zonal scorecard including observations from all AZMP regions is presented in DFO 2021.

Annual nutrient, phytoplankton, and zooplankton index anomalies are based on the mean annual concentration (mmol m^{-2} for nutrients and mg chl a m^{-2} for phytoplankton biomass) or density (cells L^{-1} for phytoplankton abundance and ind m^{-2} for zooplankton abundance) estimated at each high-frequency monitoring station and each Gulf region. These annual estimates are the results of general linear models (GLM) of the form

$Log_{10}(Density+1) = \alpha + \beta_{YEAR} + \delta_{MONTH} + \varepsilon$ for the high-frequency monitoring stations and
$Log_{10}(Density+1) = \alpha + \beta_{YEAR} + \delta_{STATION} + \gamma_{SEASON} + \varepsilon$ for the regions,

as in Pepin et al. (2013) and Johnson et al. (2016); α is the intercept, and ε is the error. The GLM is applied to each region separately. For the high-frequency monitoring stations, β and δ are the categorical effects for year and month, respectively. For the regions, β, δ, and γ are the categorical effects of year, station, and season, respectively. Four seasons (winter, early summer, late summer, and fall) are included in the GLM estimating annual average of surface nutrient inventories; three seasons are used to estimate annual average of other nutrient and phytoplankton indices (sample collection during winter helicopter survey is limited to the collection of nutrient samples in the top layer); and two seasons are used to calculate annual estimates of zooplankton indices (samples analyzed via ZooImage are presented separately). The model's least-square mean based on type III sums of squares was used as the year average. Results of the GLM analysis for high-frequency monitoring stations and Gulf regions are presented in Appendices 2–6. We log-transformed concentrations and density values before computing anomalies to compensate for the skewed distribution of observations. One was added to the *Density* term to include observations with a value of zero.

OBSERVATIONS

PHYSICAL ENVIRONMENT

Water column temperature and salinity in 2020 are described in detail in Galbraith et al. (2021). Stratification is one of the key physical parameters controlling primary production. For this reason, we present the upper water column stratification at the high-frequency monitoring stations (Fig. 5). CTD vertical profiles are made during visits at the high-frequency monitoring

stations, but the vast majority of these data are from CTD vertical profiles autonomously collected from DFO Viking buoys. The large freshwater discharge into the Estuary during springtime (Galbraith et al. 2021) led to strong and above-normal stratification during May at Rimouski station, before returning to near-normal conditions. At Shediac Valley station, stratification stayed close to normal the whole year.

DEEP OXYGEN

In the Gulf, a dissolved oxygen value of 100 µM corresponds to approximately 30% saturation, below which the water is considered to be hypoxic and can reduce the survival of some species such as Atlantic cod (Plante et al. 1998). The lowest levels of dissolved oxygen (below 20% saturation in recent years) have been found in the deep waters at the head of the Laurentian Channel in the Estuary (Fig. 6). In 2020, concentrations of dissolved oxygen at 300 m were again well below normal everywhere along the Laurentian Channel (Fig. 6), reaching time-series record lows in the Estuary and at Rimouski station (Fig. 7). The deep waters of the Estuary have consistently been hypoxic since 1984 (Gilbert et al. 2005), and the dissolved oxygen concentration was 47 µM in 2020, corresponding to ca. 15% saturation (Fig. 7). In the northwest Gulf and Cabot Strait, deep dissolved oxygen concentrations were the second lowest of the time series, slightly above the 2019 record lows (Fig. 7).

NUTRIENTS AND PHYTOPLANKTON

Distributions of dissolved inorganic nutrients (nitrate, silicate, phosphate) strongly co-vary in space and time (Brickman and Petrie 2003). For this reason and because the availability of nitrogen controls phytoplankton growth in coastal waters of the Gulf, emphasis in this document is given to the variability in nitrate concentrations and inventories, even though the distributions of other nutrients are also briefly discussed. In this document, we use the terms “nitrate” or “total nitrate” to refer to nitrate+nitrite (NO_3^-+NO_2^-).

High-frequency monitoring stations

The main patterns of nitrate inventories and phytoplankton biomass for 2020 are illustrated in Figure 8 for both high-frequency monitoring stations. Detailed vertical profiles and anomaly patterns of nitrate and chl *a* in 2020 are shown in Figure 9 for Rimouski station along with vertical profiles in 2018 and 2019 to provide some context. Climatological nitrate and chl *a* concentrations are roughly two to three times higher at Rimouski station than at Shediac Valley station. The two stations typically exhibit a reduction in surface nitrate inventories in spring/summer mediated by phytoplankton consumption, a minimum during summer, and a subsequent increase during fall/winter once water column mixing intensifies due to cooling processes and wind forcing (Fig. 8a, b). However, the climatologies of chl *a* levels have distinct seasonal patterns at each station: it reaches its maximum during summer at Rimouski station (Fig. 8c) while maximum is reached in early spring before diminishing rapidly and staying stable for the remainder of the season at Shediac Valley station (Fig. 8d).

In 2020, Rimouski station nitrate inventories in the surface layer were generally close to or above normal for most of the year and associated with chl *a* inventories that were either close to or below normal, with the exception of three samples showing high phytoplankton biomass in early July and during October (Fig. 8a, c). Overall, the mean annual nitrate inventory was slightly above normal in the surface and mid layers, and close to normal in the deep layer. The annual average chl *a* inventory anomaly was normal (Fig. 8 scorecard). Most of the phytoplankton biomass was in the upper 15 m of the water column from July to September, where nitrate inventories were depleted (Fig. 9). The strong mixing event that occurred in

September (Galbraith et al. 2021) allowed replenishment of the nitrate inventory in the surface layer, which was followed by a subsurface (10–20 m) phytoplankton bloom in October (Fig. 9).

Phytoplankton abundances at Rimouski station were generally near normal during summer except for two samples collected in July that showed very high abundances, and then diminished to below normal abundances during fall (Fig. 10a). The seasonal phytoplankton community composition was similar to the climatology (Fig. 10b, c). The annual diatom average abundance showed a positive anomaly while dinoflagellates and ciliates had negative anomalies in 2020. Negative anomalies for dinoflagellates and positive anomalies of the diatom:dinoflagellate ratio have been observed since 2014 (Fig. 11).

Gulf regions

An overview of the seasonal spatial distributions of nitrate inventories and their anomalies in the Gulf is presented in Figures 12 to 14. Annual time series of regional anomalies for nitrate and nutrient ratios are presented in Figures 15 to 17. The distribution of nitrate in the surface layer during winter 2020 was similar to the climatology, with the inventory being above normal in the southern part of the Magdalen Shallows (Fig. 12). During late summer, nitrate anomalies were mostly below normal in the surface layer, close to normal in the mid-layer, and above normal in the deep layer of the northern Gulf and Estuary (Fig. 13). During fall, positive anomalies of nitrate were generally encountered in all regions and water column layers except in the surface layer of the northeast Gulf and Magdalen Shallows, where nitrate inventories were below normal (Fig. 14). Overall, annual nitrate anomalies in 2020 were either normal or positive in almost all regions and water column layers (Fig. 15). Since 2012, deep nitrate inventories have regularly shown positive annual anomalies in Cabot Strait and the central Gulf. Strong positive anomalies of deep nitrate inventories were also recorded throughout the Gulf in 2020 (Fig. 15). The Redfield-Brzezinski C:Si:N:P ratio, that supposes equilibrium between phytoplankton composition and deep ocean nutrient inventory, is 106:15:16:1 (Brzezinski 1985; Redfield 1958). In the deep waters of the Gulf, the N:P ratio is lower and typically ranges from 9.5 to 13.5 (Fig. 16) while Si:N ratio tends to be higher, ranging between 1 and 2.2 (Fig. 17). In 2020, the N:P ratio in the surface and mid layers was either close to or above normal in all regions, while it was generally close to or below normal in the deep layer (Fig. 16). The Si:N ratio showed the reverse pattern, with mostly negative anomalies in the surface and mid layers, and positive anomalies in the bottom layer (Fig. 17). Interestingly, the N:P ratio has mostly shown negative anomalies in the deep layer over the last five years, while Si:N ratio anomalies have mostly been positive. Moreover, there is a decrease in the climatological deep N:P ratio and an increase in the climatological deep Si:N ratio as water progresses up the deep channel from Cabot Strait through the Central Gulf and northwest Gulf to the Estuary (Figs. 16, 17).

Seasonal spatial distributions of phytoplankton biomass are presented in Figure 18 and their time series of regional anomalies are presented in Figure 19. In 2020, the seasonal phytoplankton biomass distribution was similar to that of the climatology, with noticeable positive anomalies north of Anticosti Island (northeastern Gulf) during late summer and in the Estuary during fall (Fig. 18). In both cases, it led to record high seasonal anomalies for these regions and seasons (Fig. 19). Smaller positive anomalies were also recorded in central Gulf during fall (Figs. 18, 19). Overall, annual average chl a inventories over the Gulf were quite heterogeneous. They were above normal in the Estuary, central Gulf, and on the Magdalen Shallows, while they were near normal in the northeastern Gulf and below normal in the northwestern Gulf and Cabot Strait (Fig. 19).

These large spatial patterns were somewhat mirrored by local conditions encountered at the high-frequency monitoring stations, with above-normal nitrate inventories at Rimouski station

and in the Estuary (Fig. 8). The sparse sampling at Shediac Valley prevents a proper comparison of its local conditions with those of the Magdalen Shallows region.

Remote sensing of ocean colour

Satellite imagery suggests that the spring phytoplankton bloom started in early April near Cabot Strait and on the Magdalen Shallows, where it continued until late April. In the northeastern and northwestern Gulf, the spring bloom started in the second half of April and continued until mid-May in the northwestern Gulf (Figs. 20, 21). Maximum chl *a* concentrations in the surface layer during spring averaged ca. 3 mg chl *a* m^{-3} over the gulf and were close to or higher than the climatology (Fig. 20). A look at surface chl *a* distribution during fall suggests that negative anomalies were widely distributed over the Gulf and were stronger during the second half of fall (Fig. 22). Spring bloom metrics were mostly close to normal in all regions, with amplitude and magnitude showing small positive anomalies on the Magdalen Shallows and in Cabot Strait (Fig. 23). Overall, phytoplankton biomass during spring was similar to the climatology average in all four ocean colour boxes (Fig. 23). However, it was generally below normal during summer and fall, reaching record lows in the northeastern Gulf and Cabot Strait during fall (Fig. 23). The strong mixing event that created the record-high chl *a* anomaly in the Estuary during fall (Fig. 19) was hardly seen from satellite imagery (only small positive anomalies in October; Fig. 22), but the vertical structure of phytoplankton biomass at Rimouski station over the same period suggests that it was a subsurface bloom (Fig. 9). Mean annual surface chl *a* was below normal in all ocean colour boxes except for Cabot Strait, where it was close to normal (Fig. 23).

These observations contrast somewhat with in situ observations considering that many regions showed positive chl *a* anomalies (Fig. 19). These diverging patterns could be caused by the vertical structure of phytoplankton in the water column, as indicated for the subsurface fall bloom in the Estuary. Moreover, the seasonal anomalies derived from satellites are calculated for three-month periods while our at-sea sampling is generally completed within a few days, so these different time frames might also explain divergences between in situ and remote sensing data. In addition, bias in remote sensing data during fall due to higher cloud cover as well as the influence field sampling timing can have on annual anomalies of phytoplankton indexes could also account for some of the discrepancies between satellite and field data.

ZOOPLANKTON

High-frequency monitoring stations

In 2020, the zooplankton biomass at Rimouski station followed the monthly climatology, with near-normal values for most of the period covered by sampling (Fig. 24a). At Shediac Valley, however, the two samples indicated that zooplankton biomass was below normal (Fig. 24b). Total copepod abundances were close to normal during summer and below normal during fall at Rimouski station, and the composition of the copepod community was highly similar to the climatology (Fig. 25) Copepod abundance and community composition at Shediac Valley were similar to normal during the limited occupations (Fig.26).

Calanus finmarchicus abundances at Rimouski station in 2020 were close to the climatology, but the proportion of early copepodite stages (CI–CIII) was somewhat reduced compared with the climatology (Fig. 27). This could be explained by the late start of sampling this year, which possibly occurred after the *C. finmarchicus* CI–CIII peak. The proportion of early copepodite stages was high compared with climatology for the two samples collected at Shediac Valley (Fig. 27). At Rimouski station, *Calanus hyperboreus* abundances were below normal during summer and close to normal afterwards, with a copepodite assemblage similar to the climatology (Fig. 28). The stable stage composition of the population from July onward indicates

that an equivalent proportion of individuals went into diapause at stage CIV and CV, which is similar to the climatology (Fig. 28b, c). At Shediac Valley, *C. hyperboreus* individuals were retrieved in only one sample out of two and they were exclusively CIV copepodite stage (Fig. 28f). Finally, *Pseudocalanus* spp. abundances were mostly below normal at Rimouski station. The copepodite assemblage was also similar to the climatology despite the very low contribution of early stages during October and November and a contribution of this group almost twice as high as for the climatology in December (Fig. 29).

Gulf regions

Seasonal distribution and time series of zooplankton biomass and key taxa abundances are shown in Figures 30 to 34. During fall 2020, Gulf zooplankton biomass was largely concentrated in the deep channels of the Estuary and the northwestern Gulf region (zooplankton biomass is very low on coastal portion of sections), and of central Gulf and Cabot Strait, where a higher abundance of *C. hyperboreus* occurred (Figs. 30, 32). Zooplankton biomass during fall was close to normal in most regions except in central Gulf/Cabot Strait, where it was below normal (Fig. 30). Similarly, the mean regional abundance of *C. hyperboreus* during fall was slightly below normal in that region as well, but above normal in the Estuary/northwestern Gulf and close to normal elsewhere (Fig. 32). The abundance of *C. finmarchicus* during fall was more similar among regions, and its regional averages were highly similar to regional climatologies (Fig. 31). The highest abundances of *Pseudocalanus* spp. were recorded on the Magdalen Shallows during fall 2020 but were largely below normal in that region; this was the case in other regions as well, but to a lesser extent (Fig. 33). Time series of zooplankton indices from the northern Gulf late summer survey also show similar findings with large calanoid indices—including *C. finmarchicus* and *C. hyperboreus*—being either close to or above normal. Small calanoid abundance was also above normal in northern Gulf at that time (Fig. 34).

Copepod phenology

Changes in the timing of zooplankton development were described using the detailed seasonal pattern of the relative copepodite stage abundances of *C. finmarchicus* at Rimouski station from 1994 to 2020 (Fig. 35). A scorecard showing the anomaly of the first and last day when the normalized proportion of CI–CIII copepodite stages was higher than 0.3 (visually defining early stage peaks in most cases) was also added to provide an objective tool to determine *C. finmarchicus* phenology. Unfortunately, the absence of sampling prior to July does not allow an adequate characterization of *C. finmarchicus* phenology at Rimouski station in 2020. Overall, there is a trend towards earlier population development, with negative anomalies in the “First day” index strengthening in recent years. The positive anomalies of the “Last day” index from 2010 to 2014 are associated with a second pulse of early stages in late summer. However, in recent years—likely including 2020—the negative anomalies of this index are mostly associated with single and long-lasting pulses of CI–CIII copepodite stages. The large proportion of adults (CVI) in August is likely a bias due to the normalization of copepodite proportions and the absence of sampling prior to July, when the maximum proportion of adults is normally observed (Fig. 35).

Scorecards

The time series of annual zooplankton biomass anomalies highlights recent major changes in the community, with mostly negative anomalies across the Gulf since 2009 (Fig. 36). In 2020, zooplankton biomass anomalies were close to normal across the Gulf except in the central Gulf/Cabot Strait region, where it was below normal (Fig. 36). A synthesis of standard AZMP zooplankton indices (abundances of *C. finmarchicus*, *Pseudocalanus* spp., total copepods, non-

copepods) was performed using annual normalized abundance anomalies and is presented as a scorecard (Fig. 37). *Calanus finmarchicus* anomalies were close to normal in 2020 in all Gulf regions whereas *Pseudocalanus* spp. did not show any regional positive anomaly for the first time since 2012. A record low of *Pseudocalanus* spp. abundance was even observed in the Magdalen Shallows region. However, this record low must be interpreted carefully considering the absence of sampling in June, when *Pseudocalanus* spp. typically shows its highest abundance (Fig. 33). Considering the large contribution of this taxa to the total copepod abundance, the widespread negative anomalies of this latter index in 2020 is not surprising and is also a first since 2013. After several years of widespread positive anomalies, non-copepod anomalies were mostly close to normal throughout the Gulf in 2020. Only the northeastern Gulf region showed a positive anomaly of non copepods (Fig. 37).

The annual normalized abundance anomalies for six additional zooplankton indices (*C. hyperboreus* and five zooplankton groups: small calanoids, large calanoids, cyclopoids, warm-water species, and cold/arctic species) are presented in Figure 38. A detailed list of species included in each of these indices is presented in Appendix 1. *Calanus hyperboreus* abundance was above normal in the Estuary/northwestern Gulf, below normal on the Magdalen Shallows during 2020, and normal elsewhere. However, since the abundance of *C. hyperboreus* in these regions in early summer is quite variable and considering that there was no sampling done in June, these annual anomalies are mostly representative of *C. hyperboreus* abundance during fall. While overall there has been a decline in large calanoid abundance and an increase in small calanoid abundance since 2009 (Fig. 38), these two groups showed near-normal anomalies across the Gulf in 2020. There was only a small negative anomaly of large calanoids in the central Gulf/Cabot Strait region. Annual abundances of cyclopoids were below normal in most regions in 2020. Warm-water-associated copepods is another group that has seen its abundance increasing since about 2010. This was generally true again in 2020, even though the positive anomalies were relatively weak in most regions. The exception is on the Magdalen Shallows, where the abundance of *Paracalanus* spp. was at a record high and the abundance of *Centropages* spp. was among the highest recorded over the time series (data not shown). Cold-water-associated copepods showed heterogeneous anomaly patterns, with positive anomalies at Rimouski station and in the Estuary/northwestern Gulf, near-normal abundances in northeastern Gulf and on the Magdalen Shallows, and a negative anomaly in central Gulf/Cabot Strait—a first since 2004. These annual anomalies were relatively coherent among the high-frequency monitoring stations and their associated Gulf region (Figs. 36, 37, 38).

DISCUSSION

Despite the absence of sampling during early summer 2020, no change was made to our GLM analysis for the estimation of annual index averages. However, to provide an estimate of the bias associated with the missing sampling season for variables showing strong seasonality (i.e., nutrients and chl *a* concentrations, zooplankton biomass and abundances), comparisons of real annual anomalies with annual anomalies estimated from truncated datasets (removing data collected during early summer prior to the GLM analysis) were performed for each year of the time series. The anomaly bias, in terms of the difference between real and truncated annual anomalies, was relatively small for nutrient and chl *a* estimates (ca. ± 0.25 SD) but was larger for zooplankton indices (ca. 50% of the comparisons would have a bias of ± 0.5 SD and a bias between ± 0.5 SD and ± 1.5 SD for the remaining 50%). Annual anomalies of nutrients and chl *a* depend on the collection of samples during three or four seasons whereas annual anomalies of zooplankton indices are estimated only from two field seasons, likely explaining the difference in the bias obtained for these groups of indices. In any case, one must keep in mind that variables showing strong seasonality must be interpreted carefully when a sampling season is missing.

ENVIRONMENTAL CONDITIONS

The timing of the onset and extent of water column stratification plays a role in defining spring bloom phenology, phytoplankton production, species succession, and trophic interactions over the complete growth season (Levasseur et al. 1984). In 2020, the timing of upper water column stratification and strength of stratification was very similar to the climatology except in May at Rimouski station, where high freshwater inflows from the St. Lawrence River led to stronger stratification than normal. In addition to the effect of water column stratification on phytoplankton dynamics, thermal properties of the surface, intermediate, and deep water masses play a role in defining zooplankton dynamics (Plourde et al. 2002). Galbraith et al. (2021) reported on the physical conditions that prevailed in the Gulf during 2020, showing near-normal conditions in the surface layer and the cold intermediate layer (CIL), and warm conditions in deep waters. This document reports on the chemical and biological conditions in the Gulf in the context of these conditions.

Changes in dissolved oxygen of the deep waters entering the Gulf at the continental shelf are related to the varying proportions of Labrador Current water (cold/fresh, high dissolved oxygen levels) and slope water (warm/salty, low dissolved oxygen levels), which together form the source of Gulf deep water (McLellan 1957, Lauzier and Trites 1958, Gilbert et al. 2005). These waters travel from the mouth of the Laurentian Channel to the Estuary in roughly three to four years (Gilbert 2004), decreasing in dissolved oxygen because of in situ respiration and oxidation of organic material by microbes as they progress to the channel heads. Based on interdecadal variability, the inflow of warmer waters to the Estuary is expected to exacerbate the hypoxic conditions since these waters are typically poor in dissolved oxygen (McLellan 1957, Lauzier and Trites 1958, Gilbert et al. 2005). Given the inherent properties of Gulf source waters (North Atlantic Central Water vs Labrador Current water; Gilbert et al. 2005), changes in their mixing ratio at Cabot Strait imply that a decrease of 1.46 µM might be expected for each 0.1°C temperature increase. However, today's deep oxygen concentrations at Cabot Strait represent a drop of 90 µM compared with their concentrations in the early 1970s (data not shown), for a 1.98°C increase in temperature over the same period (Fig. 46 in Galbraith et al. 2021). In the St. Lawrence Estuary, temperature of the deep-water layer is well correlated with deep oxygen concentration over the time series ($r = -0.84$), and water temperature has increased by 1.63°C at 300 m between the early 1970s and 2020 (Fig. 46 in Galbraith et al. 2021). Based on the mixing ratio of source waters, this should translate into a decrease in dissolved oxygen of 24 µM in the Estuary over the same period, but the decrease has exceeded 50 µM. Thus, warming of bottom water and changes in the mixing ratio of source waters are not the only factors contributing to the decrease in oxygen concentrations in the Gulf. Other factors that can cause variability in oxygen concentration include interannual changes in the vertical flux of organic matter and microbial metabolic processes of the bottom waters of the Lower St. Lawrence Estuary.

Winter mixing is a critical process for bringing nutrient-rich deep water to the surface. In the Gulf, winter convection is partly caused by buoyancy loss of surface waters attributable to cooling and reduced freshwater runoff, brine rejection associated with sea-ice formation, and wind-driven mixing prior to ice formation (Galbraith 2006). Warmer-than-normal surface waters throughout the winter and minimal sea-ice formation imply low winter convection and may reduce the amount of nutrients available for spring primary production. The CIL represents the winter surface mixed layer that has been insulated from the atmosphere by near-surface stratification and whose nutrient inventory will supply primary producers during the growth season through vertical mixing. In 2020, the CIL temperature and winter mixed-layer volume suggest that winter convection was near normal, and nutrient content was indeed close to normal during winter. Despite generally near-normal nitrate inventories in the surface layer in

2020, negative nitrate anomalies in the surface layer have been regularly encountered in the Gulf since 2010, a period over which several temperature and ice-cover indices have shown clear warming of the Gulf (Galbraith et al. 2021). Surface layer nitrate time series suggest a diminution of 25 to 40% of the nutrient content in all regions but the Estuary and northwestern Gulf over the past 20 years. Seasonal linear regressions revealed that this decrease is not only attributable to a specific season, but that it is significant ($p < 0.01$) over all seasons but late summer. Interestingly, the N:P ratio in the surface layer diminishes in the same regions over the time series, but its diminution is only significant during fall (linear regression; $p < 0.001$). Thus, low winter convection and strengthening of the stratification in association with global warming could have limited the nutrient flux to the surface layer nitrate, but the significant change in the N:P ratio during fall suggests that a change in biological activity likely accounts for some part of the reduced nitrate content during this season.

Positive anomalies in deep-water (300 m) nitrates have been regularly observed since 2012 in the central Gulf and Cabot Strait in association with high temperature/high salinity water intrusions into the Gulf from Cabot Strait (Galbraith et al. 2021). These higher-than-average deep inventories are associated with a water mass composition that has a greater contribution of slope water than Labrador Shelf water, intensifying the effect of a shallower thermocline that reduces exchanges between the upper and bottom layers (Galbraith et al. 2021 and references therein). For the first time in the past five years, a positive deep nitrate anomaly was also observed in the Estuary. This could indicate that waters with a larger proportion of slope water have reached the Estuary, as suggested by bottom water temperature in the Estuary (Galbraith et al. 2021). The recent change in deep water nutrient ratios suggests that despite a rise in nitrate content of the deep layer, the regeneration of nitrate does not seem to occur at the same pace as other nutrients, which could eventually lead to nitrate limitation of primary production. The change in nutrient ratio as water progresses from Cabot Strait to the Estuary also supports this hypothesis of differential nutrient regeneration time. This could be the result of changes in the nitrogen cycle due to microbial activity, such as decreased nitrification or increased denitrification associated with low oxygen concentrations. The routine measurement of NH_4 concentrations has recently been added to AZMP sampling in the Gulf and will eventually be helpful in verifying this latter hypothesis. Moreover, the ongoing modelling of processes involved in the nitrogen cycle in the Gulf (Diane Lavoie, DFO, Mont-Joli, QC) will allow a detailed understanding of key processes involved in nitrate distribution.

PHYTOPLANKTON

Except at Rimouski station, where sampling regularly covers the spring bloom period, phytoplankton production during the spring bloom must be inferred either from indirect indices, such as the difference in the nutrient inventory of the surface mixed layer between the winter and the early summer surveys, or from satellite observations. Unfortunately, nutrient drawdown during spring could not be estimated in 2020. However, bloom metrics derived from satellite imagery revealed that timing, duration, and intensity of the spring bloom were all close to normal over the Gulf in 2020, in accordance with near-normal spring chl a concentration in the surface layer. No distinct trends in bloom metrics can be identified over the time series. Under global warming scenarios, an earlier onset of stratification is expected to trigger an early spring bloom. However, the expected concomitant large freshet (due to an increase in precipitation) may prevent the accumulation of phytoplankton biomass in the water column in regions under the influence of freshwater, which may instead delay detection of bloom start in these regions. Densities of overwintering copepods, which have been generally low in the gulf for the 2016–2018 period (low annual biomass) in association with a higher proportion of long-lasting and intense blooms, will also impact spring bloom intensity (Sommer and Lengfellner 2008) and the determination of bloom metrics from remote sensing. Together, these key players will largely

influence bloom metrics and likely account for the large interannual variability seen in these metrics.

For all other seasons, ocean colour data is complemented by field data. These two datasets have regularly offered different conclusions in terms of anomalies of the seasonal phytoplankton biomass. This was the case again in 2020, even though major changes were made to the analysis of ocean colour data, including the use of an improved algorithm for retrieval of chl a in coastal waters of the Gulf (Laliberté et al. 2018). Possible causes of discrepancies between methods were presented in the results (Remote sensing section). Among the recurrent differences is the observation of below-normal chl a concentrations in the thin surface layer during fall while field data have regularly suggested positive phytoplankton biomass anomalies in recent years. Removing the effect of the fall survey timing by selecting only field data collected within a two-week period (27 Oct–6 Nov), linear regressions suggest that the increase in phytoplankton biomass during fall is significant over the time series on the Magdalen Shallows ($p = 0.019$) and in central Gulf/Cabot Strait ($p < 0.001$), and almost significant in the northeast Gulf ($p = 0.076$). It corresponds to an increase of fall phytoplankton biomass of roughly 65% when comparing the beginning and the end of the time series. An increased occurrence of fall storms, as observed during the last two years (Galbraith et al. 2020, 2021), may favour ideal growth conditions for phytoplankton, especially if combined with a reduction of grazing pressure due to the diminution of grazer biomass and changes in their community composition, and may explain the diminution of N:P ratio overtime.

ZOOPLANKTON

Zooplankton biomass has generally been below normal in recent years, with record lows in 2016–2017. This has resulted in a significant ($p < 0.0001$) biomass decrease over the time series, representing a biomass loss of about 15% over the time series in the northwestern and northeastern Gulf and 40% on the Magdalen Shallows and in the central Gulf/Cabot Strait. Lower biomass is typically associated with a decrease in the abundance of large-sized zooplankton species. The mean weight of large-sized calanoids (e.g., *C. hyperboreus*: 3.5 mg per adult female) is between one and two orders of magnitude greater than that of small-sized calanoids (e.g., *Pseudocalanus* spp.: 0.02 mg per adult female) (Conover and Huntley 1991, Plourde et al. 2003). Thus, the decrease in large calanoid abundance has a greater impact on zooplankton biomass than, for instance, the increase of *Pseudocalanus* spp. abundance that has been regularly recorded over recent years. The increase in small calanoids seems to be coupled with an increase in non-copepod abundance, mostly larvae of benthic organisms. Suitability of environmental conditions, competition for food, the availability of large vs small phytoplankton cells, and/or differential predation pressure might favour the dominance of either one of these communities, i.e., one dominated by large calanoids versus one dominated by a combination of small calanoids and non-copepods (Hall et al. 1976; Daewel et al. 2014), with potential implications for the pelagic food web and pelago–benthic coupling. In 2020, results indicate a return to normal conditions for most zooplankton indices, including its biomass and its size structure. *Pseudocalanus* spp., total copepod, and cyclopoid abundances have all showed mostly positive anomalies since 2014, but their anomalies were negative in 2020. Annual indices in 2020 were only derived from fall samples, which certainly altered our interpretation of these results, as discussed previously. However, near-normal thermal properties of the surface layer and CIL combined with the on-time spring bloom start likely led to a zooplankton community that would also have shown close-to-normal indices during early summer. This is especially likely when considering the relatively long lifetime of zooplankton individuals (in comparison with phytoplankton), suggesting that the fall zooplankton community is generally representative of the early summer community.

Life cycle strategies vary among large copepod species and the timing of reproduction relative to the freshet—considering its influence on water-mass circulation and transport—could explain dissimilarities in the distribution patterns of these species (Runge et al. 1999) in regions that are under the influence of freshwater, for instance the positive anomaly of *C. hyperboreus* in northwestern Gulf in 2020 and its negative anomaly on the Magdalen Shallows. The northeastern Gulf and the central Gulf/Cabot Strait regions are less influenced by freshwater; environmental conditions modifying the zooplankton community in these regions might instead include CIL conditions or the mixing ratio of source waters that enters the deep Laurentian Chanel through Cabot Strait. Differences in these environmental drivers might explain why these two regions often show distinct anomaly patterns for the zooplankton assemblage compared to what is observed elsewhere. However, anomaly patterns in 2020 were particularly coherent among regions.

PERSPECTIVES

Questions that may arise from these indications of changes in nutrient inventories, phytoplankton biomass, and zooplankton community composition and size structure are related to the underlying explanatory drivers and what is to be expected in the near future. While the roles of predation and of changing predator stocks in the observed trends have yet to be determined, it is possible to get some insight regarding the effect of environmental variables using a simple correlation matrix (Fig. 39). Among other things, this matrix shows that a cold CIL—which would imply higher winter convection and a later onset of stratification—promotes a late bloom start and high nitrate inventories. Interestingly, high nitrate inventories in the surface layer are well correlated with higher zooplankton biomass and a community dominated by large copepods rather than the combination of small calanoids and non-copepods. While nutrients likely have little direct effect on the zooplankton community composition, thermal properties of the CIL and spring bloom—especially its timing—could be major drivers of zooplankton assemblage. Indeed, it seems that a cold CIL favours high zooplankton biomass (dry weight; negative correlation) while it reduces the abundance of non-copepods (positive correlation). Phytoplankton community composition and changes in specie succession may also be important drivers for the zooplankton assemblage but they were not included in this correlation matrix since information is only available at the high-frequency monitoring stations. These environmental drivers may also trigger changes in the developmental timing of zooplankton taxa (not illustrated on the figure), such as the earlier development of *C. finmarchicus* at Rimouski station in recent years. Overall, these preliminary analysis highlights the importance of bottom-up controls in shaping zooplankton communities, although the relative importance of these processes is not yet well understood.

SUMMARY

This document reports on the chemical and biological (plankton) conditions in the Gulf in 2020 in the context of a strong warming event initiated in 2010. Data from 2020 are compared to time-series observations.

- Concentrations of dissolved oxygen at 300 m reached record lows in the Estuary and at Rimouski station. In the northwestern Gulf and Cabot Strait, deep dissolved oxygen concentrations were the second lowest of the time series, slightly above the 2019 record lows.
- Nitrate inventories were generally near or above normal in all water column layers and Gulf regions. Positive deep nitrate anomalies have been frequently observed since 2012 in Cabot Strait and the central Gulf, and are associated with intrusions of high temperature/high salinity water into the Gulf through Cabot Strait.
- The recent rise in nitrate content of the bottom layer is mostly associated with negative anomalies of the N:P ratio and positive anomalies of the Si:N ratio.
- Annual averages of in situ chl a inventory over the Gulf were heterogeneous: anomalies were positive in the Estuary, central Gulf, and on the Magdalen Shallows; near normal in the northeastern Gulf; and below normal in the northwestern Gulf and Cabot Strait. Strong blooms occurred during late summer in the northeastern Gulf and during fall in the Estuary.
- Ocean colour data showed negative annual surface chl *a* anomalies in most ocean colour boxes over the last three years, including 2020. Spring bloom metrics were mostly near normal in 2020 except for high bloom amplitude and magnitude in the Magdalen Shallows and Cabot Strait boxes.
- The phytoplankton community was similar to the climatology community at Rimouski station, but dinoflagellate abundance has declined since 2014.
- After a few years of below-normal zooplankton biomass accompanied by changes in the proportion of large and small copepods, most zooplankton indices—including biomass and size structure—returned to near-normal conditions in 2020.
- Zooplankton indices that did not show a return to normal include abundances of *Pseudocalanus* spp. and total copepods, which mostly showed negative anomalies—a first since 2013, and warm-water-associated copepod abundances, which were again above the climatology, similar to what has been observed since 2010.
- The cancelled early summer sampling campaign made it impossible to describe the entire phenology of *C. finmarchicus* at Rimouski station. Sampling from July suggests that there was only one long-lasting peak of early copepodite stages (CI–III).

ACKNOWLEDGEMENTS

We thank Jean-Yves Couture, Marie-France Beaulieu, Caroline Lebel, Isabelle St-Pierre, and Caroline Lafleur for preparation and standardization of the phytoplankton and zooplankton data. The data used in this report would not be available without the work of François Villeneuve and his AZMP team (Rémi Desmarais, Marie-Lyne Dubé, Line McLaughlin, Roger Pigeon, Michel Rousseau, Félix St-Pierre, Liliane St-Amand, Sonia Michaud, David Leblanc, Marie-Noëlle Bourassa, Brian Boivin, and Caroline Lafleur) in organizing and carrying out AZMP surveys, analyzing samples, and ensuring quality control of the data. We thank Jeff Spry and Kevin Pauley for providing data from Shediac Valley station and Lindsay Beazley and her team, who collected samples at Cabot Strait during DFO/Maritimes Region's fall mission. We also thank NASA Ocean Biology Processing Group for the raw satellite data. We are grateful to Catherine Johnson and Gary Maillet for their critical reviews.

REFERENCES CITED

Brickman, D., and Petrie, B. 2003. Nitrate, silicate and phosphate atlas for the Gulf of St. Lawrence. Can. Tech. Rep. Hydrogr. Ocean Sci. 231: xi + 152 pp.

Brzezinski, M. A. 1985. The Si:C:N ratio of marine diatoms: interspecific variability and the effect of some environmental variables. J. Phycol. 21: 347-357.

Clay, S., and Layton, C. BIO-RSG/PhytoFit: First release (Version v1.0.0).

Conover, R. J., and Huntley, M. 1991. Copepods in ice-covered seas - Distribution, adaptations to seasonally limited food, metabolism, growth patterns and life cycle strategies in polar seas. J. Mar. Syst. 2: 1–41.

Daewel, U., Hjøllo, S.S., Huret, M., Ji, R., Maar, M., Niiranen, S., Travers-Trolet, M., Peck, M.A., and van de Wolfshaar, K. E. 2014. Predation control of zooplankton dynamics: a review of observations and models. ICES J. Mar. Sci. 71(2): 254–271.

DFO. 2021. Oceanographic conditions in the Atlantic zone in 2020. DFO Can. Sci. Advis. Sec. Sci. Advis. Rep. 2021/026.

Galbraith, P. S. 2006. Winter water masses in the Gulf of St. Lawrence. J. Geophys. Res. 111, C06022, doi: 10.1029/2005JC003159.

Galbraith, P.S., Chassé, J., Shaw, J.-L., Dumas, J., Caverhill, C., Lefaivre, D., and Lafleur, C. 2020. Physical oceanographic conditions in the Gulf of St. Lawrence during 2019. DFO Can. Sci. Advis. Sec. Res. Doc. 2020/030. iv + 81 p.

Galbraith, P.S., Chassé, J., Shaw, J.-L., Dumas, J., Caverhill, C., Lefaivre, D., and Lafleur, C. 2021. Physical oceanographic conditions in the Gulf of St. Lawrence during 2020. DFO Can. Sci. Advis. Sec. Res. Doc. 2021/045. iv + 81 p.

Gilbert, D. 2004. Propagation of temperature signals from the northwest Atlantic continental shelf edge into the Laurentian Channel. ICES CM, 2004/N: 7, 12 pp.

Gilbert, D., Sundby, B., Gobeil, C., Mucci, A., and Tremblay, G.-H. 2005. A seventy-two-year record of diminishing deep-water oxygen in the St. Lawrence estuary: The Northwest Atlantic connection. Limnol. Oceanogr., 50(5): 1654–1666.

Grégoire, F., Girard, L. and Boudreau, M. 2014. Résultats des relevés du programme de monitorage zonal atlantique (PMZA)-maquereau bleu (*Scomber scombrus* L.) réalisés dans le sud du golfe du Saint-Laurent en 2012 et 2013. Secr. can. de consult. sci. du MPO. Doc. de rech. 2014/075. v + 82 p.

Grosjean, P., Denis K., and Wacquet G. 2018. ZooImage: Analysis of Numerical Plankton Images. R package version 5.5.2.

Hall, D.J., Threlkeld, S.T., Burns, C.W., and Crowley, P.H. 1976. The size-efficiency hypothesis and the size structure of zooplankton communities. Ann. Rev. Ecol. Evol. Syst. 7: 177–208.

Johnson, C., Casault, B., Head, E., and Spry, J. 2016. Optical, chemical, and biological oceanographic conditions on the Scotian Shelf and in the Eastern Gulf of Maine in 2014. DFO Can. Sci. Advis. Sec. Res. Doc. 2016/003. v + 51 p.

Laliberté, J., Larouche, P., Devred, E., and Craig, S. 2018. Chlorophyll-a concentration retrieval in the optically complex waters of the St. Lawrence Estuary and Gulf using principal component analysis. Remote Sens. 10, 265, doi: 10.3390/rs10020265.

Lauzier, L.M., and Trites, R.W. 1958. The deep waters of the Laurentian Channel. J. Fish. Res. Board Can. 15: 1247–1257.

Lehoux, C., Plourde S., and Lesage, V. 2020. Significance of dominant zooplankton species to the North Atlantic Right Whale potential foraging habitats in the Gulf of St. Lawrence: a bio-energetic approach. DFO Can. Sci. Advis. Sec. Res. Doc. 2020/033. iv + 44 p.

Levasseur, M., Therriault, J.-C., and Legendre, L. 1984. Hierarchical control of phytoplankton succession by physical factors. Mar. Ecol. Prog. Ser. 19: 211–222.

McLellan, H.J. 1957. On the distinctness and origin of the slope water off the Scotian Shelf and its easterly flow south of the Grand Banks. J. Fish. Res. Board Can. 14: 213–239.

Mitchell, M. R., Harrison, G., Pauley, K., Gagné, A., Maillet, G., and Strain, P. 2002. Atlantic Zonal Monitoring Program sampling protocol. Can. Tech. Rep. Hydrogr. Ocean Sci. 223: iv + 23 pp.

Ouellet, P. 1987. Distribution automnale des stades larvaires de capelan (*Mallotus villosus*) et de hareng (*Clupea harengus*) dans le nord du golfe Saint-Laurent en Octobre 1985. Rapp. tech. Can. sci. halieut. aquat. 1583: 27 p.

Parent, G.J., Plourde, S., and Turgeon, J. 2011. Overlapping size ranges of *Calanus* spp. off the Canadian Arctic and Atlantic coasts: impact on species' abundances. J. Plankton Res. 33: 1654–1665.

Pepin, P., Maillet, G., Fraser, S., Shears, T., and Redmond, G. 2013. Optical, chemical, and biological oceanographic conditions on the Newfoundland and Labrador Shelf during 2011-12. DFO Can. Sci. Advis. Sec. Res. Doc. 2013/051. v + 38 p.

Plante, S., Chabot, D., and Dutil, J.-D. 1998. Hypoxia tolerance in Atlantic cod. J. Fish Biol. 53: 1342–1356.

Plourde, S., Dodson, J. J., Runge, J. A., and Therriault, J.-C. 2002. Spatial and temporal variations in copepod community structure in the lower St. Lawrence Estuary, Canada. Mar. Ecol. Prog. Ser. 230: 221–224.

Plourde, S., Joly, P., Runge, J.A., Dodson, J., and Zakardjian B. 2003. Life cycle of *Calanus hyperboreus* in the lower St. Lawrence Estuary and its relationship to local environmental conditions. Mar. Ecol. Prog. Ser. 255: 219–233.

Plourde, S., Maps, F., and Joly, P. 2009. Mortality and survival in early stages control recruitment in *Calanus finmarchicus*. J. Plankton Res. 31(4): 371–388.

Plourde, S., Lehoux, C., Johnson, C. L., Perrin, G., and Lesage, V. 2019. North Atlantic right whale (*Eubalaena glacialis*) and its food: (I) a spatial climatology of *Calanus* biomass and potential foraging habitats in Canadian waters. J. Plankton Res. 41(5): 667–685.

Redfield A. C. 1958. The biological control of chemical factors in the environment. Am. Sci. 46, 205–221.

Runge, J. A., Castonguay, M., de Lafontaine, Y., Ringuette, M., and Beaulieu, J. L. 1999. Covariation of climate, zooplankton biomass and mackerel recruitment in the southern Gulf of St. Lawrence. Fish. Oceanogr. 8(2): 139–149.

Sommer, U., and Lengfellner, K. 2008. Climate change and the timing, magnitude, and composition of the phytoplankton spring bloom. Global Change Biol. 14: 1199–1208.

Therriault, J.-C., Petrie, B., Pépin, P., Gagnon, J., Gregory, D., Helbig, J., Herman, A., Lefaivre, D., Mitchell, M., Pelchat, B., Runge, J., and Sameoto, D. 1998. Proposal for a Northwest Atlantic zonal monitoring program. Can. Tech. Rep. Hydrogr. Ocean Sci. 194: vii + 57 pp.

Xiong, X., Angal, A., Chang, T., Chiang, K., Lei, N., Li, Y., Sun, J., Twedt, K., and Wu, A. 2020. MODIS and VIIRS calibration and characterization in support of producing long-term high-quality data products. Remote Sensing. 12:3167; doi:10.3390/rs12193167

Zhai, L., Platt, T., Tang, C., Sathyendranath, S., and Hernández Walls, R. 2011. Phytoplankton phenology on the Scotian Shelf. ICES J. Mar. Sci. 68: 781–791, doi:10.1093/icesjms/fsq175.

TABLES

Table 1. List of oceanographic surveys with locations, dates, and sampling activities for 2020 in each Gulf region. See Figure 1 for section station locations. While numbers of CTD/bottle are indicated for each region and their subdivision, numbers of nets are only indicated for main regions.

	Station/Region	Dates (2020)	Vessel	CTD/bottle	Net
High-frequency monitoring stations	Rimouski	6 Jan – 9 Dec	Beluga II (+ others)	23	21
	Shediac Valley	11 March; 31 July; 20 Oct	Multiple	3	2
Winter Survey	Estuary	2 – 15 March	GC-945 Helicopter	6	0
	Northwest Gulf			9	
	Northeast Gulf			22	0
	Central Gulf			9	0
	Cabot Strait			7	
	Magdalen Shallows			31	0
Total				**84**	**0**
Early summer survey	Estuary	No sampling		0	0
	Northwest Gulf			0	
	Northeast Gulf			0	0
	Central Gulf			0	0
	Cabot Strait			0	
	Magdalen Shallows			0	0
Total				**0**	**0**
Late summer survey	Estuary	13 Aug – 29 Sept	Teleost	10	10
	Northwest Gulf			4	
	Northeast Gulf			7	7
	Central Gulf			17	11
	Cabot Strait			4	
	Magdalen Shallows			42	1
Total				**84**	**29**
Fall Survey	Estuary	13 – 30 Oct	Hudson	17	15
	Northwest Gulf			14	
	Northeast Gulf			13	7
	Central Gulf			11	7
	Cabot Strait			5	
	Magdalen Shallows			13	12
Total				**73**	**41**

FIGURES

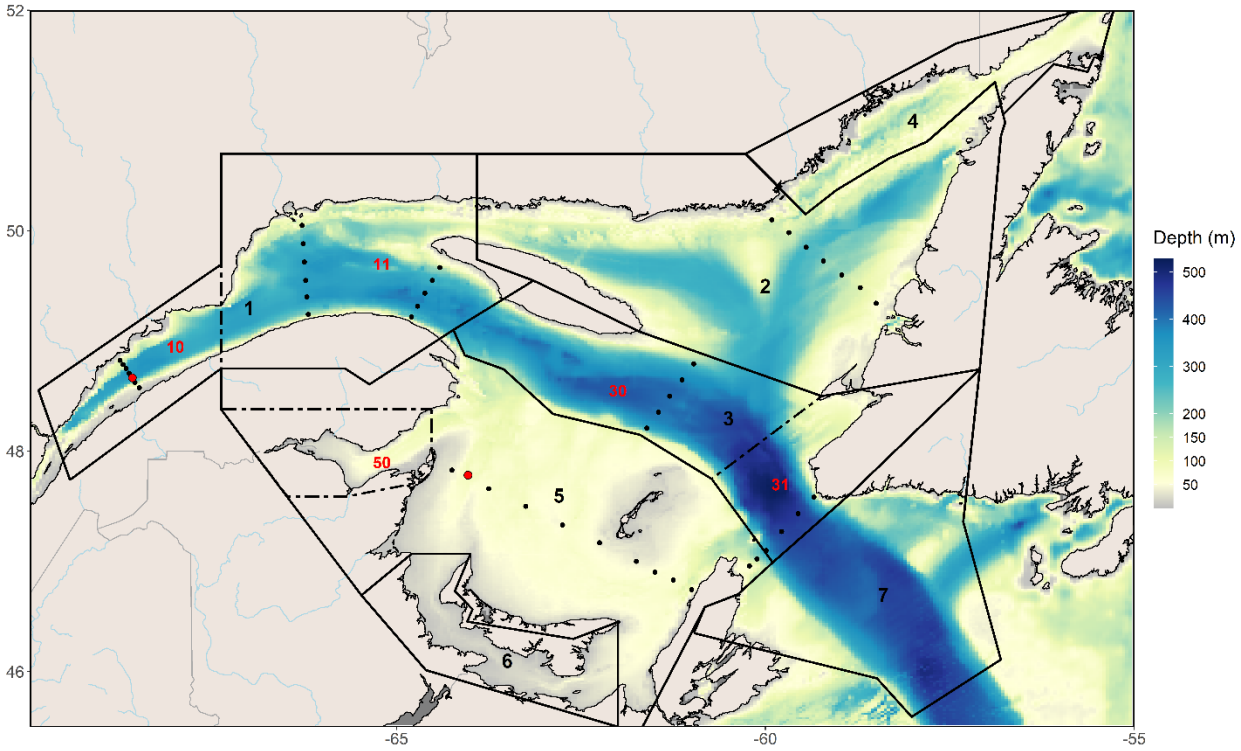

Figure 1. Bathymetric map of the Estuary and Gulf of St. Lawrence showing regular core AZMP sampling stations on the different sections (dots) and high-frequency Rimouski and Shediac Valley stations (red circles). Box 1: Estuary (subdivision 10) and northwest Gulf (subdivision 11); Box 2: northeast Gulf; Box 3: central Gulf (subdivision 30) and Cabot Strait (subdivision 31); Box 4: Mecatina; Box 5: Magdalen Shallows; Box 6: Northumberland; Box 7: Laurentien Hermitage.

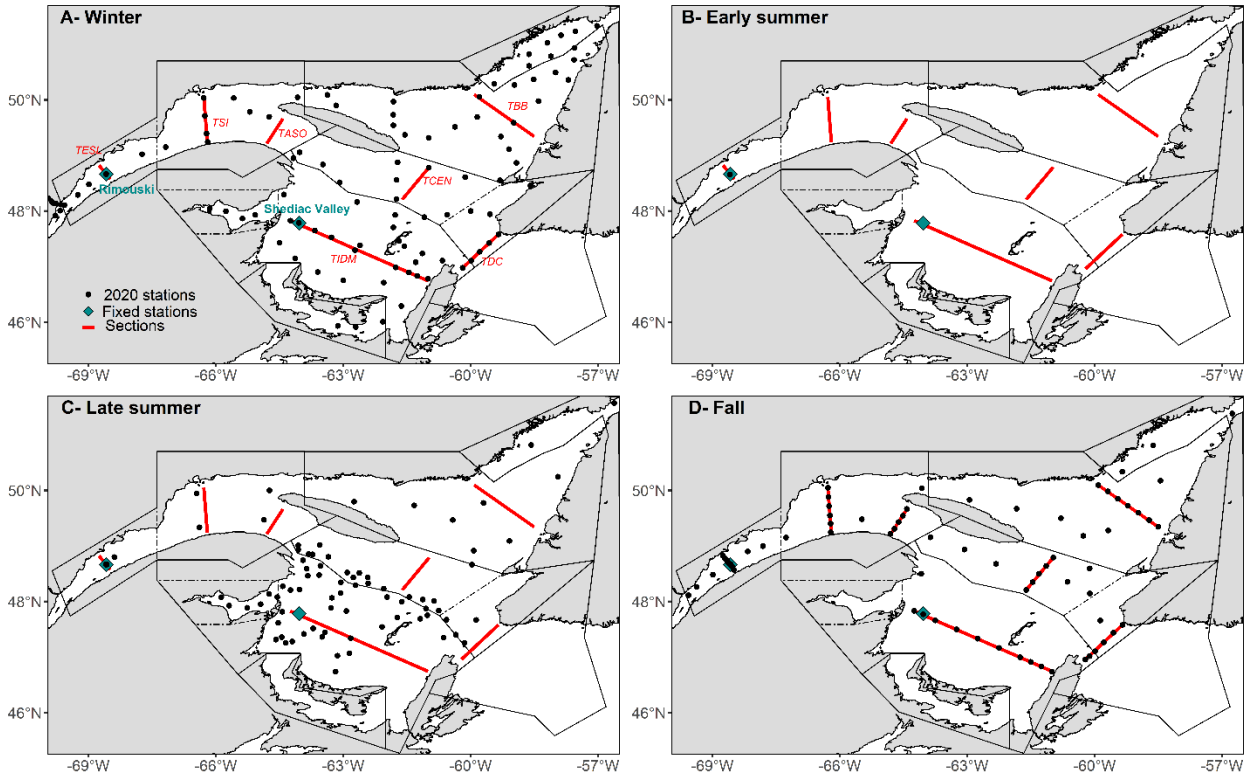

Figure 2. Locations of stations sampled during winter (A), early summer (B), late summer (C),and fall (D) 2020 (see Figure 1 caption for box descriptions).

Figure 3. Sampling frequencies at Rimouski and Shediac Valley stations through 2020. Sampling included CTD/bottle as well as plankton net tows most of the time (weather permitting).

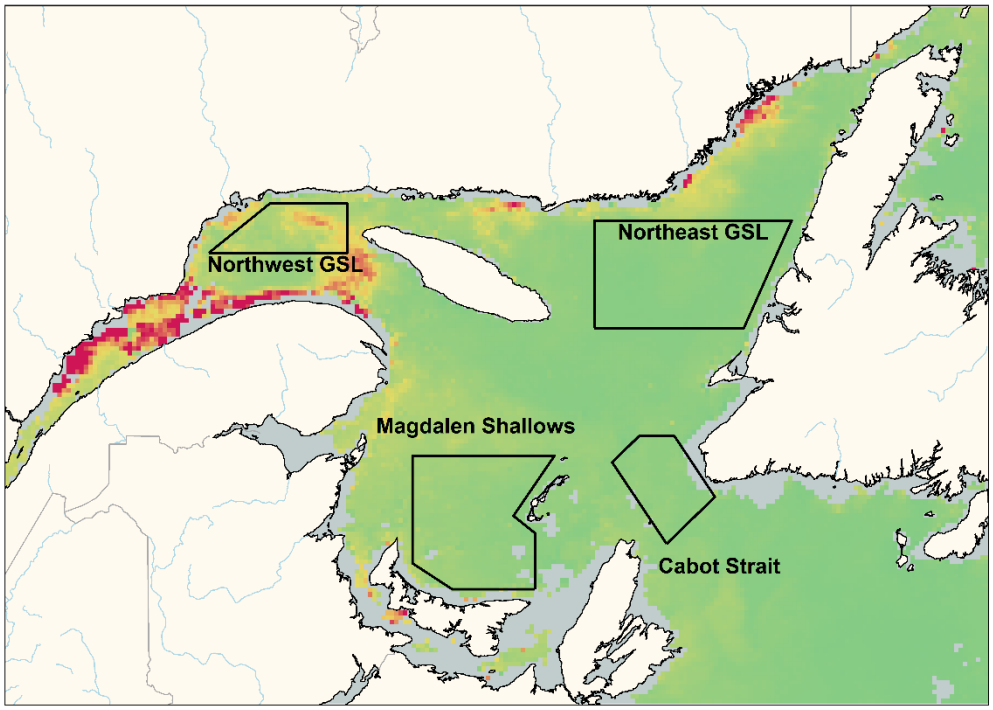

Figure 4. Statistical boxes in the Gulf identified for the spatial/temporal analysis of satellite ocean colour data. The figure is a MODIS composite image showing chlorophyll a from 1–15 June 2020. Grey areas indicate no data (near-shore regions in this case).

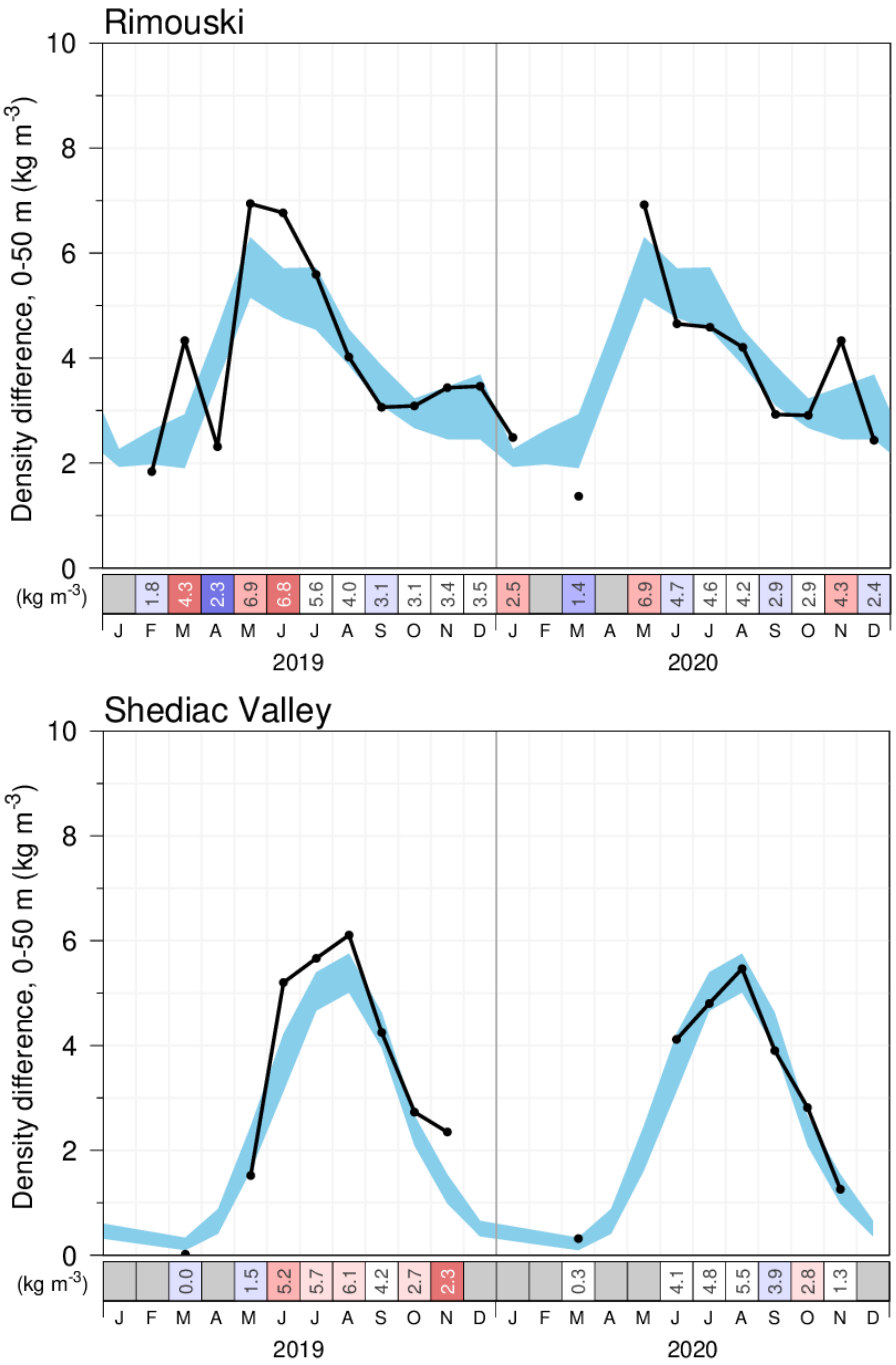

Figure 5. Seasonal stratification index (calculated as the density difference between 50 m and the surface; black solid line) during 2019 and 2020 at Rimouski station (upper panel) and at Shediac Valley station (lower panel). These data come from CTD vertical profiles made during visits at the high-frequency monitoring stations, but the majority of profiles were autonomously collected by CTDs on DFO Viking buoys. The blue area represents the climatological monthly mean ± 0.5 SD (1999–2020). The positive anomalies are shown in red and correspond to low surface salinity and strong stratification. Numbers in the scorecard are monthly density differences in kg m^{-3}.

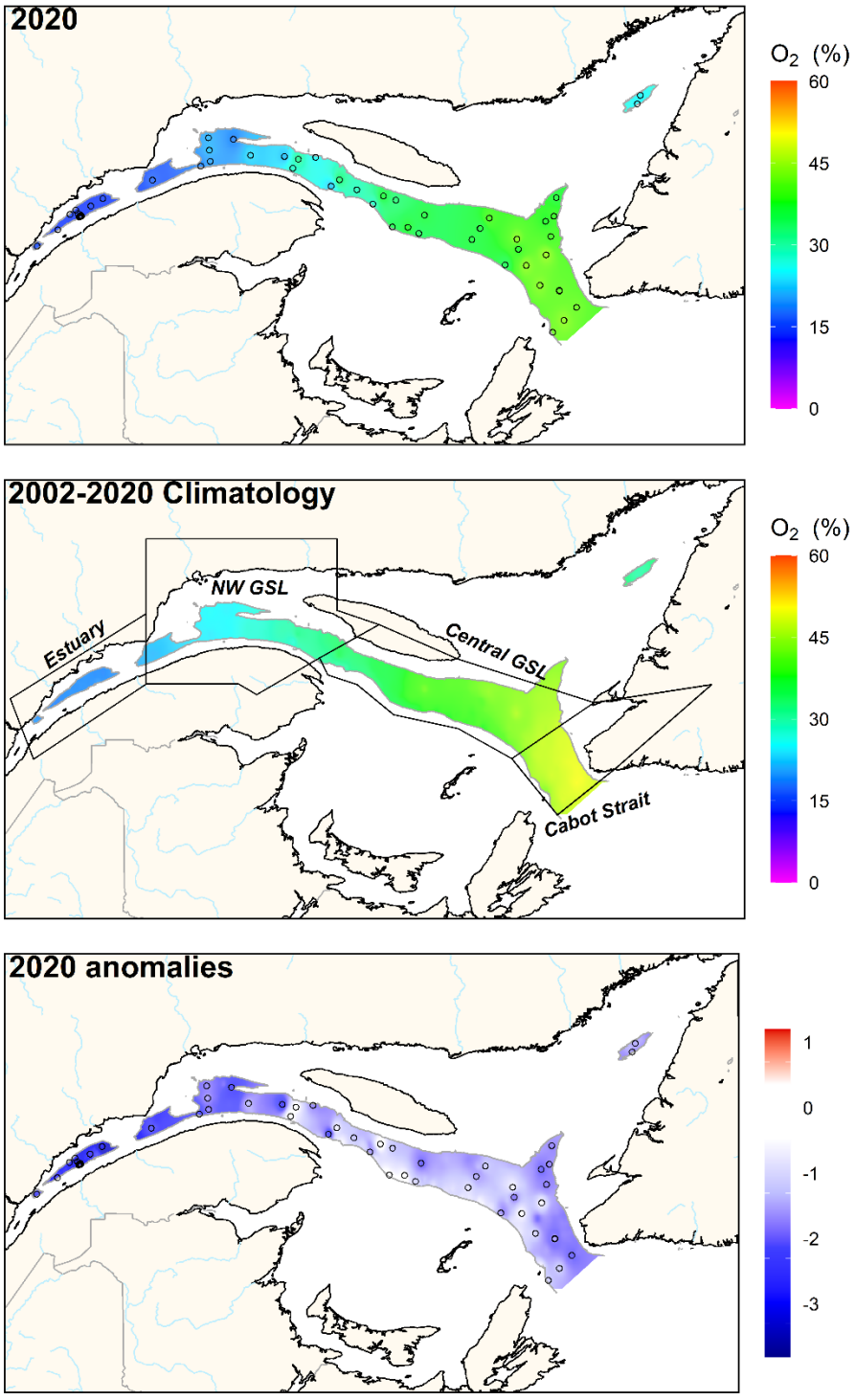

Figure 6. Annual average distribution of dissolved oxygen saturation at a depth of 300 m in the Estuary and Gulf of St. Lawrence during 2020 (upper panel). The climatology (2002–2020; middle panel) and anomalies (lower panel) are also shown. Blue colours indicate anomalies below the mean, reds are anomalies above the mean, and white represents normal conditions. Polygons in the middle panel are used to calculate regional anomalies. Open circles represent station locations in 2020.

Dissolved oxygen concentrations (µM) at 300m

	2002	2003	2004	2005	2006	2007	2008	2009	2010	2011	2012	2013	2014	2015	2016	2017	2018	2019	2020	Mean	SD
Rimouski	64.1	58.7	62	64.1	67.6	65	63.5	65.9	60.7	67.5	64.7	67	60.6	58.5	56.6	55.6	57.5	51.8	45.8	60.9	5.7
Estuary	65.4	59.4	63.6	65.9	68.4	67.2	64.3	67.4	62.2	68.7	66.6	68.6	63.4	60	57.8	57.7	58.4	52.5	46.8	62.3	5.9
Northwest Gulf	89	77.9	87.1	88.2	90.4	92	79	85.1	90.6	105	94	90.6	82.3	90.7	71.9	77.2	72.2	67.4	67.6	84.1	9.9
Central Gulf	152.8	116	148	162.9	152.4	158.8	137.7	152.6	154.3	162.6	150.5	153.9	143.9	140.6	128.8	126.4	123.7	118.4	121.5	142.4	15.5
Cabot Strait	125.9	109.7	123.2	127.9	133.7	126.8	115.6	133.2	130.7	139.1	135.8	132.8	129.6	127.7	113.6	109.3	103.8	101.3	102.5	122.2	12.2

Figure 7. Time series of deep-layer dissolved oxygen concentration (µM). The numbers on the right are the 2002–2020 climatological means and standard deviations, and the numbers in the boxes are the oxygen concentrations. Cell colour represents the anomaly: blue colours indicate anomalies below the mean, reds are anomalies above the mean, and white represents normal conditions.

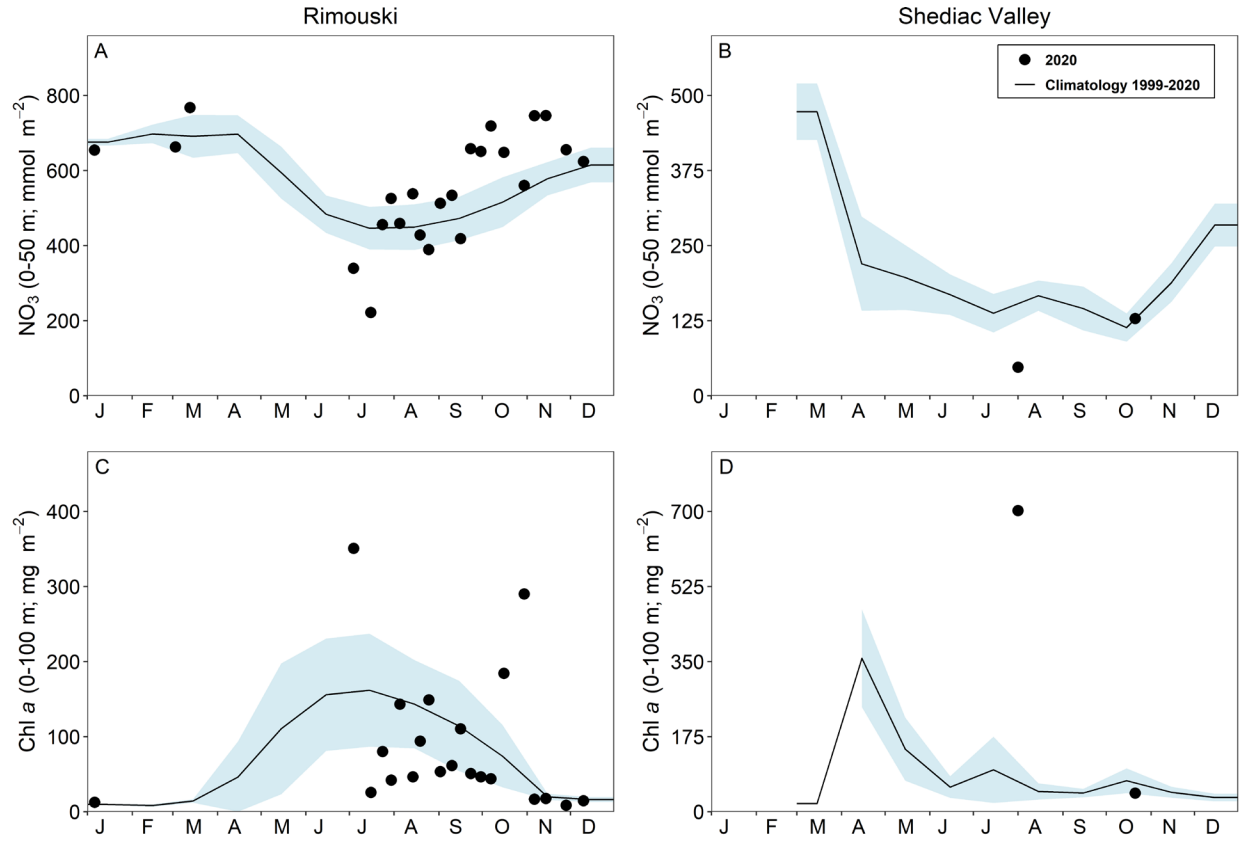

Rimouski

	1999	2000	2001	2002	2003	2004	2005	2006	2007	2008	2009	2010	2011	2012	2013	2014	2015	2016	2017	2018	2019	2020	Mean	SD
Chl *a* 0-100m	2.43	-0.79	0.71	-0.12	0.76	-1.58	-1.04	-1.01	0.61	-2.21	-0.33	-0.07	-0.09	0.35	-0.51	1.28	0.18	0.63	-0.4	0.42	0.77	0.03	34.3	17.1
NO_3 0-50m	-0.23	1.08	0.53	1.88	-0.31	1.36	-0.26	0.02	-0.4	0.8	-1.64	-2.15	-0.83	-0.57	0.42	0.76	0.7	-1.27	0.24	-1.17	0.47	0.58	570.1	73.8
NO_3 50-150m	-1.28	-0.41	0.98	1.32	-0.63	-0.16	-0.37	1.09	1.29	-0.38	0.18	-1.68	-1.23	0.19	-0.66	0.98	0.61	0.34	-0.3	-2.02	1.36	0.78	1432.8	106.5
NO_3 150-320m	2.85	-0.67	-1	0.47	0.14	0.1	1.14	1.5	0.45	-1.16	0.18	-1.49	-0.55	-0.24	-0.25	0.66	0.45	-0.79	-0.87	-1.19	0.05	0.19	3851.2	138.6

Shediac Valley

	1999	2000	2001	2002	2003	2004	2005	2006	2007	2008	2009	2010	2011	2012	2013	2014	2015	2016	2017	2018	2019	2020	Mean	SD
Chl *a* 0-100m	-1.02	-1.44	-0.14	2.48	0.18	-0.21	-0.7	-0.04	1.57	1.52	-0.05	-0.73	-1.2	0.36	0.54	-0.34	-0.4	-0.95	1.24	-0.51	-0.15		50	15.8
NO_3 0-50m	0.78	1.68	-0.04	0.59	0.68	0.93	-0.86	0.68	-2.01	-0.09	1.14	-1.94	-1.13	0.05	0.18	0.54	0	-0.16	0.92	-1.35	-0.57		173.1	43.3
NO_3 50-84m	-0.15	0.28	0.79	0.46	0.51	-0.2	-2.12	0.94	-1.72	-0.13	-0.24	-0.45	-0.17	0.69	0.76	-0.81	1.09	0.58	0.93	-2.18	1.14		225.5	40.3
	1999	2000	2001	2002	2003	2004	2005	2006	2007	2008	2009	2010	2011	2012	2013	2014	2015	2016	2017	2018	2019	2020	Mean	SD

Figure 8. Nitrate inventories (0–50 m; top panels) and phytoplankton biomass (0–100 m for Rimouski and 0–84 m for Shediac Valley; bottom panels) in 2020 (black circles) with monthly mean conditions (± 0.5 SD) for the 1999–2020 climatology (black line with blue shading) at Rimouski and Shediac Valley stations. During the March helicopter survey, no chl a sample are collected. The nutrient sample collected in March 2020 at Shediac Valley was lost. Time series of normalized annual anomalies for nitrate inventories (mmol m^{-2}) and phytoplankton biomass (mg chl a m^{-2}) are also presented with the variable means and standard deviations for the 1999–2020 climatology to the right of the scorecard. Blue colours indicate anomalies below the mean, reds are anomalies above the mean, and white represents normal conditions.

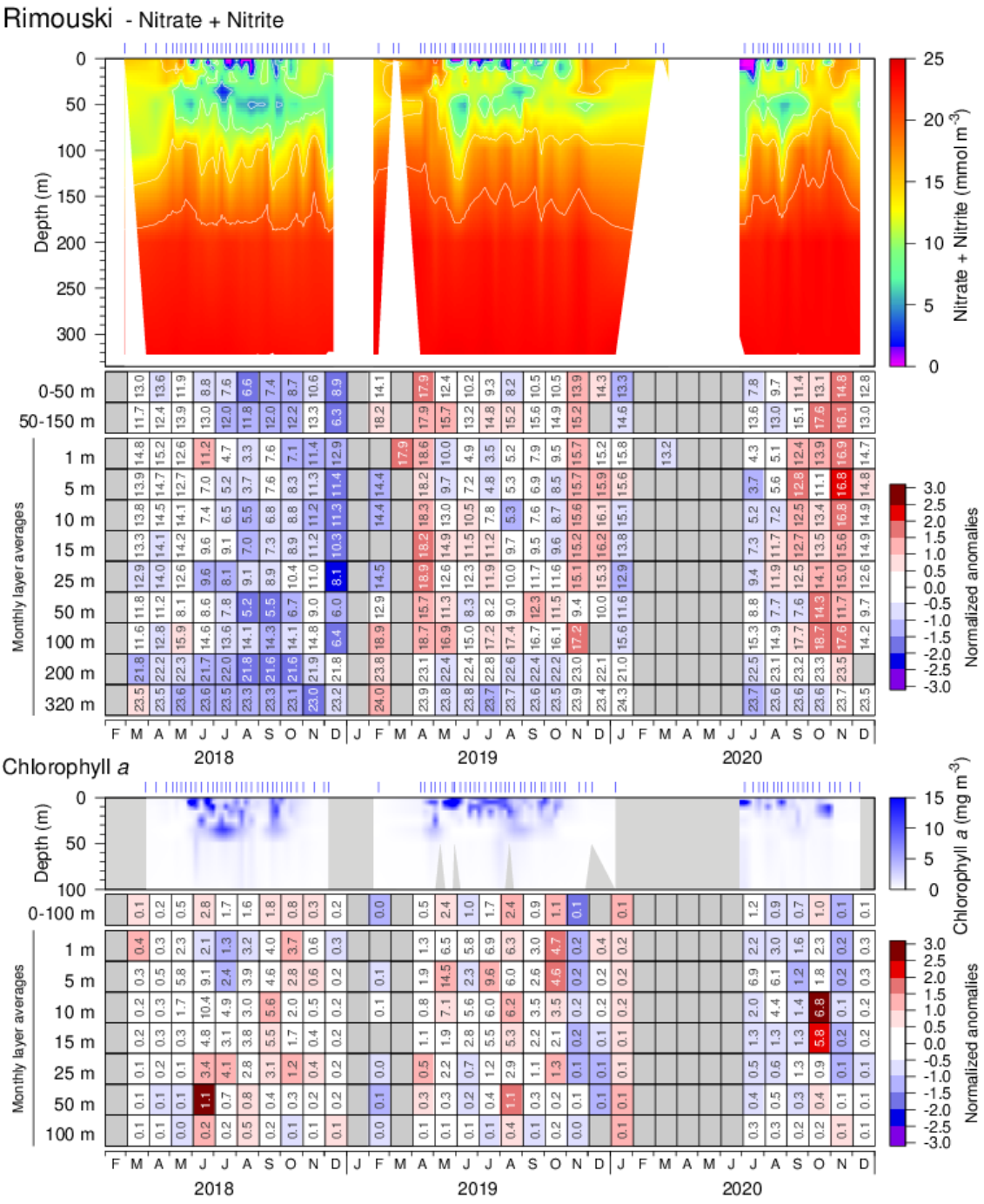

Figure 9. Nitrate (top) and chlorophyll a (bottom) concentrations at Rimouski station during the 2018 to 2020 sampling seasons. Contour plots use data from individual sorties while monthly means are shown in the tables below the graphics (nitrates: mmol m^{-3}; chl a: mg m^{-3}). Cell colours indicate normalized anomalies based on the 1999–2020 climatology: blue colours indicate anomalies below the mean, reds are anomalies above the mean, and white represents normal conditions. During March, the integrated (0–50) monthly average and the depth-specific average for nitrate for the climatology do not include the same amount of data, and this might result in inconsistent anomalies between integrated and depth-specific values.

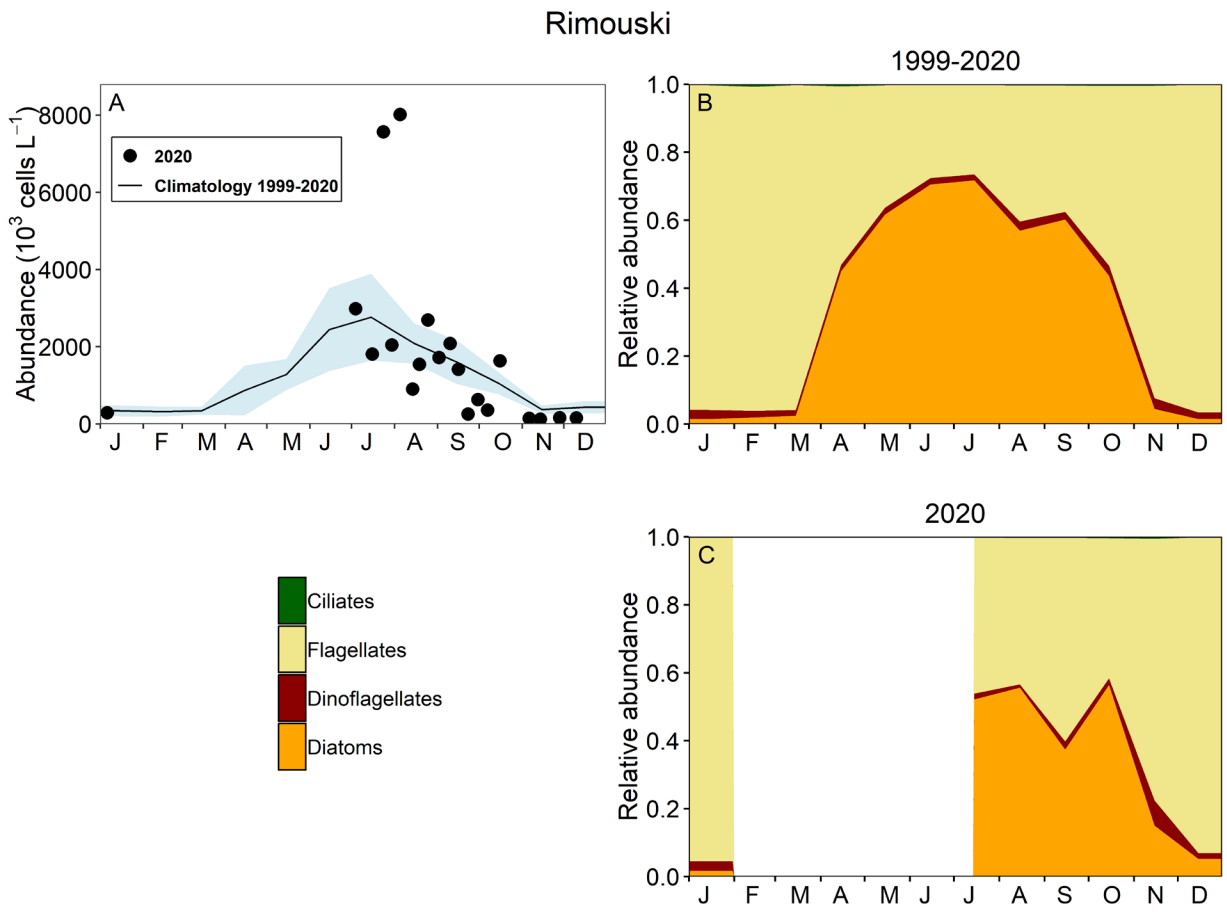

Figure 10. Phytoplankton abundance (A) and community composition at Rimouski station for the 1999–2020 climatology (B; no data in 2010) and for 2020 (C). Blue shading on panel (A) represents ± 0.5 SD of the monthly mean phytoplankton abundance for the climatology. Ciliates can hardly been seen on this figure since this group represents < 1% of phytoplankton cells each month for the climatology. It was also the case in 2020.

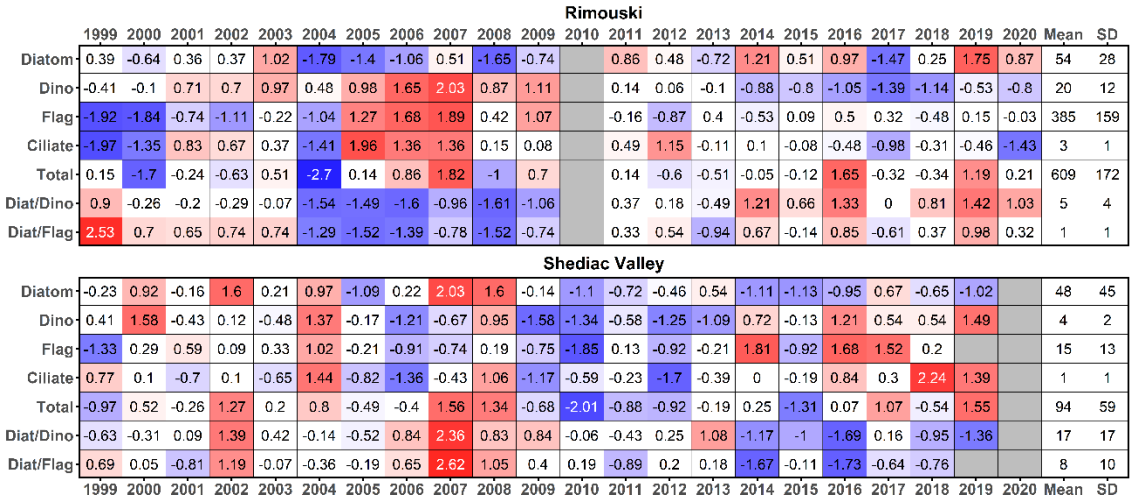

Figure 11. Time series of normalized annual (April–December) anomalies for abundance (10^3 cells L^{-1}) of the main phytoplankton taxonomic groups (diatoms, dinoflagellates, flagellates, ciliates) and total microphytoplankton, and for the diatom/dinoflagellate and diatom/flagellate ratios at Rimouski and Shediac Valley stations (calculated using GLM). Variable means and standard deviations for the 1999–2020 climatology are shown to the right of the scorecard. Blue colours indicate anomalies below the mean, reds are anomalies above the mean, and white represents normal conditions. No data are available for 2010 at Rimouski station. In 2019 and 2020, samples from Shediac Valley were analyzed by a different taxonomist; this led to a large bias in flagellate counts, so these counts were removed from anomaly calculations.

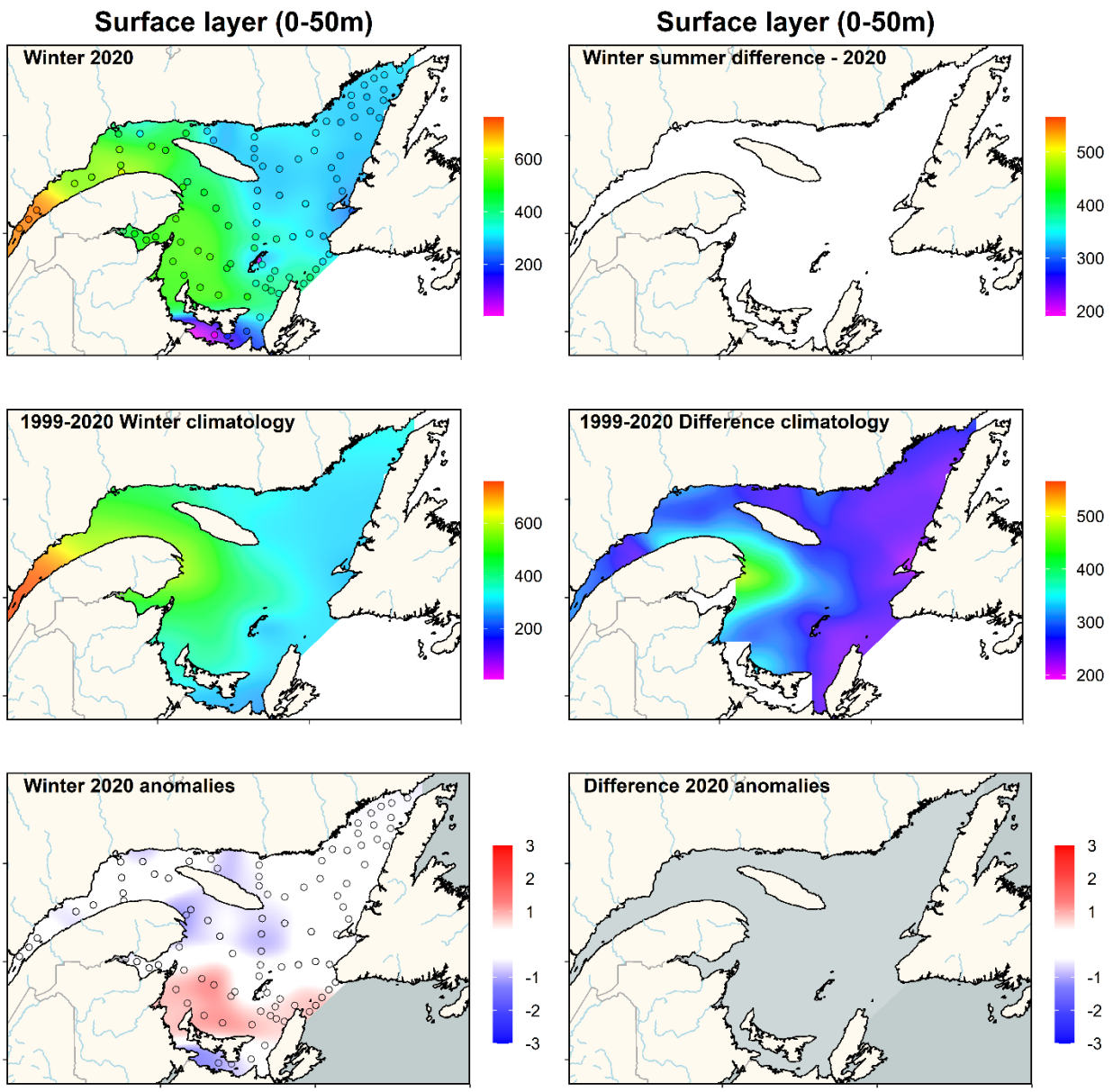

Figure 12. Total nitrate (NO_3^- + NO_2^-) inventories (mmol m^{-2}) in the surface layer (0–50 m) of the Estuary and Gulf of St. Lawrence during early March 2020 (upper left panel). Difference in total nitrate inventories (mmol m^{-2}) in the surface layer of the Estuary and Gulf of St. Lawrence between winter and early summer (upper right panel); there was no early summer oceanographic survey in 2020. The climatology (2001–2020 for winter and 2001–2019 for difference; middle panels) and anomalies (lower panels) are shown. Blue colours indicate anomalies below the mean, reds are anomalies above the mean, and white represents normal conditions.

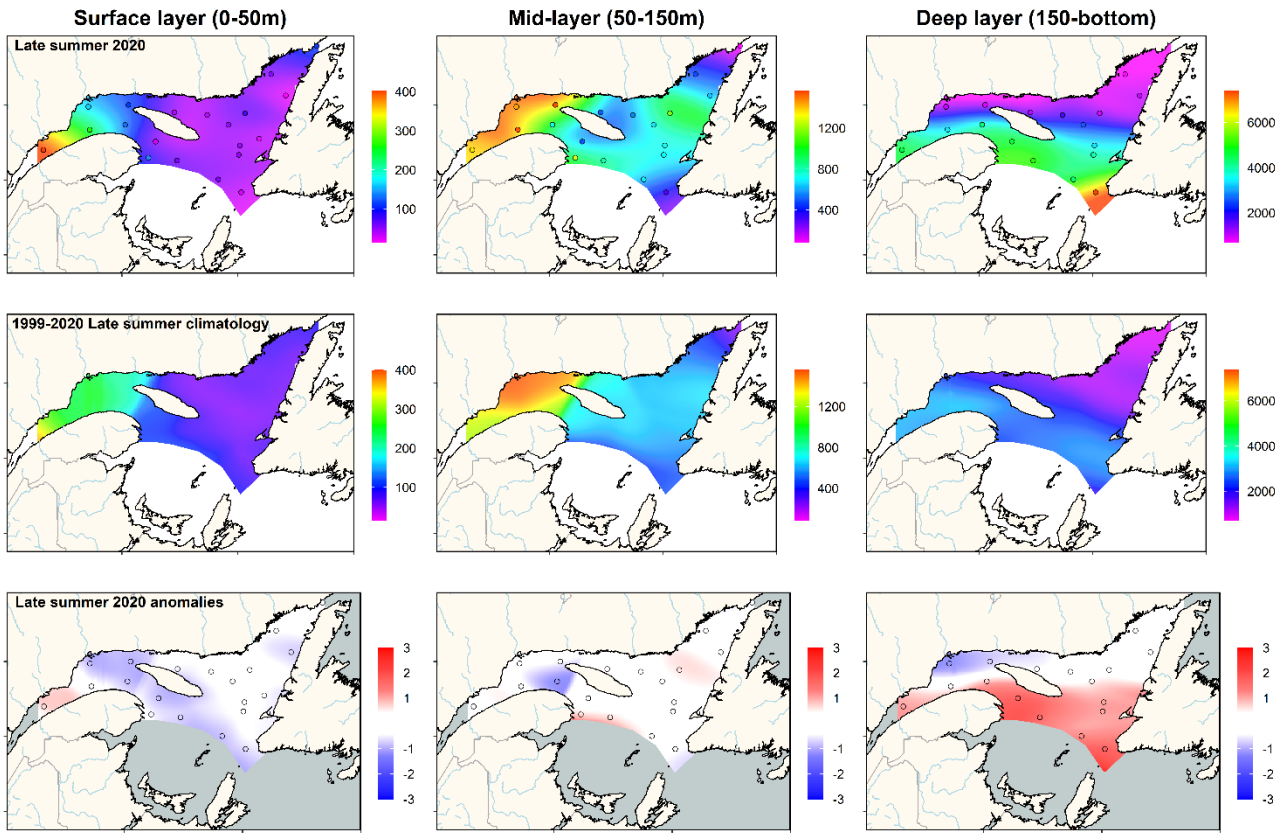

Figure 13. Total nitrate (NO_3^- + NO_2^-) inventories (mmol m^{-2}) in the surface (left panels), mid (middle panels), and deep (right panels) layers of the Estuary and Gulf of St. Lawrence during late summer 2020 (upper panels). The climatology (1999–2020; middle panels) and anomalies (lower panels) are shown for each layer. Blue colours indicate anomalies below the mean, reds are anomalies above the mean, and white represents normal conditions.

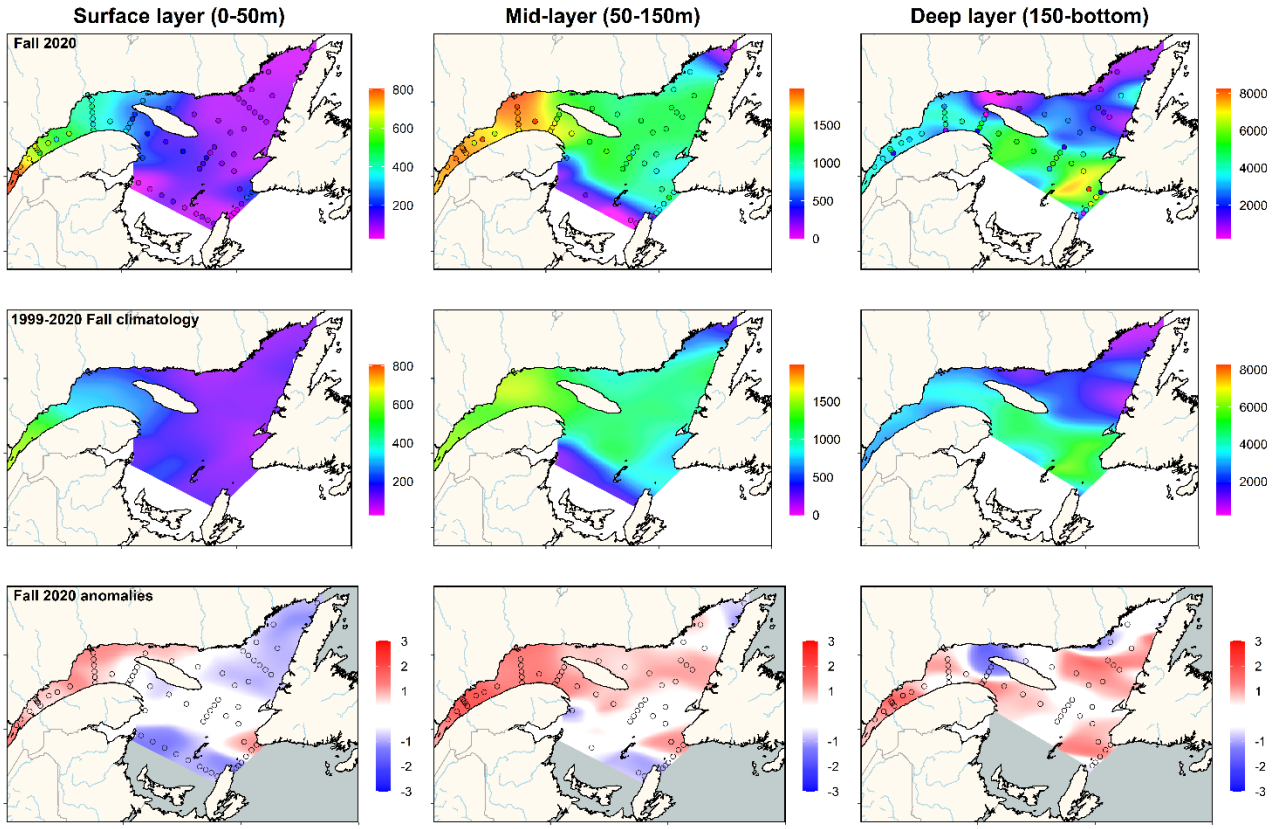

Figure 14. Total nitrate (NO_3^- + NO_2^-) inventories (mmol m^{-2}) in the surface (left panels), mid (middle panels), and deep (right panels) layers of the Estuary and Gulf of St. Lawrence during fall 2020 (upper panels). The climatology (1999–2020; middle panels) and anomalies (lower panels) are shown for each layer. Blue colours indicate anomalies below the mean, reds are anomalies above the mean, and white represents normal conditions.

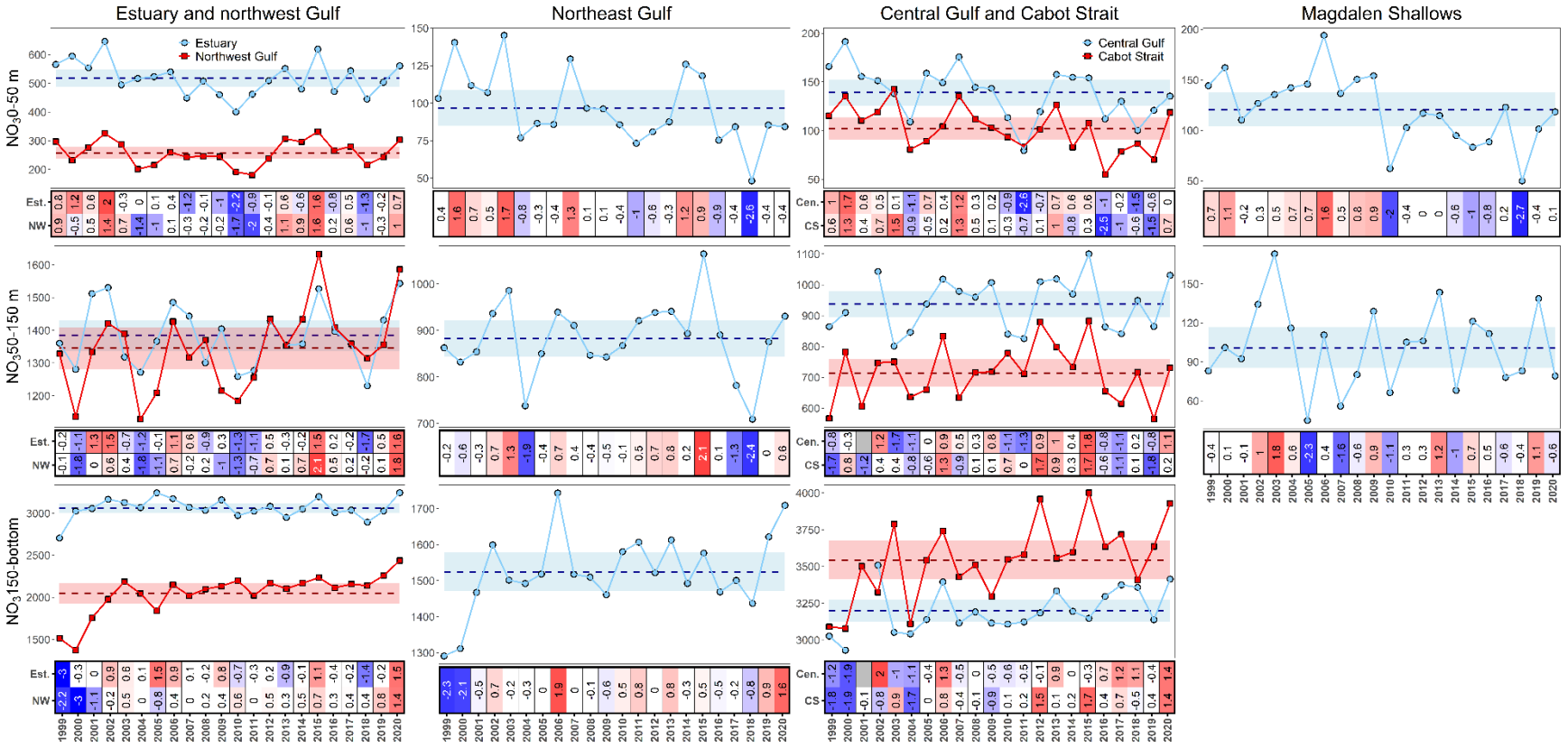

Figure 15. Time series of annual average (lines) and normalized annual anomalies (scorecard) for nitrate (mmol m^{-2}) in the surface, mid and bottom layers for Gulf regions. Means (horizontal dashed lines) and standard deviations (blue or red shading) for the 1999–2020 climatology are shown for each region and water column layer. In the scorecard, blue colours indicate anomalies below the mean, reds are anomalies above the mean, and white represents normal conditions.

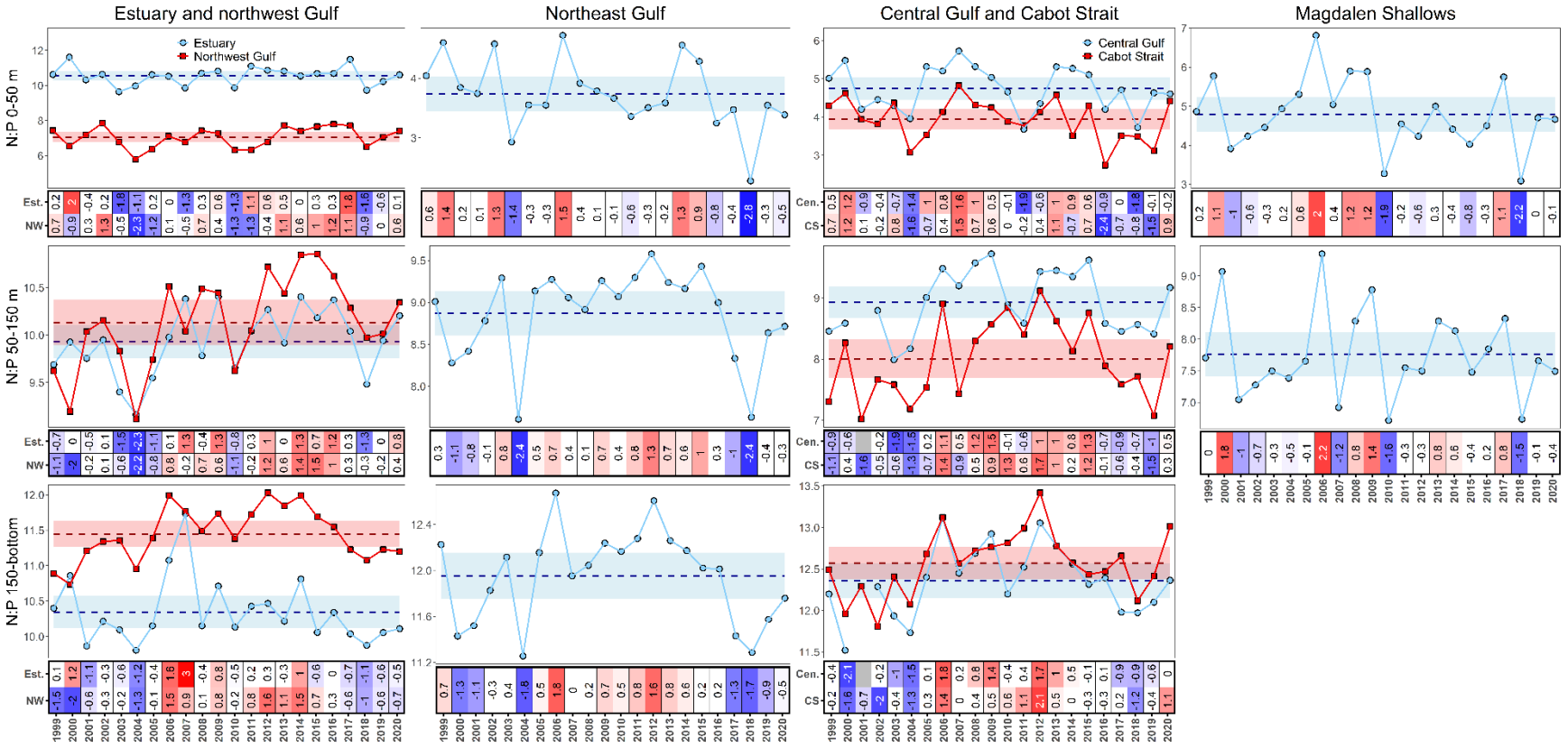

Figure 16. Time series of annual average (lines) and normalized annual anomalies (scorecard) for N:P ratio in the surface, mid and bottom layers for Gulf regions. Means (horizontal dashed lines) and standard deviations (blue or red shading) for the 1999–2020 climatology are shown for each region and water column layer. In the scorecard, blue colours indicate anomalies below the mean, reds are anomalies above the mean, and white represents normal conditions.

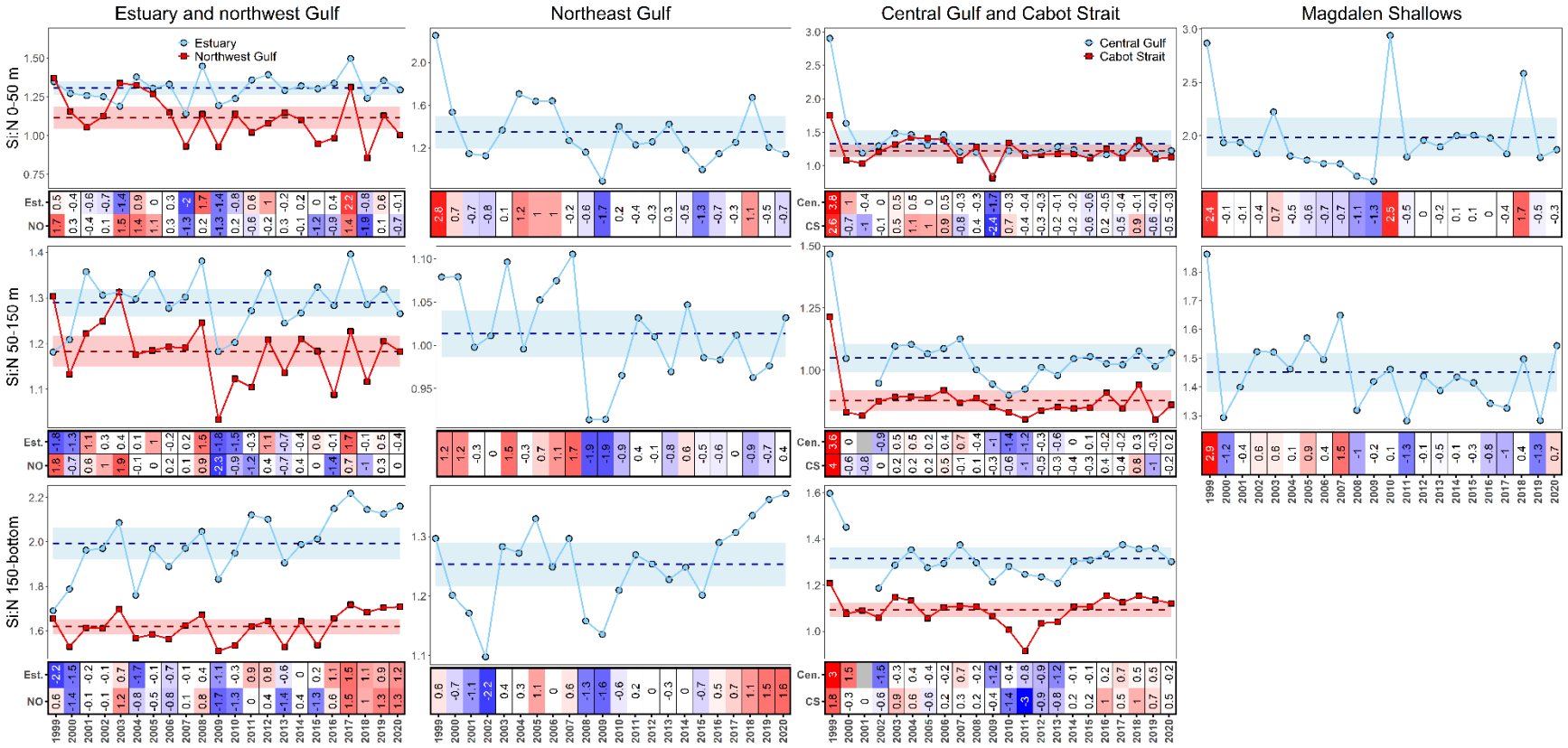

Figure 17. Time series of annual average (lines) and normalized annual anomalies (scorecard) for Si:N ratio in the surface, mid and bottom layers for Gulf regions. Means (horizontal dashed lines) and standard deviations (blue or red shading) for the 1999–2020 climatology are shown for each region and water column layer. In the scorecard, blue colours indicate anomalies below the mean, reds are anomalies above the mean, and white represents normal conditions.

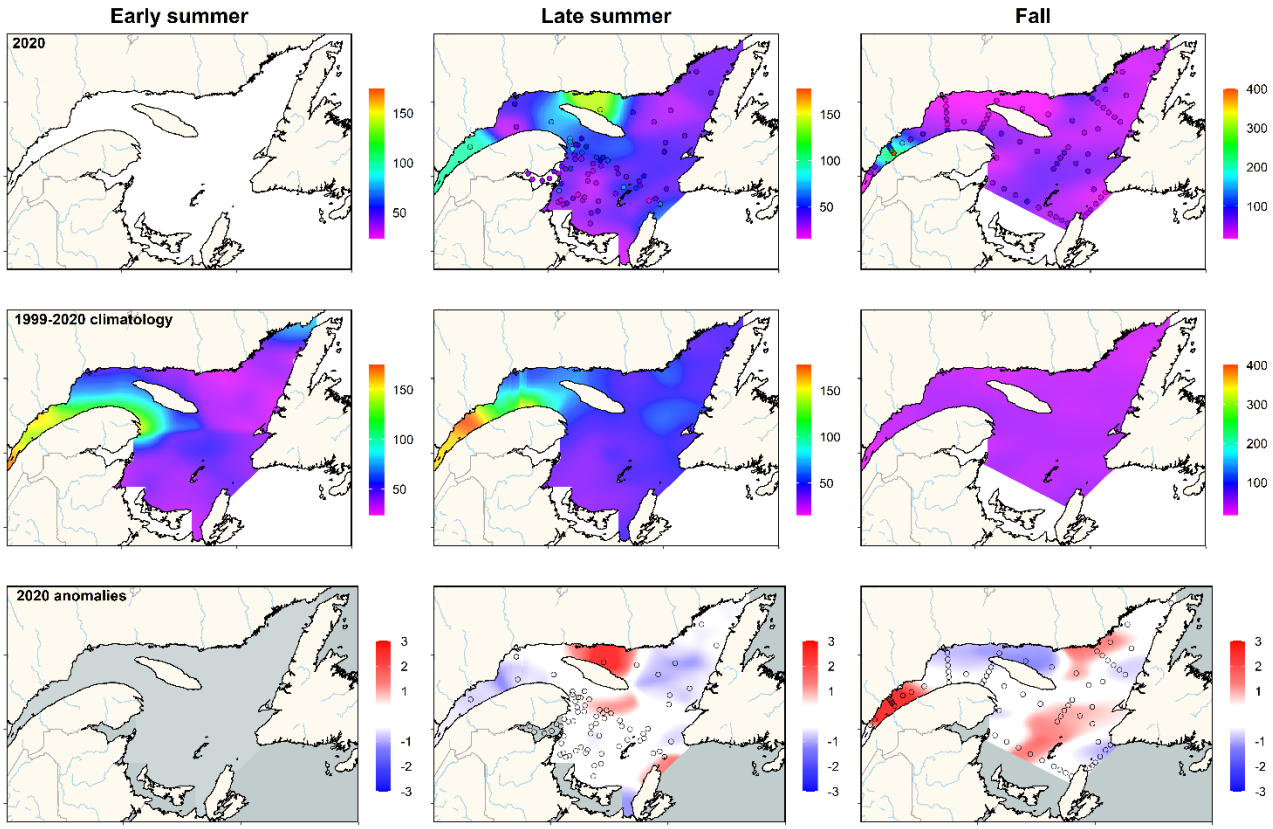

Figure 18. Vertically integrated (0–100 m) chlorophyll a concentrations (mg m^{-2}) in the Estuary and Gulf of St. Lawrence during early summer (left panels), late summer (middle panels), and fall (right panels) 2020. There was no early summer oceanographic survey in 2020. The climatology (1999–2020; middle panels) and anomalies (lower panels) are shown for each season. Blue colours indicate anomalies below the mean, reds are anomalies above the mean, and white represents normal conditions.

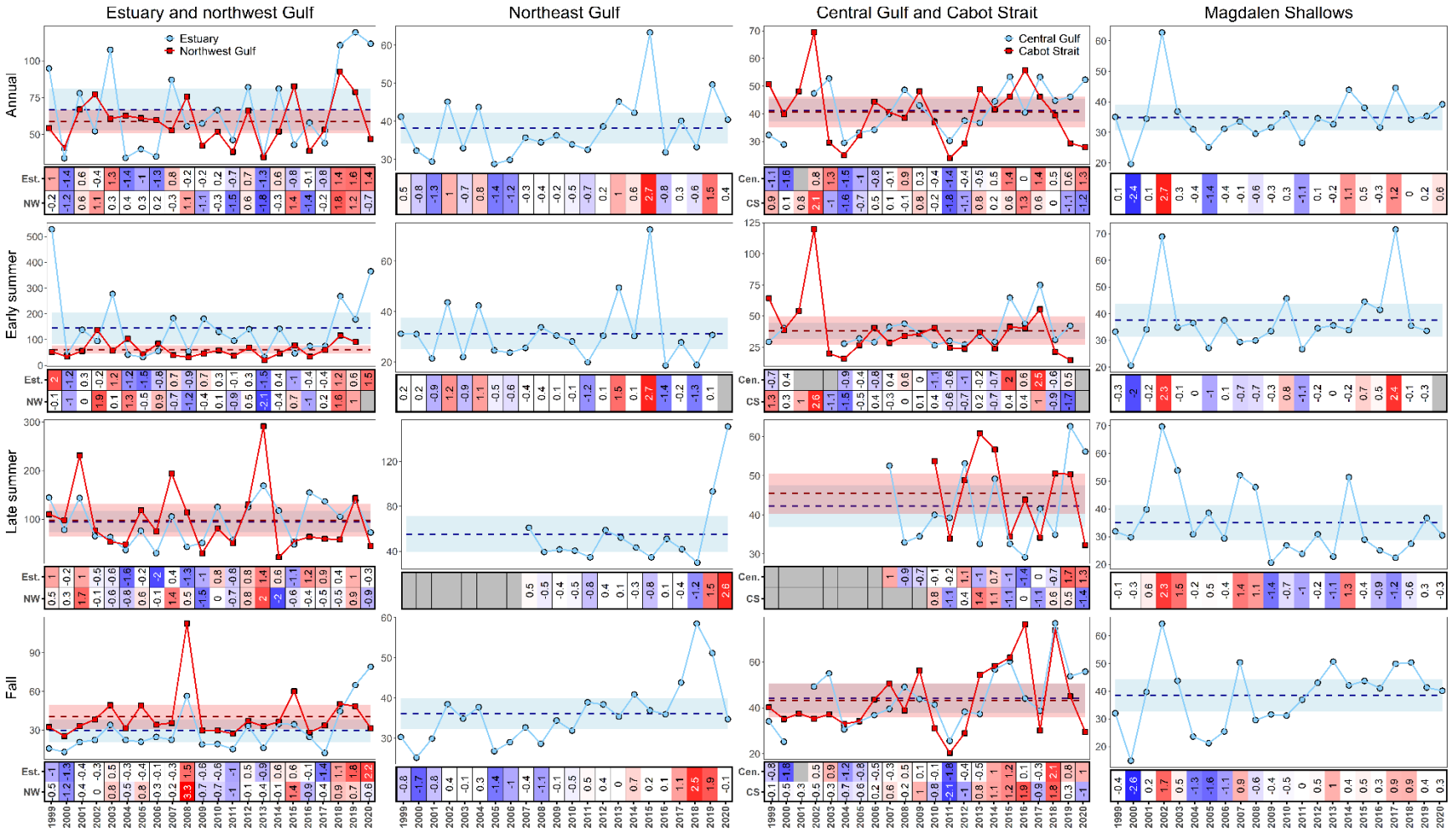

Figure 19. Time series of annual and seasonal average (lines), and normalized annual and seasonal anomalies (scorecard) of vertically integrated chlorophyll a (0–100 m; mg m^{-2}) in the Gulf regions. Means (horizontal dashed lines) and standard deviations (blue or red shading) for the 1999–2020 climatology are shown for each region and season. In the scorecard, blue colours indicate anomalies below the mean, reds are anomalies above the mean, and white represents normal conditions.

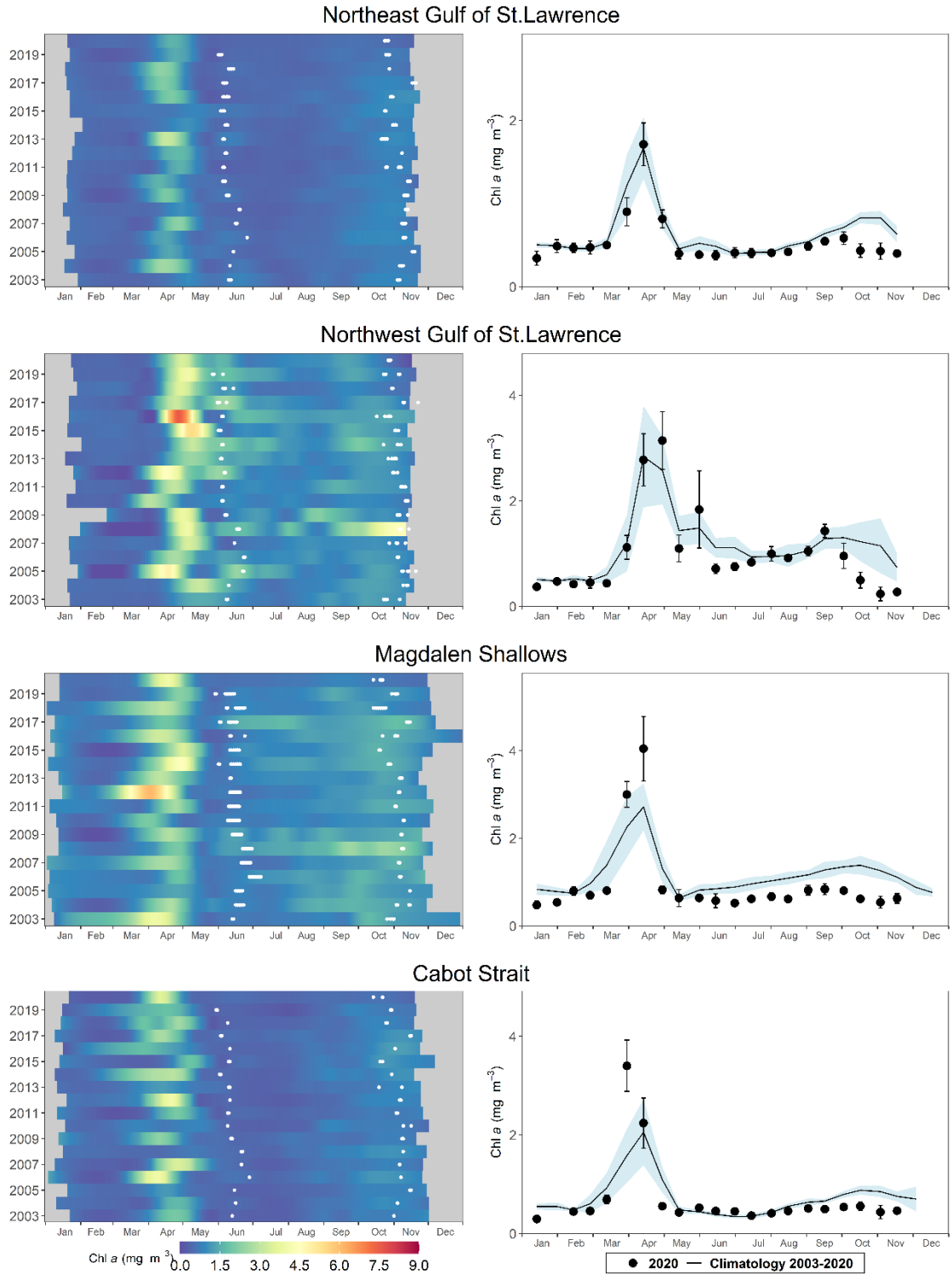

Figure 20. Left panels: LOESS-smoothed time series of surface chlorophyll a concentrations from daily MODIS ocean colour data in the northeast Gulf of St. Lawrence, northwest Gulf of St. Lawrence, Magdalen Shallows, and Cabot Strait ocean colour boxes (see Fig. 4).White dots indicate sampling time of main AZMP surveys. Right panels: comparison of semi-monthly mean (± 0.5 SD) of surface chlorophyll a estimates in 2020 (black circles) with average (± 0.5 SD) conditions from the 2003–2020 climatology (solid line with blue shading) for the same ocean colour boxes.

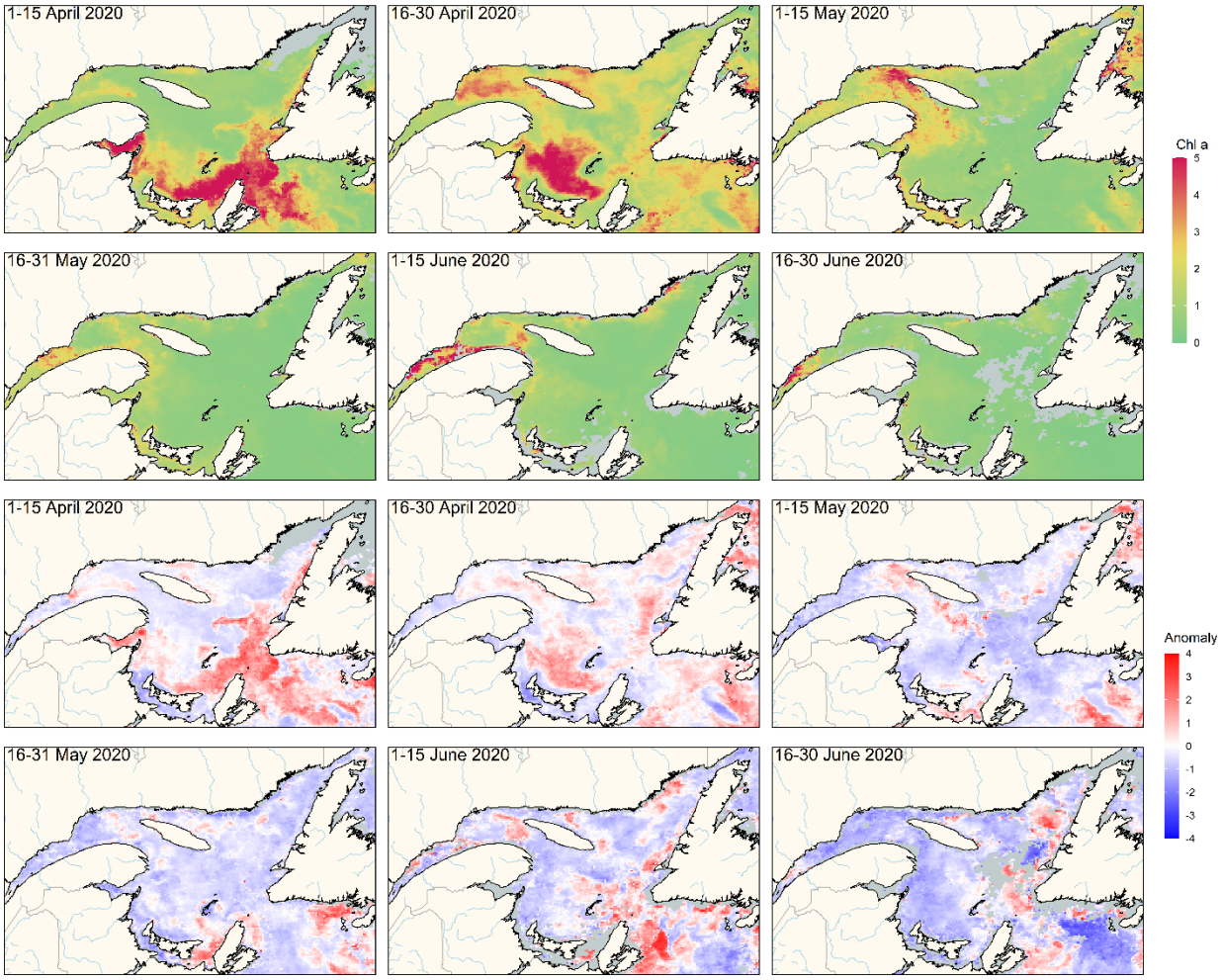

Figure 21. MODIS composite images of surface chlorophyll a (upper panels) and chlorophyll a normalized anomaly based on the 2003–2020 climatology (lower panels) in the Gulf of St. Lawrence during spring/early summer 2020.

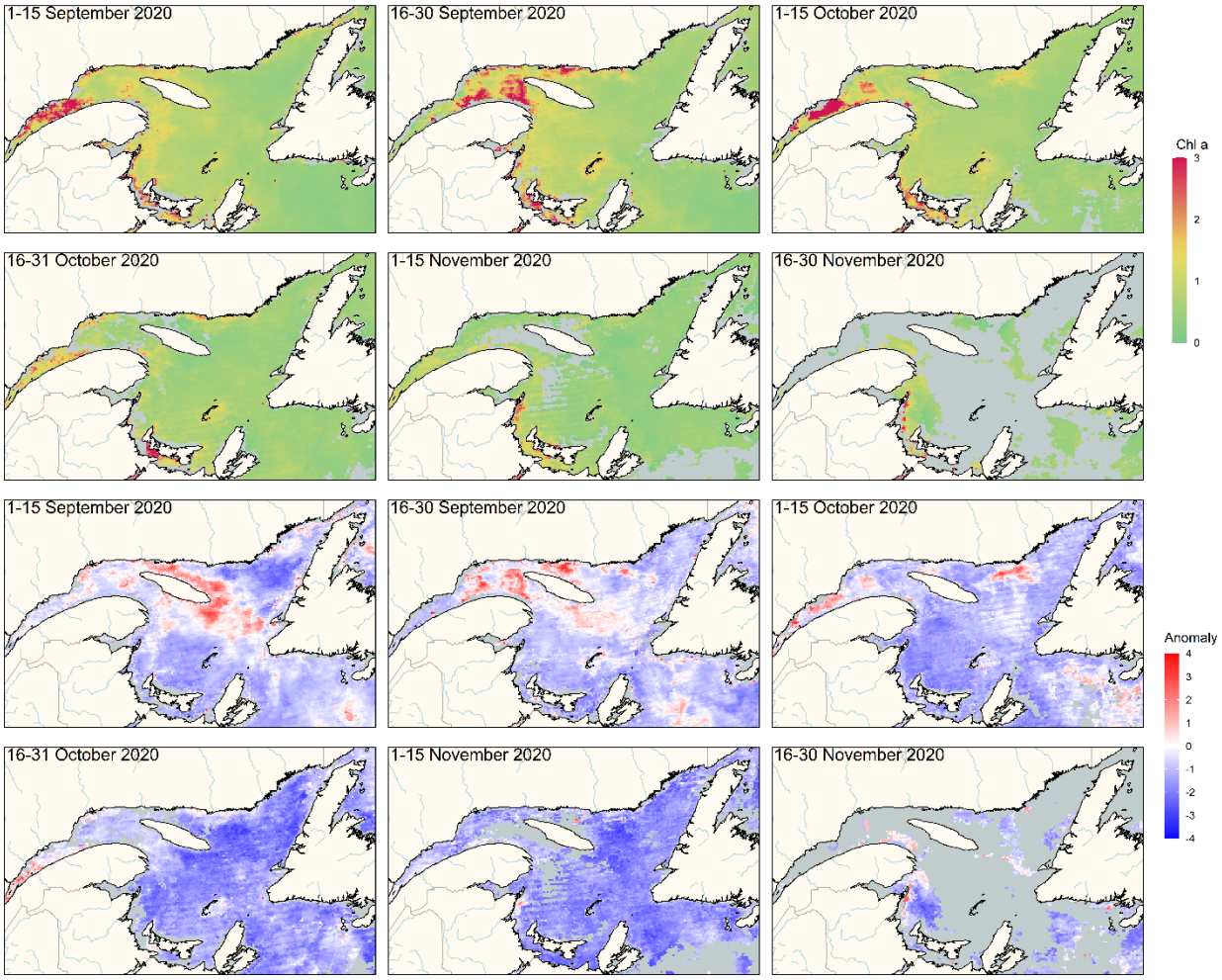

Figure 22. MODIS composite images of surface chlorophyll a (upper panels) and chlorophyll a normalized anomaly based on the 2003–2020 climatology (lower panels) in the Gulf of St. Lawrence during fall 2020.

Spring bloom metrics

		2003	2004	2005	2006	2007	2008	2009	2010	2011	2012	2013	2014	2015	2016	2017	2018	2019	2020	Mean	SD
Start	Northwest Gulf	91	102	93	102	110	112	106	77	98	95	110	112	113	105	100	100	110	96	101.8	9.3
	Northeast Gulf	115	82	101	89	103	106	87	78	102	103	90	112	125	93	83	81	103	95	97.1	12.9
	Magdalen Shallows	77	89	107	112	85	104	78	70	99	66	67	98	99	86	81	60	98	87	86.8	15.2
	Cabot Strait	98	94	89	75	97	112	80	68	103	95	75	96	121	35	81	69	101	84	87.4	19.4
Duration	Northwest Gulf	106	72	28	24	34	22	26	36	30	28	26	30	34	22	32	44	24	48	37	21
	Northeast Gulf	26	50	22	34	30	32	38	38	34	28	38	30	12	34	42	44	26	36	33	8.7
	Magdalen Shallows	56	38	22	14	48	24	52	42	30	56	68	38	38	42	42	76	38	42	42.6	15.5
	Cabot Strait	36	44	38	44	44	38	44	36	26	30	56	36	18	112	44	80	24	40	43.9	21.6
Magnitude	Northwest Gulf	60.4	88.4	76.1	38.4	45.2	56.2	46.4	57.4	41.3	80.8	27.5	35.7	86	118.4	50.7	69.3	51.8	64.9	60.8	22.7
	Northeast Gulf	5.6	63.8	11.7	25.3	30.2	10.6	34.4	30	31.4	26.5	54.3	10	3.8	37.3	42.6	48.5	20.4	28.8	28.6	16.8
	Magdalen Shallows	89.1	77.1	16.7	14.3	51.8	26.5	89.1	39.2	46.6	123.5	61.4	119.1	59.3	78.4	43.4	118.8	44.7	84	65.7	33.9
	Cabot Strait	48.5	38.3	13.8	96.1	72.1	5.7	45.7	8.7	30.1	50	22.9	64.3	16.5	88.3	44.6	70.1	35.6	72.1	45.7	27.1
Amplitude	Northwest Gulf	0.97	2.72	4.82	2.64	2.18	4.92	3.81	3.26	2.92	5.2	2.04	3.96	4.88	12.03	2.86	3.42	4.3	3.13	3.89	2.33
	Northeast Gulf	0.33	3.06	1.09	1.2	2.15	0.71	1.9	1.43	1.81	1.6	2.78	0.62	0.55	2.26	1.84	2.25	1.39	1.78	1.6	0.76
	Magdalen Shallows	2.85	3.42	1.45	1.72	1.9	2.21	2.23	1.59	3.18	5.44	1.81	7.69	2.34	3.04	1.9	2.35	2.36	4.38	2.88	1.57
	Cabot Strait	2.54	1.73	0.68	3.86	3.64	0.41	2.55	0.43	2.48	3.21	0.81	4.92	1.5	1.36	2.02	2.55	1.79	3.69	2.23	1.28

Mean surface Chl *a*

		2003	2004	2005	2006	2007	2008	2009	2010	2011	2012	2013	2014	2015	2016	2017	2018	2019	2020	Mean	SD
Annual	Northwest Gulf	0.93	1.16	1.51	1.11	1.06	2	1.26	1	1.14	1.46	1.1	1.45	1.35	1.71	1.3	1.04	1.26	1.09	1.27	0.27
	Northeast Gulf	0.65	0.81	0.64	0.71	0.69	0.56	0.7	0.65	0.59	0.68	0.86	0.6	0.68	0.74	0.72	0.7	0.58	0.56	0.67	0.08
	Magdalen Shallows	1.33	1.29	1.05	1.14	1.2	1.53	1.38	0.95	1.12	1.58	1.22	1.49	1.25	1.35	1.38	1.25	1.03	0.99	1.25	0.18
	Cabot Strait	0.71	0.68	0.58	1.04	0.86	0.65	0.76	0.64	0.73	0.95	0.7	0.94	0.7	0.88	0.79	0.81	0.69	0.75	0.77	0.12
Spring	Northwest Gulf	0.84	1.47	2.23	1.24	1.4	1.57	1.33	1.4	1.26	2.21	1.19	1.36	1.84	2.4	1.51	1.58	1.6	1.51	1.55	0.39
	Northeast Gulf	0.6	1.29	0.76	0.77	0.93	0.59	0.95	0.87	0.78	1	1.32	0.7	0.68	0.92	0.96	1.04	0.74	0.8	0.87	0.2
	Magdalen Shallows	2.2	1.47	0.98	1.01	1.62	1.08	1.54	1.12	1.2	2.9	1.68	2.05	1.55	1.75	1.16	1.96	1.12	1.67	1.56	0.5
	Cabot Strait	1.12	0.87	0.69	1.67	1.45	0.54	1.1	0.79	1.11	1.81	0.88	1.74	0.8	1.25	1.06	1.35	1.19	1.29	1.15	0.36
Summer	Northwest Gulf	0.83	0.92	1.33	1.07	0.78	1.38	1.19	0.84	0.92	1.11	1.12	1.47	0.95	1.45	1.32	0.75	1.23	1.01	1.09	0.23
	Northeast Gulf	0.6	0.48	0.47	0.53	0.42	0.36	0.48	0.41	0.36	0.39	0.52	0.42	0.54	0.48	0.47	0.43	0.43	0.4	0.45	0.06
	Magdalen Shallows	0.73	0.99	0.89	1.05	0.75	1.39	1.21	0.78	0.86	0.7	0.9	1.1	0.92	0.94	1.47	0.81	0.83	0.61	0.94	0.23
	Cabot Strait	0.36	0.39	0.34	0.53	0.43	0.47	0.51	0.36	0.43	0.32	0.41	0.42	0.48	0.46	0.51	0.39	0.29	0.44	0.42	0.07
Fall	Northwest Gulf	1.16	1.09	1.02	1.03	0.98	3.16	1.25	0.78	1.27	1	0.98	1.51	1.25	1.26	1.03	0.74	0.94	0.74	1.18	0.53
	Northeast Gulf	0.75	0.66	0.69	0.83	0.72	0.76	0.67	0.66	0.65	0.65	0.75	0.71	0.83	0.83	0.73	0.61	0.61	0.48	0.7	0.09
	Magdalen Shallows	1.19	1.42	1.28	1.37	1.25	2.05	1.39	0.94	1.29	1.14	1.09	1.32	1.28	1.36	1.5	0.98	1.14	0.71	1.26	0.28
	Cabot Strait	0.71	0.78	0.72	0.93	0.71	0.94	0.68	0.77	0.65	0.72	0.79	0.91	0.84	0.92	0.8	0.69	0.67	0.5	0.76	0.12

Figure 23. Time series of annual mean for indices of change in spring bloom properties (upper section) and annual/seasonal mean surface chlorophyll a (lower section; mg m^{-3}) estimated from satellite ocean colour data (MODIS: 2003–present) in the Gulf of St. Lawrence ocean colour boxes (see Fig. 4). The spring bloom indices are start (day of the year), duration (days), magnitude (mg chl m^{-3} day), and amplitude (mg chl m^{-3}). Variable means and standard deviations for the 2003–2020 climatology are shown to the right of the scorecard. Blue colours indicate normalized anomalies below the mean, reds are anomalies above the mean, and white represents normal conditions. Spring is from March to May, summer from June to August, and fall from September to November.

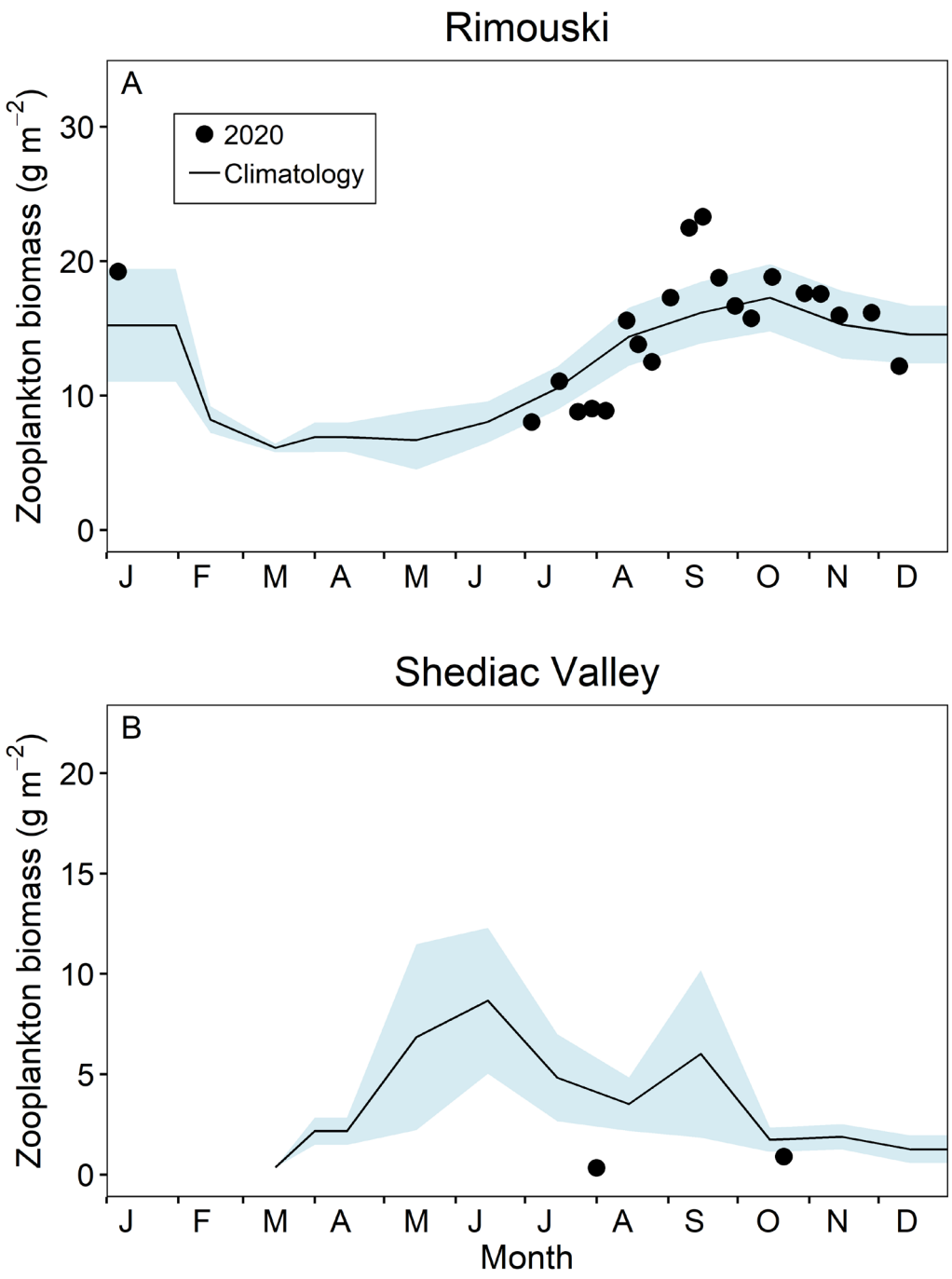

Figure 24. Comparison of total zooplankton biomass (dry weight) in 2020 (circles) with the monthly climatology from (A) Rimouski (2005–2020) and (B) Shediac Valley (1999–2020) stations (black line with blue shading). Blue shading represents ± 0.5 SD of the monthly means.

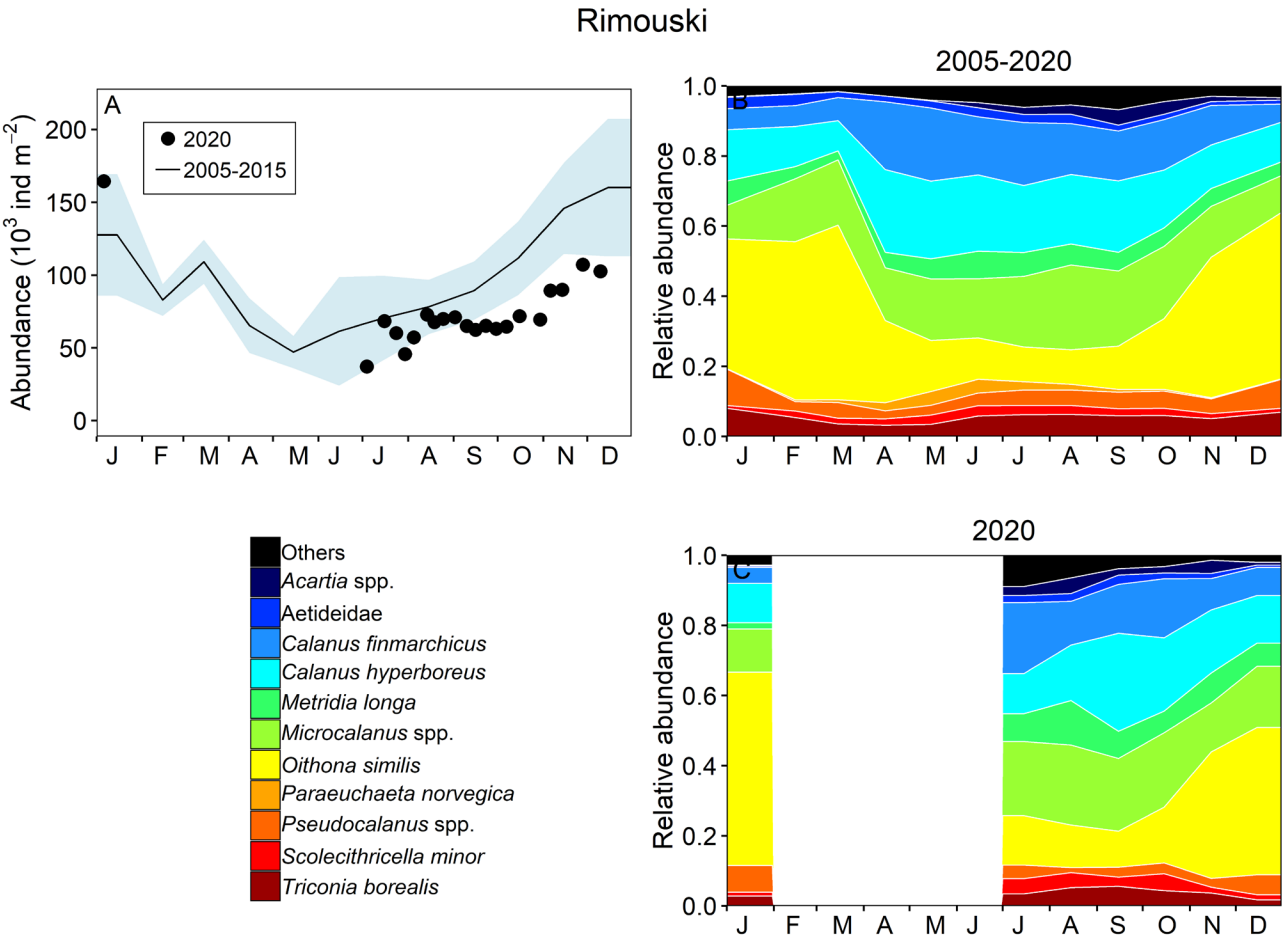

Figure 25. Seasonal variability of dominant copepods at Rimouski station. Copepod abundance (excluding nauplii) during the climatology (black line with blue shading indicating ± 0.5 SD) and in 2020 (circles) [A]; climatology of the relative abundance of the identified copepod taxa representing 95% of total copepod abundance during the 2005–2020 period (B) and in 2020 (C).

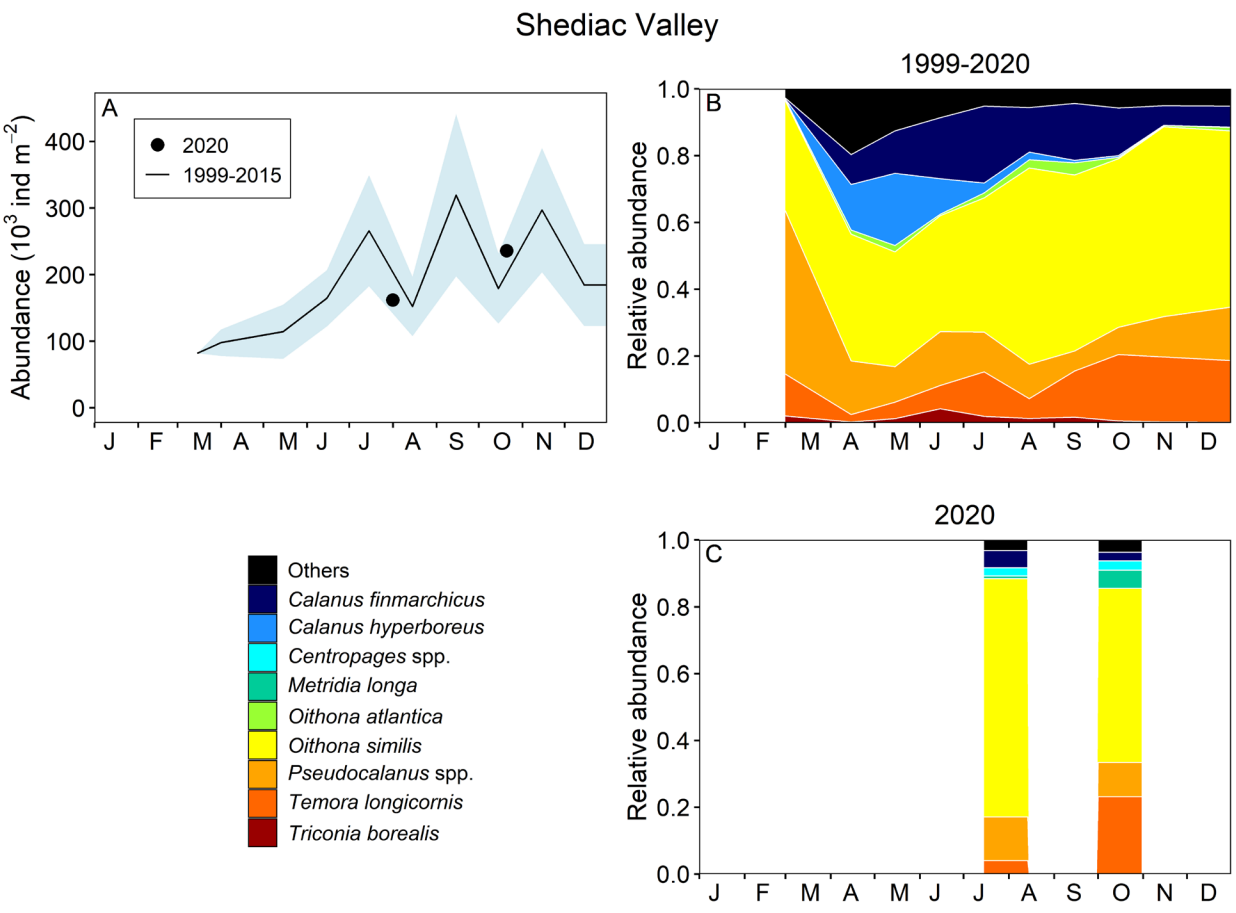

Figure 26. Seasonal variability of dominant copepods at Shediac Valley station. Copepod abundance (excluding nauplii) during the climatology (black line with blue shading indicating ± 0.5 SD) and 2020 (circles) (A); climatology of the relative abundance of the identified copepod taxa representing 95% of total copepod abundance during the 1999–2020 period (B) and in 2020 (C).

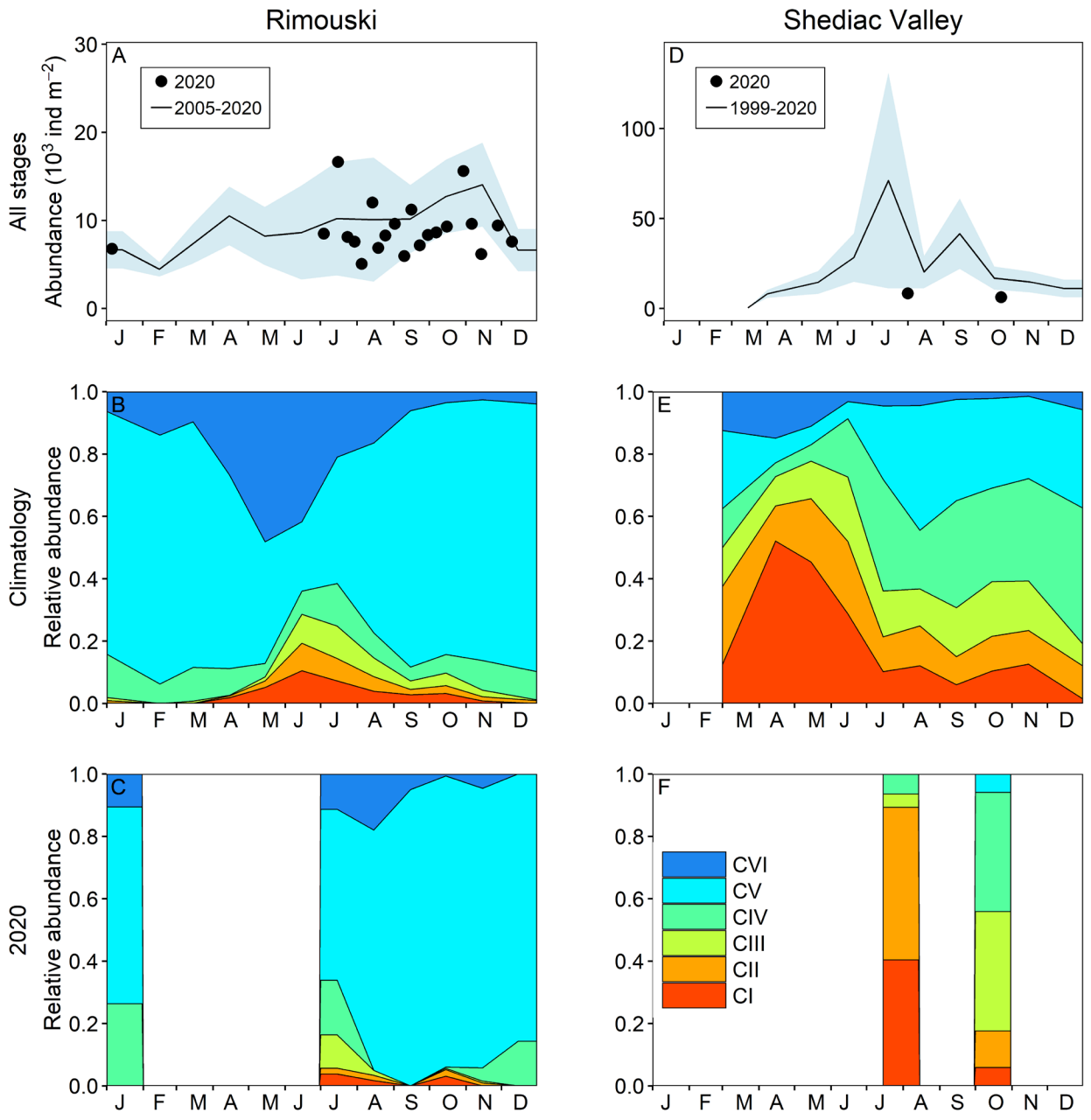

Figure 27. Seasonal variability in Calanus finmarchicus *copepodite abundance at Rimouski (A–C) and Shediac Valley (D–F) stations. The climatologies of the combined counts (black line with blue shading indicating ± 0.5 SD) are plotted with data from 2020 (circles) (A, D). The seasonal variabilities for the individual copepodite stages for the climatologies (B, E) and for 2020 (C, F) are also shown.*

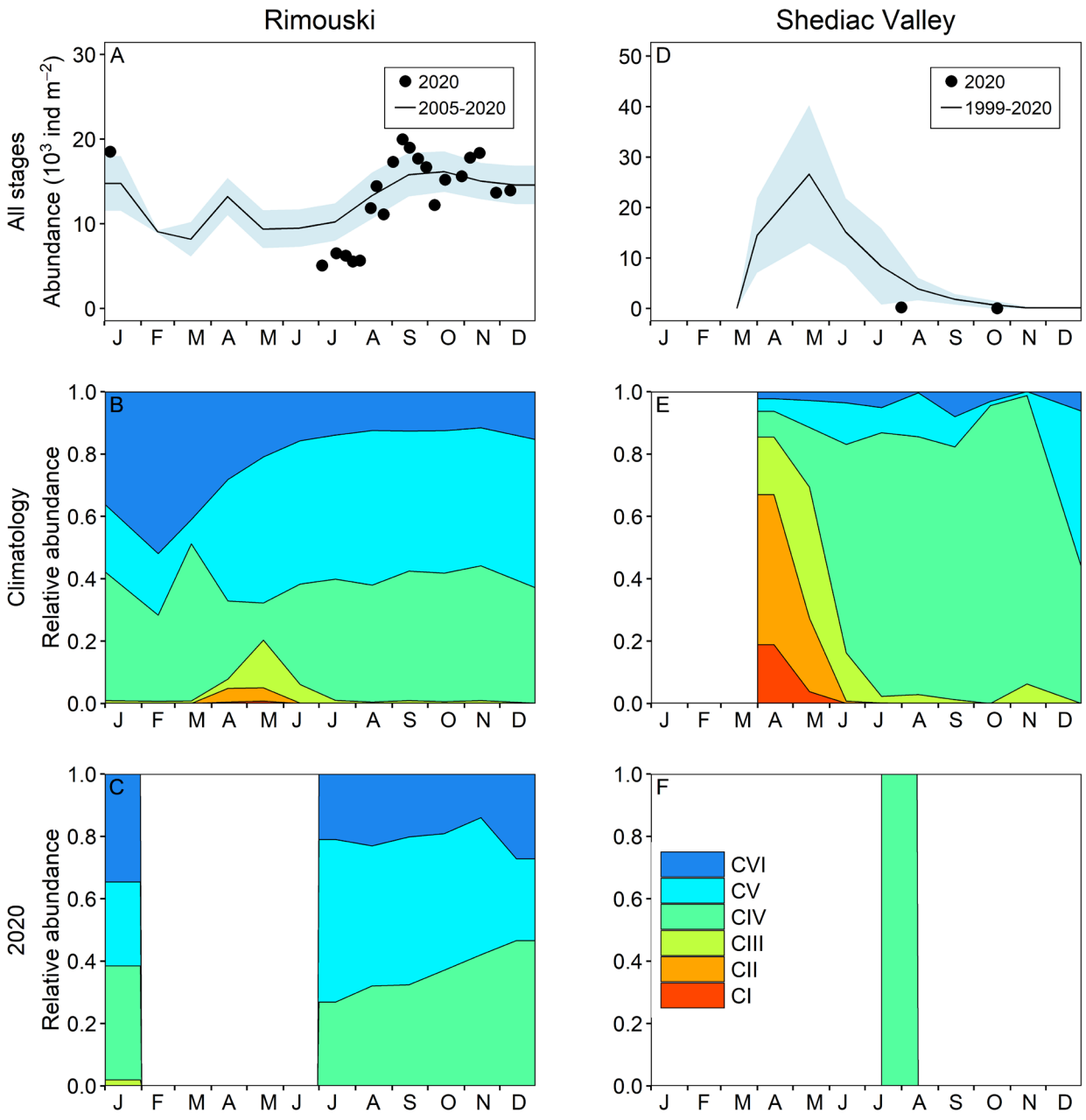

Figure 28. Seasonal variability in Calanus hyperboreus *copepodite abundance at Rimouski (A–C) and Shediac Valley (D–F) stations. The climatologies of the combined counts (black line with blue shading indicating ± 0.5 SD) are plotted with data from 2020 (circles) (A, D). The seasonal variabilities for the individual copepodite stages for the climatologies (B, E) and for 2020 (C, F) are also shown. No* C. hyperboreus *individual was collected in the October sample at Shediac Valley.*

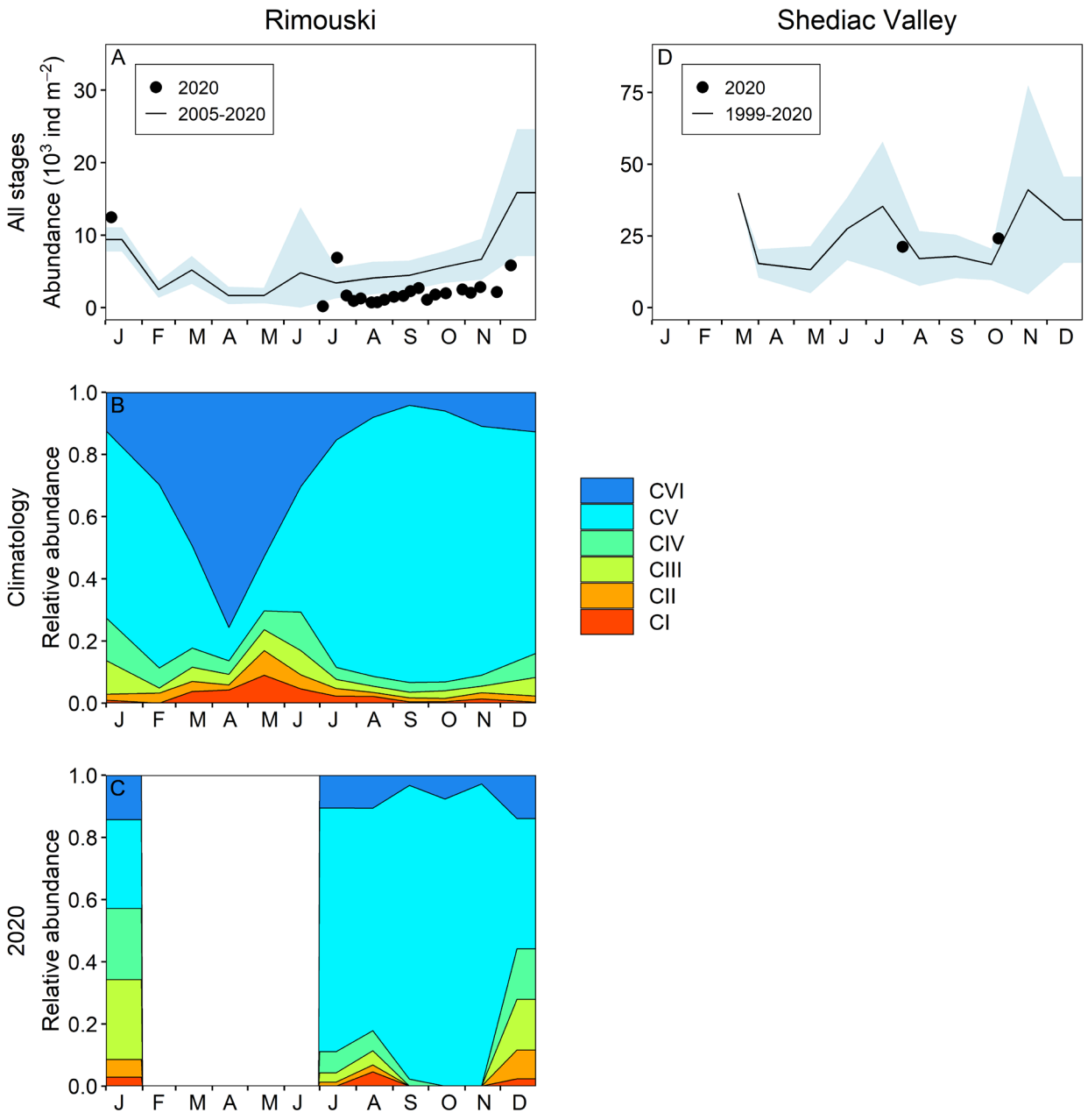

Figure 29. Seasonal variability in Pseudocalanus *spp. copepodite abundance at Rimouski (A–C) and Shediac Valley (D) stations. The climatologies of the combined counts (black line with blue shading indicating ± 0.5 SD) are plotted with data from 2020 (circles) (A, D). The seasonal variabilities for the individual copepodite stages for the climatologies (B) and for 2020 (C) are also shown. No stage information is available for Shediac Valley.*

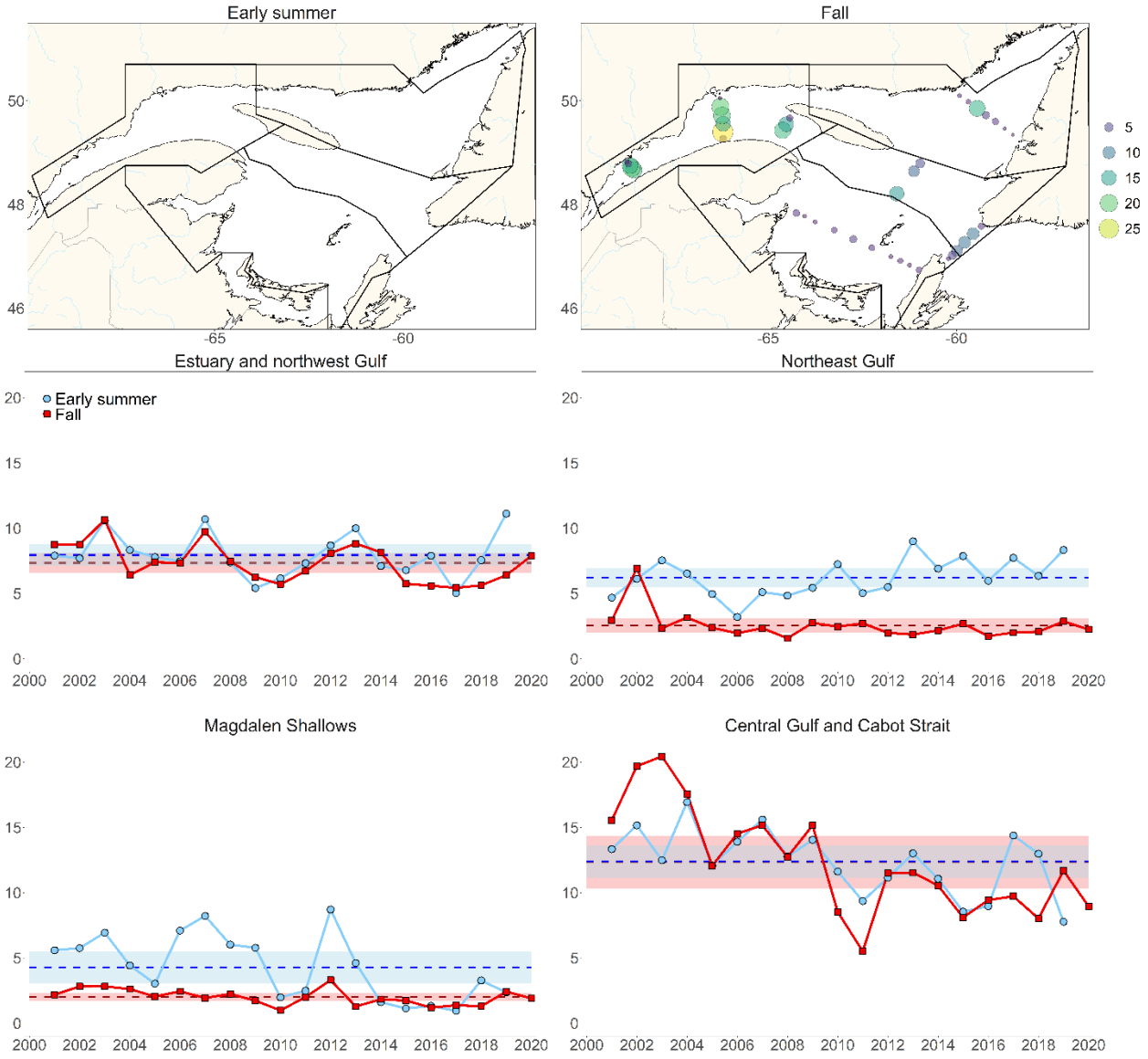

Figure 30. Zooplankton biomass (dry weight; g m^{-2}) at each sampling station during early summer and fall 2020 (upper panels) and regional seasonal time series of mean total zooplankton biomass (g m^{-2}; middle and bottom panels) calculated using GLM. Dashed blue and red lines represent the climatology (2001–2020) *averages (shading represents ± 0.5 SD) for early summer and fall, respectively.*

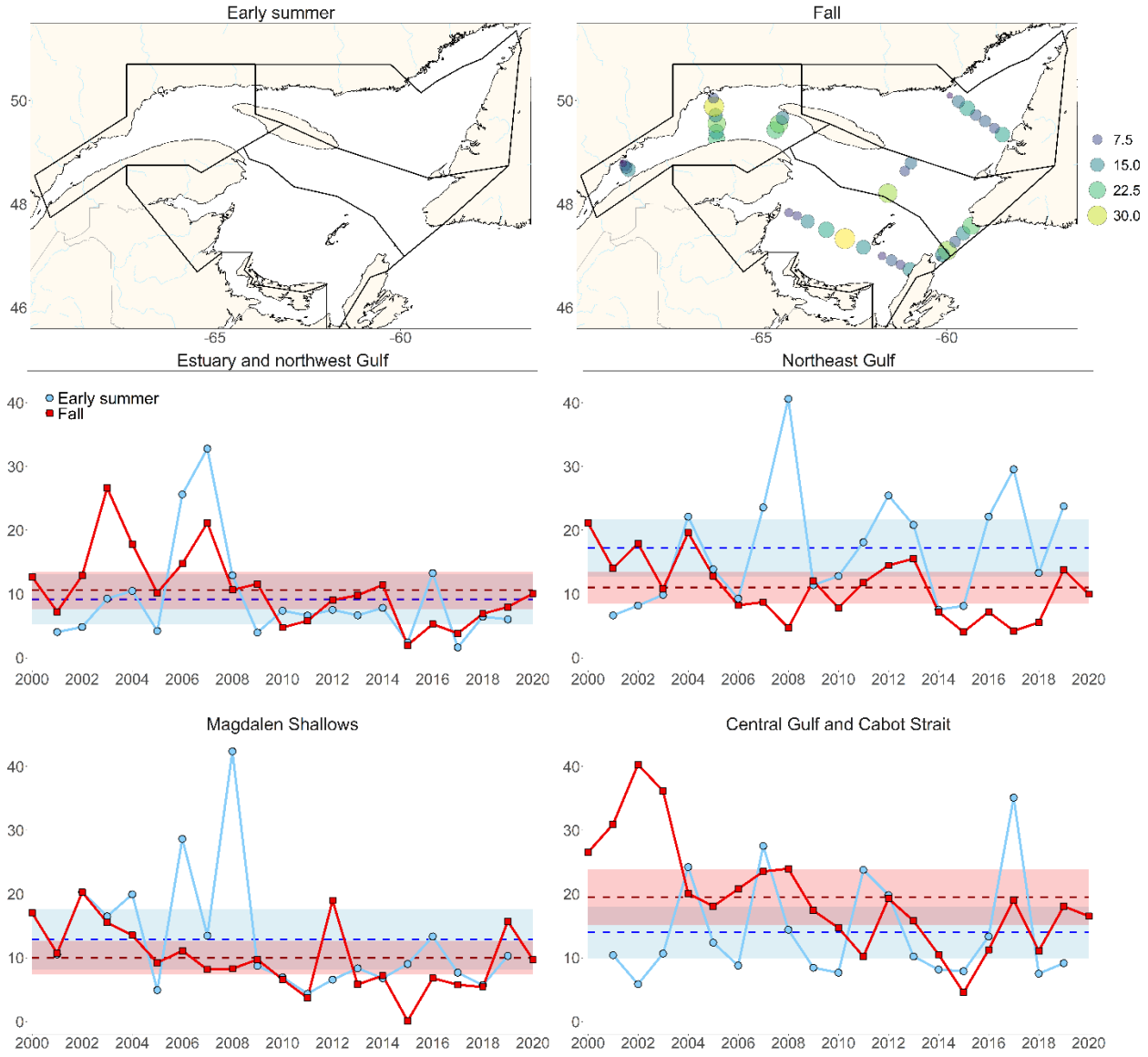

Figure 31. Calanus finmarchicus *abundance (10^3 ind m^{-2}) at each sampling station during early summer and fall 2020 (upper panels) and regional seasonal time series of mean total* Calanus finmarchicus *abundance (10^3 ind m^{-2}; middle and bottom panels) calculated using GLM. Dashed blue and red lines represent the climatology* (2000–2020) *averages (shading represents ± 0.5 SD) for early summer and fall, respectively.*

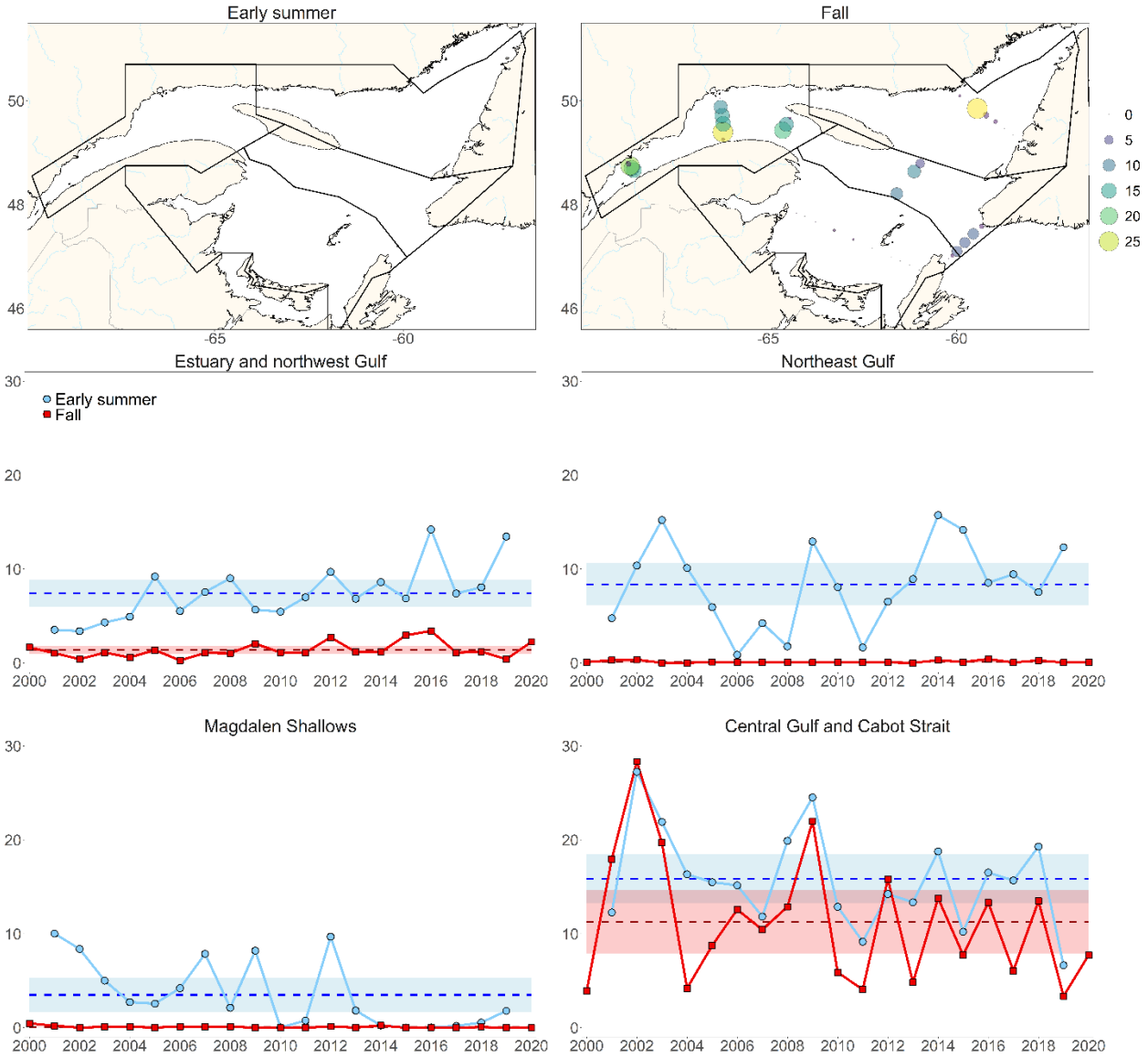

Figure 32. Calanus hyperboreus *abundance (10^3 ind m^{-2}) at each sampling station during early summer and fall 2020 (upper panels) and regional seasonal time series of mean total* Calanus hyperboreus *abundance (10^3 ind m^{-2}; middle and bottom panels) calculated using GLM. Dashed blue and red lines represent the climatology* (2000–2020) *averages (shading represents ± 0.5 SD) for early summer and fall, respectively.*

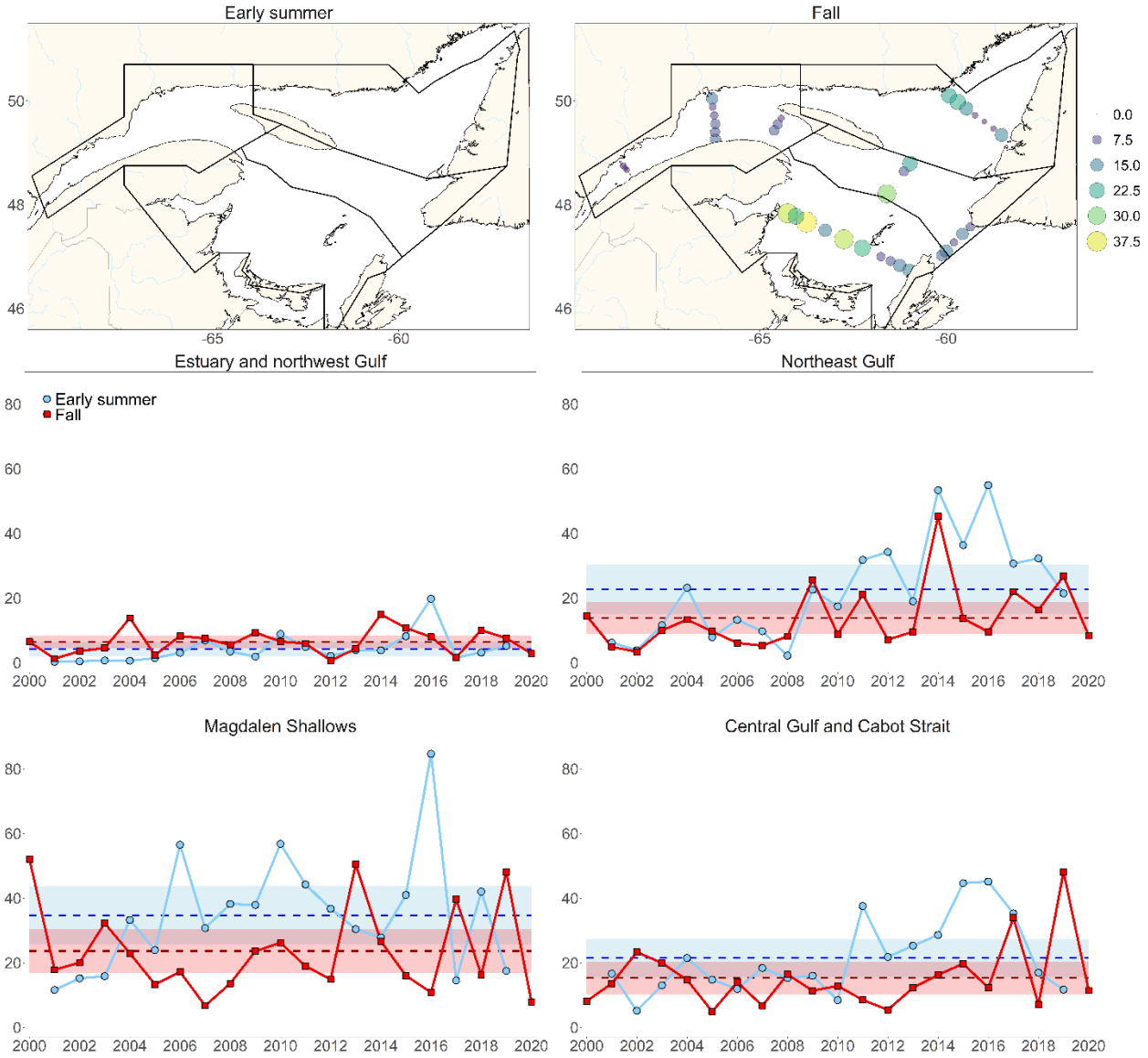

Figure 33. Pseudocalanus *spp. abundance (10^3 ind m^{-2}) at each sampling station during early summer and fall 2020 (upper panels) and regional seasonal time series of mean total* Pseudocalanus *spp. abundance (10^3 ind m^{-2}; middle and bottom panels) calculated using GLM. Dashed blue and red lines represent the climatology* (2000–2020) *averages (shading represents ± 0.5 SD) for early summer and fall, respectively.*

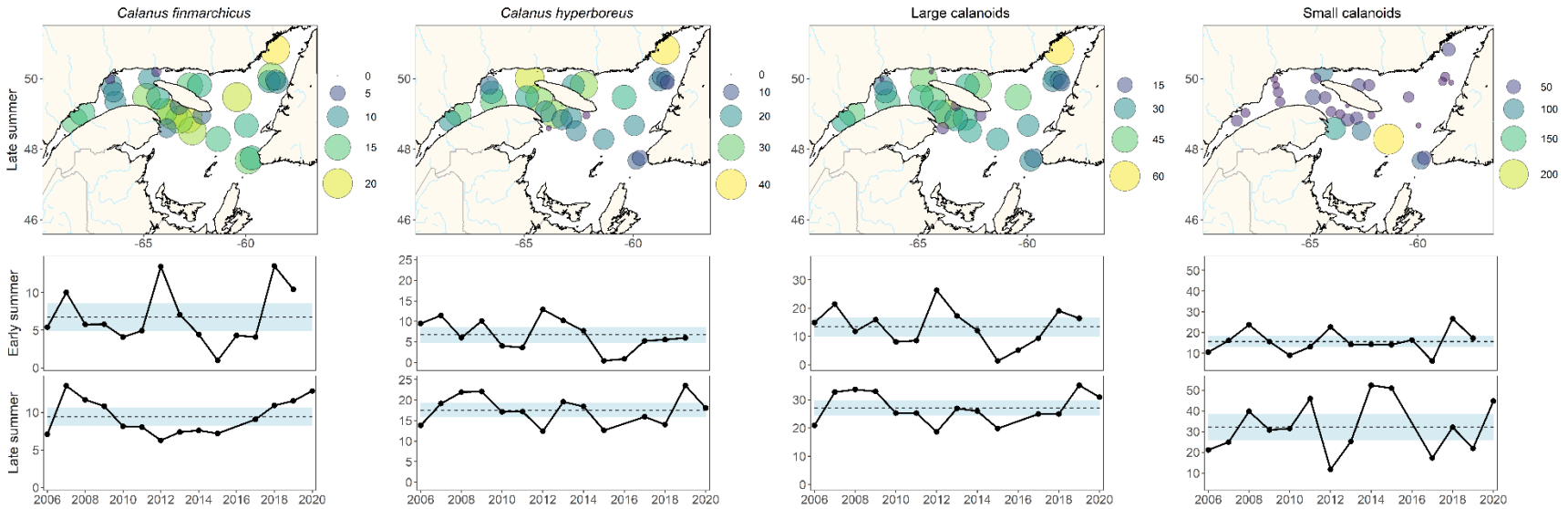

Figure 34. Abundances (10^3 ind m^{-2}) of main taxa identified through automated numerical zooplankton images analysis (ZooImage) at each sampling station during early summer on the Magdalen Shallows (no abundance maps: no sampling in 2020) and late summer 2020 in the northern Gulf (upper panels). The regional seasonal time series of mean total abundances are also shown for these taxa (10^3 ind m^{-2}; bottom panels). Dashed lines represent the climatology (2006–2020) *averages (shading represents ± 0.5 SD). The abundances of* C. finmarchicus *and* C. hyperboreus *include copepodite stages CIV – CVI only. ZooImage does not distinguish between* C. finmarchicus *and* C. glacialis*; thus both species are included in* C. finmarchicus *index. In this figure, large calanoid abundances correspond to the the sum of these* C. finmarchicus *and* C. hyperboreus *indices; and small calanoid abundances correspond to the sum of the following taxa:* Temora *spp.,* Eurytemora *spp.,* Pseudocalanus *spp.,* Microcalanus *spp. and* Scolecithricella *spp.*

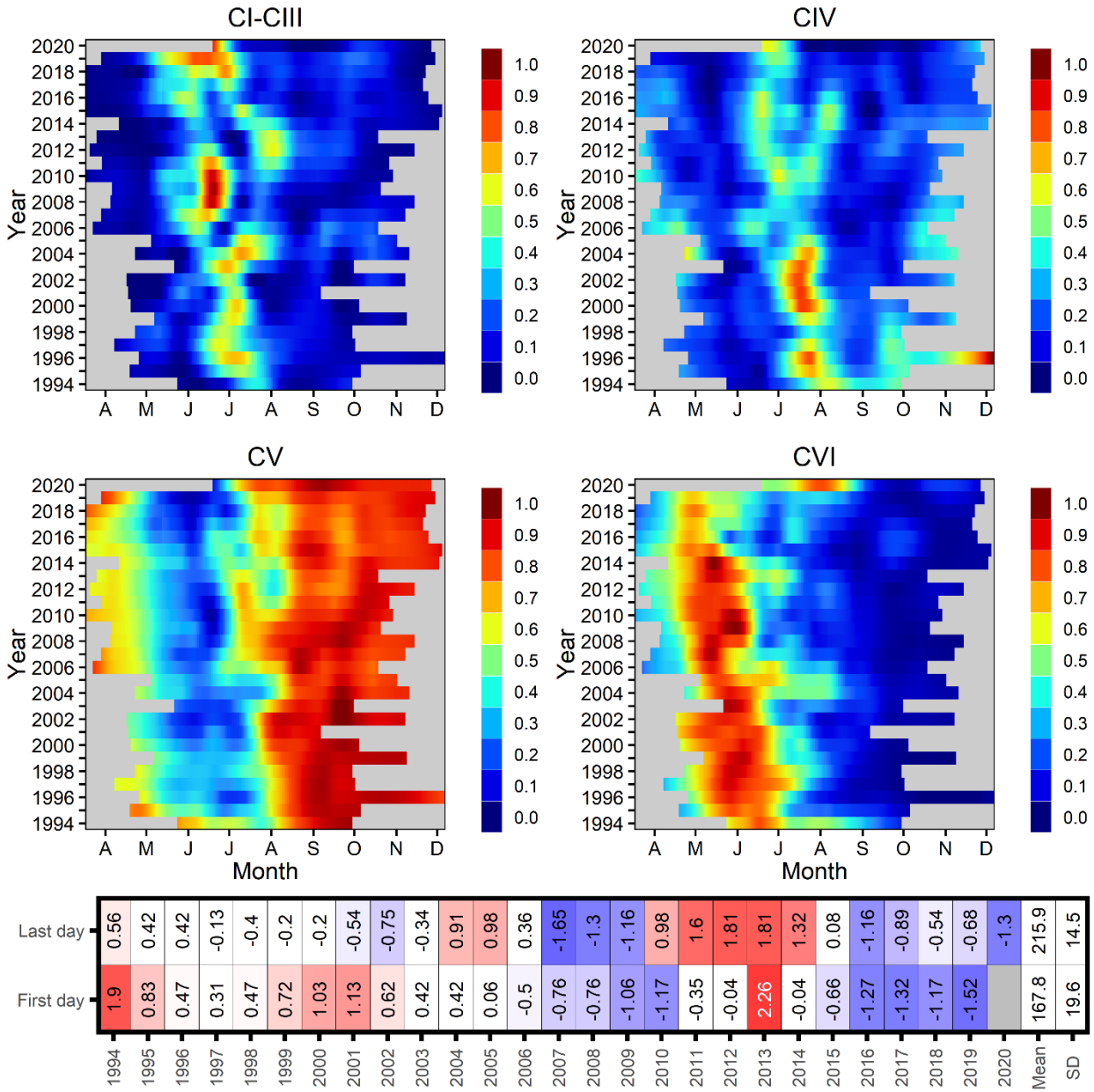

Figure 35. Time series of the seasonal cycle in relative proportion of total abundance for Calanus finmarchicus *copepodite stages (CI–CIII, CIV, CV, and CVI male + female) at Rimouski station. Proportions are normalized by their annual maximum and smoothed using a Loess regression. Bottom scorecard shows the anomaly time series (climatology 1994–2020) associated with the first and last day when the normalized proportion of CI–CIII was higher than 0.3.*

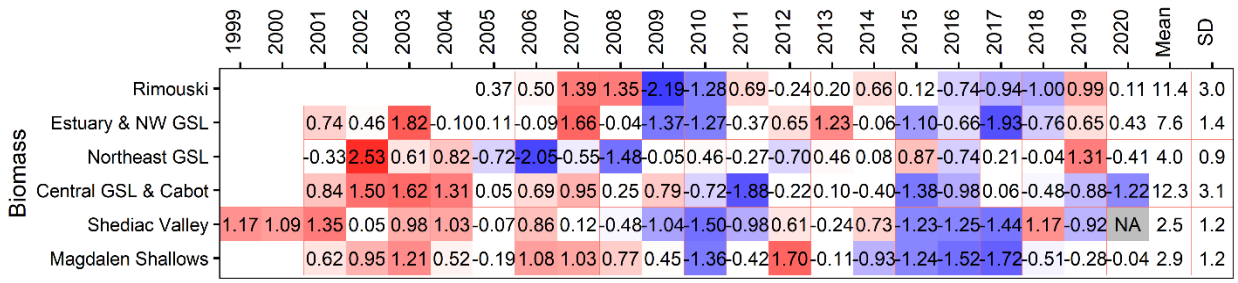

Figure 36. Time series of normalized annual anomalies of zooplankton biomass (dry weight; g m^{-2}) for the high-frequency monitoring stations and the regions of the Gulf of St. Lawrence (calculated using GLM). Variable means and standard deviations for the 2001–2020 (2005–2020 for Rimouski; 1999–2020 for Shediac Valley) climatology are shown to the right of the scorecard. Blue colours indicate anomalies below the mean, reds are anomalies above the mean, and white represents normal conditions. GSL: Gulf of St. Lawrence.

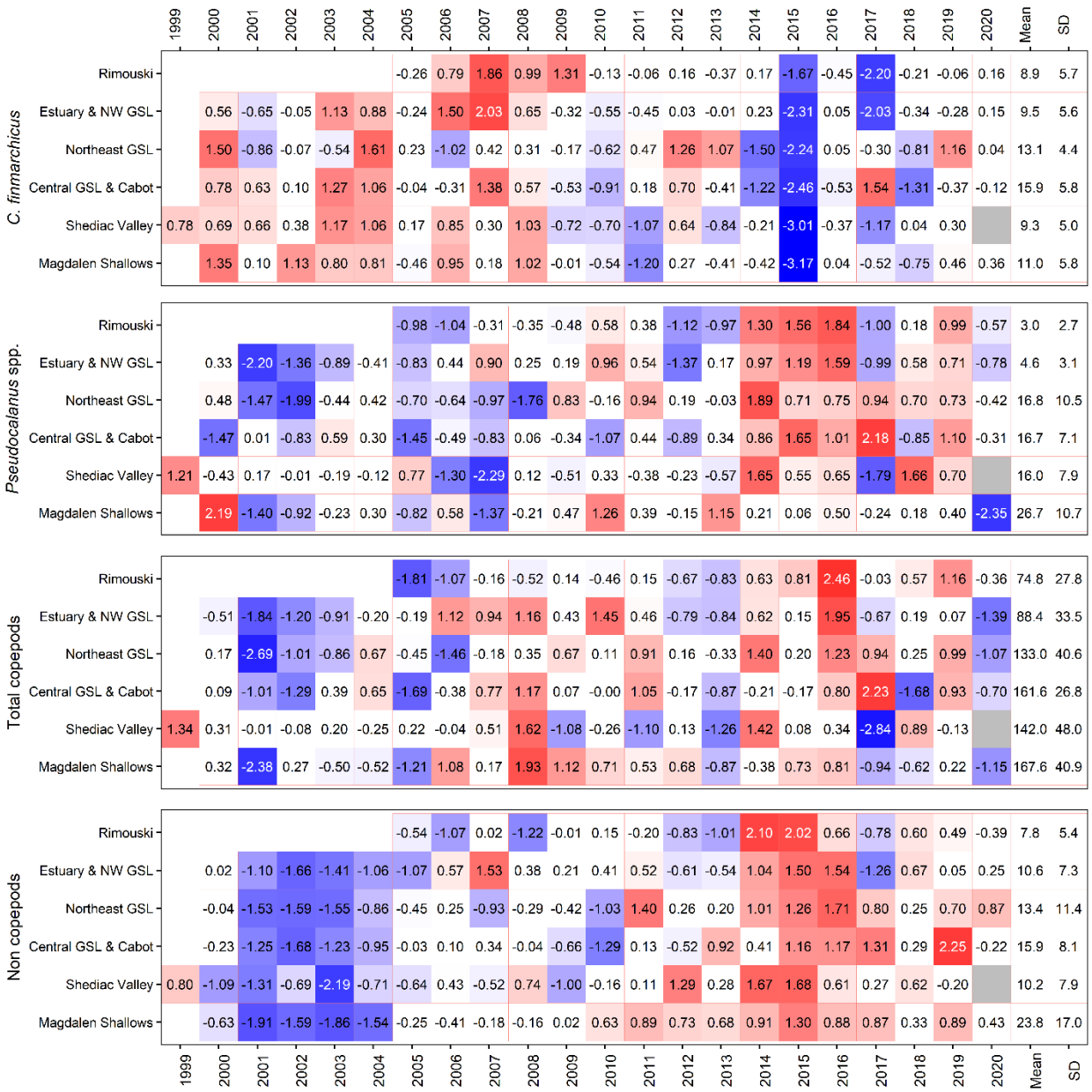

Figure 37. Time series of normalized annual anomalies for the abundance (×10^3 ind m^{-2}) of four zooplankton categories for the high-frequency monitoring stations and the regions of the Gulf of St. Lawrence (calculated using GLM). Variable means and standard deviations for the 2000–2020 (2005–2020 for Rimouski, 1999–2020 for Shediac Valley) climatology are shown to the right of the scorecard. Blue colours indicate anomalies below the mean, reds are anomalies above the mean, and white represents normal conditions. GSL: Gulf of St. Lawrence.

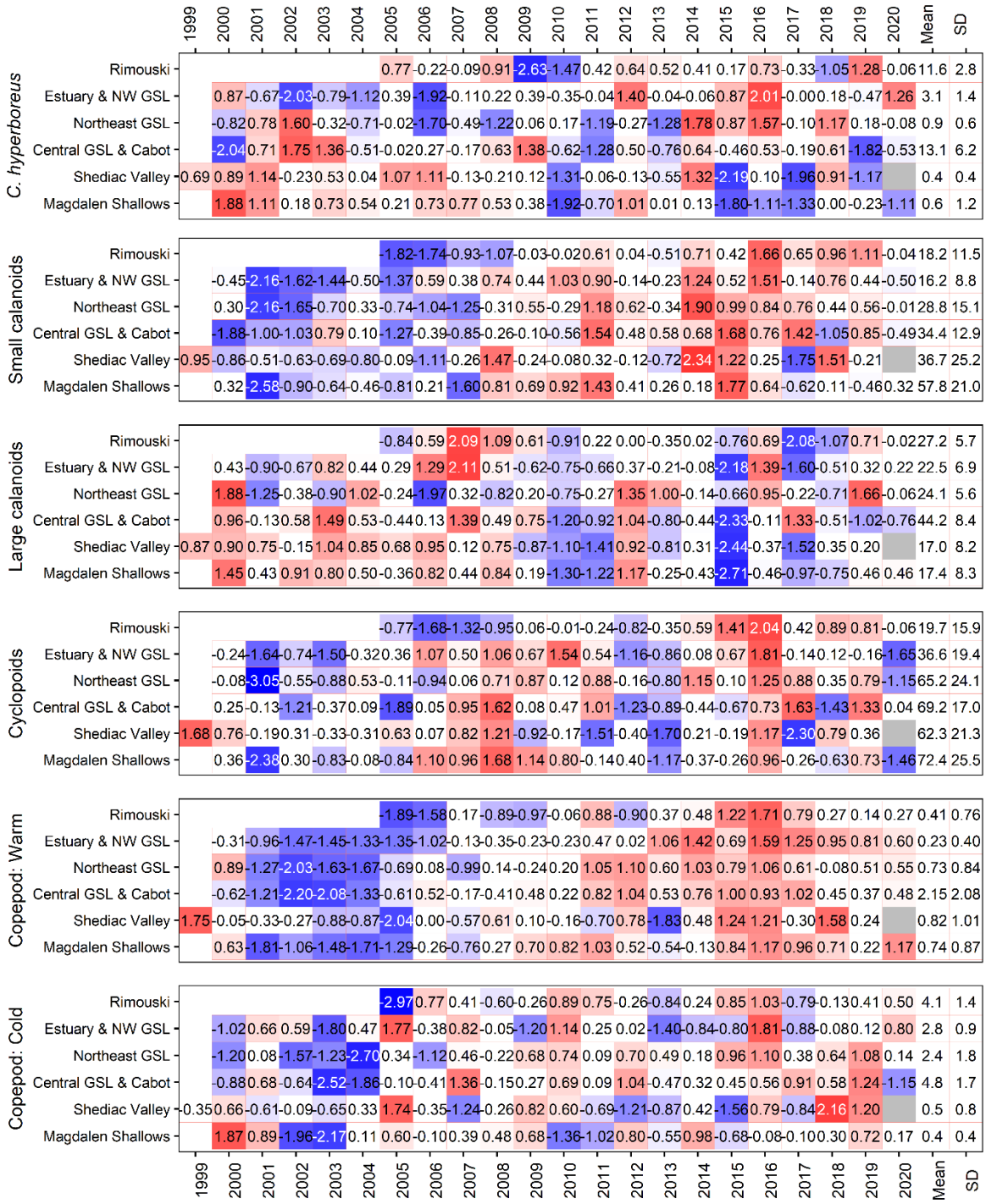

Figure 38. Time series of normalized annual anomalies for the abundance (×10³ ind m⁻²) of six categories of zooplankton assemblages for the high-frequency monitoring stations and the regions of the Gulf of St. Lawrence (calculated using GLM). Variable means and standard deviations for the 2000–2020 (2005–2020 for Rimouski, 1999–2020 for Shediac Valley) climatology are shown to the right of the scorecard. Blue colours indicate anomalies below the mean, reds are anomalies above the mean, and white represents normal conditions. A detailed list of species included in each large copepod index is presented in Appendix 1. GSL: Gulf of St. Lawrence.

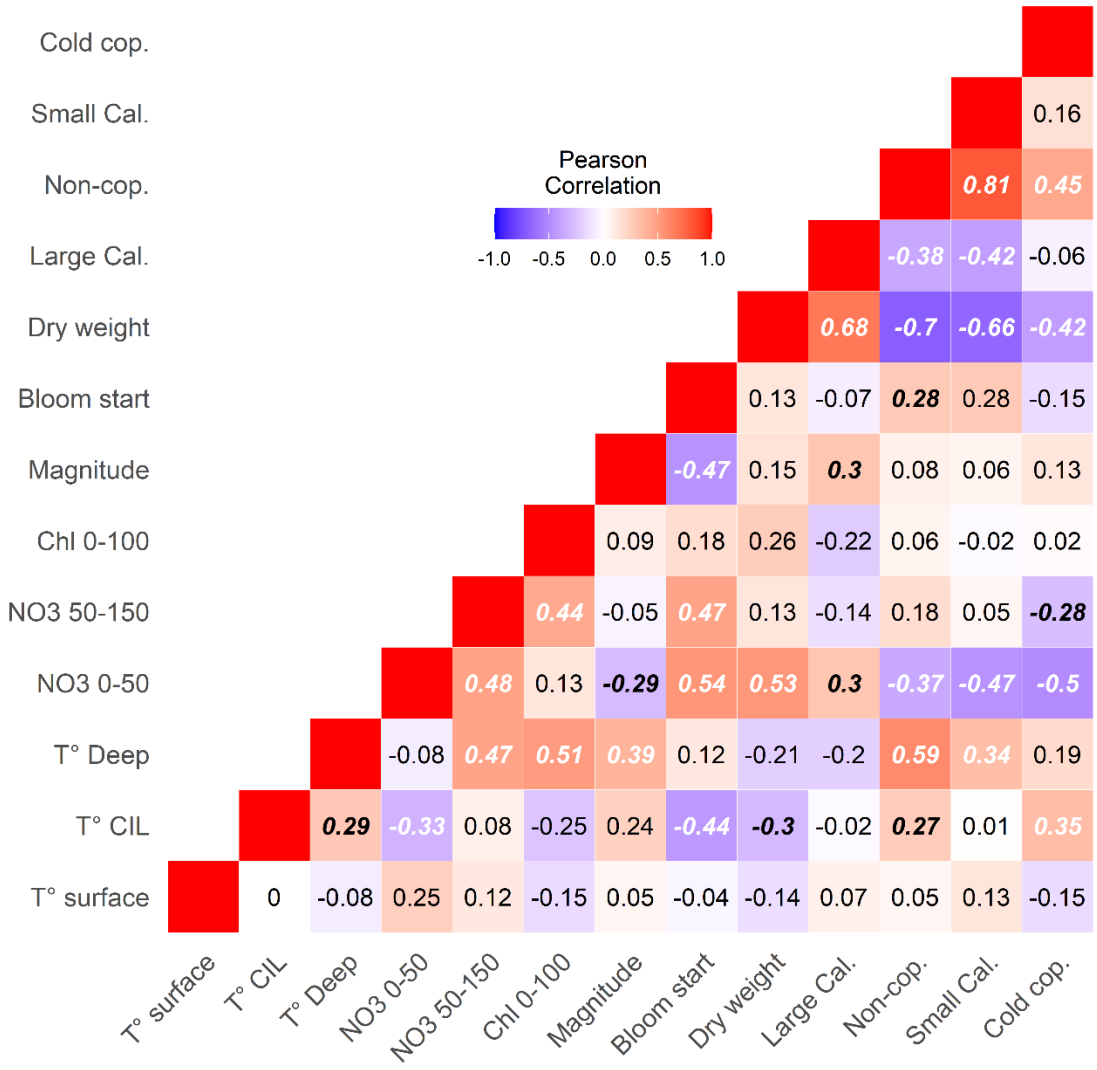

Figure 39. Correlation matrix for summed anomalies of some Gulf indices. Blue colours indicate negative correlations and reds are positive correlations. Significant correlations are indicated in black bold-italic ($p < 0.1$) or in white bold-italic ($p < 0.05$). CIL: cold intermediate layer.

APPENDICES

Appendix 1. List of taxa associated with each copepod index.

Small calanoids	*Acartia* spp.
	Aetideidae
	Centropages spp.
	Clausocalanus spp.
	Eurytemora spp.
	Microcalanus spp.
	Nannocalanus minor
	Paracalanus parvus
	Pseudocalanus spp.
	Scolecithricella spp.
	Spinocalanus spp.
	Temora spp.
	Tortanus spp.
Large calanoids	*Anomalocera* spp.
	Calanus finmarchicus
	Calanus glacialis
	Calanus hyperboreus
	Euchaeta spp.
	Metridia spp.
	Paraeuchaeta norvegica
	Pleuromamma borealis
	Pleuromamma robusta
Warm copepods	*Centropages* spp.
	Clausocalanus spp.
	Metridia lucens
	Nannocalanus minor
	Paracalanus spp.
	Pleuromamma borealis
	Pleuromamma robusta
Cyclopoids	*Oithona* spp.
	Oncaea spp.
	Triconia borealis
	Triconia conifer
	Triconia similis
Cold copepods	*Metridia longa*
	Calanus glacialis

Appendix 2. GLM results for Rimouski and Shediac Valley stations. Significance of the year and month effects as well as the adjusted R squared of the regression for nutrients and chorophyll a *are presented.*

Station	Index	Year (*p*)	Month (*p*)	R^2
Rimouski	Chlorophyll *a* (0–100m)	<0.0001	<0.0001	0.42
	Nitrate (0–50m)	<0.0001	<0.0001	0.35
	Nitrate (50–150m)	<0.0001	<0.0001	0.27
	Nitrate (150–320m)	<0.0001	<0.0001	0.39
Shediac Valley	Chlorophyll *a* (0–100m)	<0.0001	<0.0001	0.37
	Nitrate (0–50m)	<0.001	<0.0001	0.33
	Nitrate (50–84m)	<0.0001	0.0001	0.21

Appendix 3. GLM results for Rimouski and Shediac Valley stations. Significance of the year and month effects as well as the adjusted R squared of the regression for phytoplankton groups are presented.

Region	Index	Year (*p*)	Month (*p*)	R^2
Rimouski	Diatoms	<0.0001	<0.0001	0.37
	Dinoflagellates	<0.0001	<0.0001	0.53
	Flagellates	<0.0001	<0.0001	0.38
	Ciliates	<0.0001	<0.0001	0.36
	Total	0.0001	<0.0001	0.26
	Diatoms/Dinoflagellates	<0.0001	<0.0001	0.33
	Diatoms/Flagellates	<0.0001	<0.0001	0.24
Shediac Valley	Diatoms	<0.0001	<0.001	0.33
	Dinoflagellates	<0.0001	0.07	0.34
	Flagellates	<0.0001	<0.0001	0.42
	Ciliates	0.09	0.5	0.06
	Total	<0.0001	<0.001	0.36
	Diatoms/Dinoflagellates	<0.0001	<0.001	0.35
	Diatoms/Flagellates	<0.0001	<0.0001	0.41

Appendix 4. GLM results for Gulf regions. Significance of the year, season, and station effects as well as the adjusted R squared of the regression for nutrients or chorophyll a are presented.

Region	Index	Year (*p*)	Season (*p*)	Station(*p*)	R^2
Estuary	Chlorophyll *a* (0–100m)	<0.0001	<0.0001	0.5	0.48
	Nitrate (0–50m)	<0.0001	<0.0001	<0.0001	0.41
	N:P (0–50m)	<0.0001	<0.0001	<0.0001	0.4
	Si:N (0–50m)	<0.0001	<0.0001	0.6	0.5
	Nitrate (50–150m)	<0.0001	<0.0001	<0.0001	0.23
	N:P (50–150m)	<0.0001	0.5	<0.01	0.18
	Si:N (50–150m)	<0.0001	<0.0001	<0.0001	0.33
	Nitrate (150-btm)	<0.0001	<0.0001	<0.0001	0.88
	N:P (150-btm)	<0.001	0.03	0.5	0.1
	Si:N (150-btm)	<0.0001	<0.001	<0.0001	0.42
Northwest Gulf	Chlorophyll *a* (0–100m)	<0.0001	<0.0001	<0.0001	0.32
	Nitrate (0–50m)	<0.0001	<0.0001	<0.0001	0.53
	N:P (0–50m)	<0.0001	<0.0001	<0.0001	0.47
	Si:N (0–50m)	<0.0001	<0.001	<0.0001	0.24
	Nitrate (50–150m)	<0.0001	<0.0001	<0.0001	0.42
	N:P (50–150m)	<0.0001	<0.0001	<0.0001	0.34
	Si:N (50–150m)	<0.0001	<0.01	<0.0001	0.31
	Nitrate (150-btm)	<0.0001	<0.0001	<0.0001	0.81
	N:P (150-btm)	<0.0001	0.03	<0.0001	0.31
	Si:N (150-btm)	<0.0001	<0.001	<0.0001	0.41
Northeast Gulf	Chlorophyll *a* (0–100m)	<0.0001	<0.0001	0.2	0.23
	Nitrate (0–50m)	<0.0001	<0.0001	<0.01	0.73
	N:P (0–50m)	<0.0001	<0.0001	<0.01	0.75
	Si:N (0–50m)	<0.0001	<0.0001	<0.0001	0.24
	Nitrate (50–150m)	<0.0001	<0.0001	<0.0001	0.54
	N:P (50–150m)	<0.0001	<0.0001	<0.0001	0.58
	Si:N (50–150m)	<0.0001	0.2	<0.0001	0.34
	Nitrate (150-btm)	<0.0001	<0.0001	<0.0001	0.91
	N:P (150-btm)	<0.0001	<0.0001	<0.0001	0.58
	Si:N (150-btm)	<0.0001	<0.01	<0.0001	0.53
Central Gulf	Chlorophyll *a* (0–100m)	<0.0001	0.08	0.3	0.15
	Nitrate (0–50m)	<0.0001	<0.0001	<0.0001	0.73
	N:P (0–50m)	<0.0001	<0.0001	<0.0001	0.73

Region	Index	Year (*p*)	Season (*p*)	Station(*p*)	R^2
	Si:N (0–50m)	<0.0001	<0.001	0.09	0.27
	Nitrate (50–150m)	<0.0001	<0.0001	<0.0001	0.35
	N:P (50–150m)	<0.0001	<0.0001	<0.0001	0.44
	Si:N (50–150m)	<0.0001	<0.0001	<0.0001	0.49
	Nitrate (150-btm)	<0.0001	<0.0001	<0.0001	0.9
	N:P (150-btm)	<0.0001	<0.0001	<0.0001	0.48
	Si:N (150-btm)	<0.0001	0.2	<0.0001	0.28
Cabot Strait	Chlorophyll *a* (0–100m)	<0.0001	<0.001	0.2	0.23
	Nitrate (0–50m)	<0.0001	<0.0001	0.1	0.69
	N:P (0–50m)	<0.0001	<0.0001	0.5	0.7
	Si:N (0–50m)	<0.001	<0.01	0.02	0.15
	Nitrate (50–150m)	<0.0001	<0.0001	<0.0001	0.4
	N:P (50–150m)	<0.0001	<0.0001	<0.0001	0.44
	Si:N (50–150m)	<0.0001	0.01	<0.0001	0.41
	Nitrate (150-btm)	<0.0001	<0.0001	<0.0001	0.94
	N:P (150-btm)	<0.0001	<0.0001	<0.0001	0.44
	Si:N (150-btm)	<0.001	0.4	<0.0001	0.51
Magdalen Shallows	Chlorophyll *a* (0–100m)	<0.0001	<0.0001	<0.0001	0.22
	Nitrate (0–50m)	<0.0001	<0.0001	<0.0001	0.56
	N:P (0–50m)	<0.0001	<0.0001	<0.0001	0.57
	Si:N (0–50m)	<0.0001	<0.0001	<0.0001	0.34
	Nitrate (50–150m)	<0.0001	<0.0001	<0.0001	0.7
	N:P (50–150m)	<0.0001	<0.0001	<0.0001	0.45
	Si:N (50–150m)	<0.0001	0.02	<0.0001	0.35

Appendix 5. GLM results for Rimouski and Shediac Valley stations. Significance of the year and month effects as well as the adjusted R squared of the regression for each zooplankton index are presented.

Station	Index	Year (*p*)	Month (*p*)	R^2
Rimouski	*Calanus finmarchicus*	<0.0001	<0.0001	0.5
	Pseudocalanus spp.	<0.0001	<0.0001	0.55
	Total copepods	<0.0001	<0.0001	0.57
	Non-copepods	<0.0001	<0.0001	0.42
	Calanus hyperboreus	<0.0001	<0.0001	0.43
	Small calanoids	<0.0001	<0.0001	0.66
	Large calanoids	<0.0001	<0.0001	0.33
	Cyclopoids	<0.0001	<0.0001	0.59
	Copepods: Warm	<0.0001	0.8	0.47
	Copepods: Cold	<0.0001	<0.0001	0.45
	Dry weight	<0.0001	<0.0001	0.65
Shediac Valley	*Calanus finmarchicus*	<0.0001	<0.0001	0.33
	Pseudocalanus spp.	0.1	0.2	0.06
	Total copepods	0.2	<0.0001	0.18
	Non-copepods	0.001	<0.001	0.21
	Calanus hyperboreus	<0.0001	<0.0001	0.67
	Small calanoids	0.01	<0.0001	0.19
	Large calanoids	<0.0001	<0.0001	0.35
	Cyclopoids	0.3	<0.0001	0.25
	Copepods: Warm	0.1	0.05	0.07
	Copepods: Cold	0.07	<0.0001	0.3
	Dry weight	<0.0001	<0.0001	0.36

Appendix 6. GLM results for Gulf regions. Significance of the year, season, and station effects as well as the adjusted R squared of the regression for each zooplankton index are presented.

Region	Index	Year (*p*)	Season (*p*)	Station(*p*)	R^2
Estuary and Northwest Gulf	*Calanus finmarchicus*	<0.0001	<0.001	<0.0001	0.66
	Pseudocalanus spp.	<0.0001	<0.0001	<0.0001	0.55
	Total copepods	<0.0001	<0.0001	<0.0001	0.77
	Non-copepods	<0.0001	<0.0001	<0.0001	0.58
	Calanus hyperboreus	0.02	<0.0001	<0.0001	0.6
	Small calanoids	<0.0001	<0.0001	<0.0001	0.68
	Large calanoids	<0.0001	0.007	<0.0001	0.77
	Cyclopoids	<0.0001	<0.0001	<0.0001	0.73
	Copepods: Warm	<0.0001	0.009	<0.0001	0.51
	Copepods: Cold	<0.0001	<0.0001	<0.0001	0.68
	Dry weight	<0.0001	<0.0001	<0.0001	0.79
Northeast Gulf	*Calanus finmarchicus*	<0.0001	<0.0001	0.01	0.22
	Pseudocalanus spp.	<0.0001	<0.01	<0.0001	0.3
	Total copepods	<0.0001	<0.0001	<0.001	0.38
	Non copepods	<0.0001	0.01	<0.0001	0.46
	Calanus hyperboreus	0.03	<0.0001	<0.0001	0.59
	Small calanoids	<0.0001	0.9	<0.0001	0.42
	Large calanoids	0.02	<0.0001	<0.0001	0.45
	Cyclopoids	<0.0001	<0.0001	0.1	0.51
	Copepods: Warm	<0.0001	<0.0001	0.003	0.49
	Copepods: Cold	<0.0001	<0.0001	<0.0001	0.45
	Dry weight	0.002	<0.0001	<0.0001	0.68
Central Gulf and Cabot Strait	*Calanus finmarchicus*	<0.0001	<0.01	0.04	0.26
	Pseudocalanus spp.	<0.0001	<0.0001	<0.0001	0.28
	Total copepods	0.02	<0.0001	<0.01	0.15
	Non-copepods	<0.0001	<0.0001	<0.0001	0.46
	Calanus hyperboreus	<0.0001	<0.001	<0.0001	0.5
	Small calanoids	<0.0001	0.7	<0.0001	0.3
	Large calanoids	<0.0001	0.9	<0.0001	0.3
	Cyclopoids	<0.001	<0.0001	<0.01	0.23
	Copepods: Warm	<0.0001	<0.0001	<0.0001	0.48
	Copepods: Cold	<0.001	0.2	0.3	0.09
	Dry weight	<0.0001	0.3	<0.0001	0.58
	Calanus finmarchicus	<0.0001	<0.001	<0.0001	0.32

Region	Index	Year (*p*)	Season (*p*)	Station(*p*)	R^2
Magdalen Shallows	*Pseudocalanus* spp.	<0.0001	<0.0001	0.6	0.11
	Total copepods	<0.0001	<0.0001	<0.001	0.24
	Non-copepods	<0.0001	<0.0001	<0.0001	0.49
	Calanus hyperboreus	<0.0001	<0.0001	<0.0001	0.5
	Small calanoids	<0.0001	<0.001	<0.01	0.19
	Large calanoids	<0.0001	<0.0001	<0.0001	0.5
	Cyclopoids	<0.0001	<0.0001	<0.0001	0.34
	Copepods: Warm	<0.0001	<0.0001	0.01	0.49
	Copepods: Cold	<0.0001	<0.0001	<0.0001	0.4
	Dry weight	<0.0001	<0.0001	<0.0001	0.4